REVIEW

EnergyChem

www.journals.elsevier.com/energychem

Luminescent inorganic-organic hybrid semiconductor materials for energy-saving lighting applications

Wei Liu,[a] William P. Lustig,[b] and Jing Li*,[b,a]

[a] Hoffmann Institute of Advanced Materials, Shenzhen Polytechnic, 7098 Liuxian Blvd, Nanshan District, Shenzhen 518055, China

[b] Department of Chemistry and Chemical Biology, Rutgers University, 123 Bevier Road, Piscataway, NJ, 08854, USA

*Correspondence: jingli@rutgers.edu (J. L.)

ABSTRACT: Solid-state-lighting (SSL) technologies are gradually replacing conventional lighting sources due to their advantages in energy efficiency and reduced environmental impact. As such, developing high-performance luminescent materials to be used in SSL devices for lighting related applications has become a very hot topic in the past decade. These luminescent materials can be designed as either phosphors or emissive layers for light-emitting diodes (LEDs) or organic light-emitting diodes (OLEDs). This article provides a brief overview on the recent research and development of a variety of luminescent inorganic-organic hybrid semiconductor material classes. The structural characteristics and luminescent properties of representative examples of each material family will be discussed and summarized.

KEYWORDS: *Crystalline hybrid material, Semiconductor, LED, Luminescence, Phosphor, Solid state lighting*

Abbreviations: MLCT, metal-to-ligand-charge-transfer; XLCT, halide-to-ligand-charge-transfer; CC, metal-center change transfer; EQE, external quantum efficiency; PE, power efficiency; CE, current efficiency; VON, Turn-on voltage; Lmax, maximum luminance; KC, ligand centered; LLCT, inter-ligand (or ligand-to-ligand) charge transfer; MC, metal-centered; MMCT, metal-to-metal charge transfer; BAM, $BaMgAl_{10}O_{17}:Eu^{2+}$; XMLCT, cluster-centered halogen-metal to ligand; EWDP, excitation-wavelength-dependent photoluminescence; T_D, decomposition temperature; STE, self-trapped exciton; EA, ethylammonium; PEI, polyethyleneimine; mCPy, 3,5-bis(carbazol-9-yl)pyridine; TCIQ, 4-[3,6-di(carbazol-9-yl)carbazol-9-yl]isoquinoline; TCPy, 3-[3,6-di(carbazol-9-yl)carbazol-9-yl]pyridine; CPy, 4-(carbazol-9-yl)isoquinoline (4CIQ), and 3-(carbazol-9-yl)pyridine; CIQ, isoquinolyl carbazole; DCIQ, 9-(8-(carbazol-9-yl)isoquinolin-5-yl)-carbazole; DCDPIQ, 9-(4-(5-(4-(carbazol-9-yl)phenyl)isoquinolin-8-yl)phenyl)-carbazole; 1-Mim, 1-methyl imidazole; 2,6-dmpz, 2,6-dimethylpiperazine; 4,4′-bpy, 4,4′-bipyridine; 4,4′-dps, 4,4′-dipyridyl sulfide; 5-Br-pm, 5-bromopyrimidine; API, N-(3-Aminopropyl)-imidazole; ba, n-butylamine; bbipe, 1,5-bis(1H-benzo[d]imidazol-1-yl)pentane; bix, 1, 4-bis(imidazole-1-ylmethyl)benzene; bmbipe, 1,5-bis(5-methyl-1H-benzo[d]imidazol-1-yl)pentane; bmib, 1,4-bis(2-methyl-imidazol-1-yl)butane; Bmim, 1-butyl-3-methyl imidazolium; Bmmim, 1-butyl-2,3-dimethyl imidazolium; bp4mo, N-oxide-4,4′-bipyridine; bpp, 1,3-bis(4-pyridyl)propane; btmdb, N-((1H-benzo[d][1,2,3]triazol-1-yl)methyl)-N,N-dibutylbutan-1-aminium; bttmm, 1-(1H-benzo[d][1,2,3]triazol-1-yl)-N,N,N-trimethylmethanaminium; bza, benzylamine; Bzmim, 1-benzyl-3-methyl imidazolium; bz-ted, 1-benzyl-1,4-diazabicyclo[2.2.2]octan-1-ium; CRI, Color Rendering Index; CCT, correlated color temperature; CyBMA, 1,3-bis(methylaminohydrobromide)cyclohexane; DABCO, 1,4-Diazabicyclo(2,2,2)octane; DETA, diethylenetriamine; dipe, 1,5-di(1H-imidazol-1-yl)pentane; dppe, bis(diphenylphosphanyl)ethane; dppf, $Ph_2PCpFeCpPPh_2$; dppm, bis(diphenylphosphino)methane; dppo, $Ph_2P(CH_2)_8PPh_2$; dpppt, bis(diphenylphosphanyl)pentane; EDBE, 2,2′-(ethylenedioxy)bis(ethylammonium); EL, electroluminescence; en, ethylenediamine; EPy, 1-ethylpyridinium; EQY, external quantum yield; fbza, 4-flurobenzylamine; H_2mba, 2-mercaptobenzoic acid; ha, n-hexylamine; hep, heptamethylenimine; hex, hexamethylenimine; HMD, homopiperazine; HOOCMim, 1-carboxymethyl-3-methyl imidazolium; HLED, hybrid light emitting diode; Im, imidazole; ISC, intersystem crossing; IQY, internal quantum yield; CIE, International Commission on Illumination; LED, light-emitting diode; mbza, 4-methoxybenzylamine; N-MEDA, N^1-methylethane-1,2-diammonium; oa, octylamine; OLED, organic light-emitting diode; pca, 3-picolylamine; pda, 1,3-propanediamine; pc-WLED, phosphor-converted white light emitting diode; PL, photoluminescence; PV, photovoltaic; pm, pyrimidine; pr-ted, 1-propyl-1,4-diazabicyclo[2.2.2]octan-1-ium; py, pyridine; QCE, quantum confinement effect; QE, Quantum efficiency; QY, Quantum yield; REE, rare-earth element; SOC, spin-orbit coupling; TBA, tetrabutylammonium; thfa, tetrahydrofurfurylamine; tpp, triphenylphosphine.; tppa, N,N′,N″-tris(3-pyridinyl)phosphoric triamide; YAG, yttrium aluminum garnet.

INTRODUCTION

Inorganic-organic hybrid semiconductors for solid-state lighting

As the environmental challenges facing the planet have become clearer, the development of new energy-saving technologies has become an extremely active research topic,[1,2] with the eventual goal being the development of a sustainable and energy-efficient global society. The most effective ways to improve energy efficiency is to replace traditional energy-costly technologies with more efficient alternatives.[3,4] Solid-state lighting (SSL) technologies for general lighting, including light-emitting diodes (LEDs) and organic light-emitting diodes (OLEDs), are much more efficient than conventional lighting devices.[5] Since general lighting accounts for a significant portion of global energy consumption, SSL brings about a revolution in the lighting and display industries and is widely

Received: January 18, 2019
Revised: June 11, 2019
Accepted: June 11, 2019
Published: 13 June 2019

DOI: 10.1016/j.enchem.2019.100008
EnergyChem 1, 100008 (2019)

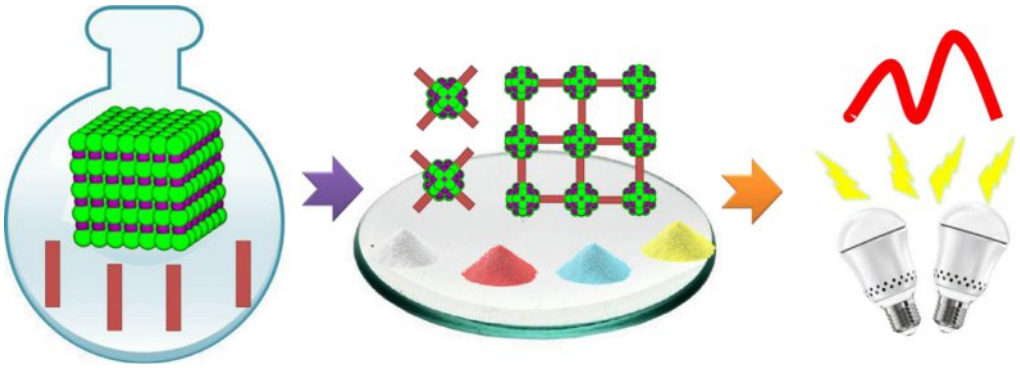

Fig. 1. Illustration of the design and synthesis of inorganic-organic hybrid materials for lighting applications.

considered to be the lighting technology of the future. While white LEDs (WLEDs) offer the highest energy efficiency for general lighting applications, commercial phosphors currently used in WLEDs are inorganic materials containing rare-earth elements (REEs). Their dependence on REEs, in particular europium, terbium, and yttrium, can become problematic due to potential supply risk and cost issues, as well as their serious environmental impact. In addition, the quality of light produced by commercial WLEDs needs further optimization. For these reasons, new types of better performing lighting materials are still in great demand (Fig. 1).

Crystalline inorganic-organic hybrid materials are composed of inorganic and organic moieties or modules blended at the atomic or molecular scale, and they have been extensively explored over the past several decades.[6–11] These materials are both fundamentally and technologically important because of their structural versatility and interesting/unique properties that result from incorporation of both inorganic and organic component in a single crystal lattice.[8,122] The integration of the inorganic modules and organic ligands allows the combination of the superior electronic, magnetic, optical, thermal, and mechanical properties of the inorganic compounds with the excellent structural flexibility, processability, light weight, and functionality of organic molecules in the resulting hybrid structures, providing greatly enhanced structural, chemical and physical properties. [8,12,13] The diversity of these structures allow scientists to optimize their properties by altering the inorganic and organic components, or the bonding between them, and the overall performance of the hybrids can also be systematically tuned by changing the reactants or reaction conditions. The structure-property relationships of these structures have been extensively studied in order to obtain high-performance functional materials.

The luminescence, either photoluminescence (PL) or electroluminescence (EL), of inorganic-organic hybrid semiconductors is particularly interesting.[14–16] Depending on their optical properties, these materials may be suitable for use as either the lighting phosphors for phosphor-converted WLEDs (pc-WLEDs) or the emissive layers in hybrid LEDs (HLEDs). In both cases the light output is primarily determined by the intrinsic emissive behaviors of excited phosphors in form of either fluorescence or phosphorescence. Fluorescence occurs when an electron relaxes to its ground state by emitting a photon from an excited singlet state.[17] Such electron transition is spin-allowed (S_1-S_0), so this process is fast, usually taking less than 1 μs to occur. In phosphorescence, an electron undergoes intersystem crossing (ISC) into a triplet state. The excited electron is then trapped in the triplet state with only "forbidden" transitions available to return to the lower energy singlet state. This transition (T_1-S_0), although "forbidden", will still occur, albeit significantly slower than fluorescence transitions.[18,19]

Luminescence from hybrid structures tends to be complicated and in most cases involves more than one energy transfer process after the compound is excited by light or an electric field.[11,14,20] Different types of hybrid structures also tend to exhibit different luminescence mechanisms. Broadly speaking, electron transition processes for typical inorganic-organic hybrids involve ligand centered (LC) transitions, inter-ligand (or ligand-to-ligand) charge transfer (LLCT), charge transfer between metal and ligand (MLCT or LMCT), metal-centered (MC) transitions, and metal-to-metal charge transfer (MMCT).[21] For hybrid semiconductor materials, band gap emission generally dominates, which involves recombination of electrons from the lowest edge of the conduction band with holes present in the highest edge of the valance band. When the electron recombines with the hole in such a way, a photon with energy equal to the band gap is emitted.[22,23] At the nano-scale, band edge emission from semiconductors is highly size dependent, owing to size-dependent quantum confinement or quantum size effect. Emissions from defects and impurities are common for nanoparticles or doped samples of hybrid semicondutors.[24] A recent study showed that, for low-dimensional perovskite based hybrids with strong electron−phonon interactions, the broadband emissions are from self-trapped excitons.[25] Strong spin-orbit coupling (SOC) effect also plays an important role influencing the band gap as well as luminescent properties of some of these materials since they often contain heavy atoms.[26–30] SOC is the interaction between the electron spin and the magnetic moment generated by the orbital motion of the electron.[31] Spin-orbital splitting of energy levels of different atoms may be different, and the extent of such splitting is generally larger for heavier atoms.[32] Many studies show that the SOC effect has strong influence on the energy levels of heavy metals (e.g. Pb, Sn), which leads to strong mixing between singlet and triplets states of the excitons and reduces band gaps of hybrid perovskites.[29] Studies also show that efficient SOC can lead to faster ISC, which results in stronger phosphorescence in hybrid molecular clusters in the solid state.[26,33–35] Due to the complexity of these structures, the study of their luminescence mechanisms is still in its infancy.

The general approach to fabricating pc-WLEDs involves the use of either single or multicomponent phosphors in combination with an excitation source (e.g. a blue LED chip) to generate white light of high quality.[36] The phosphors used are down

DOI: 10.1016/j.enchem.2019.100008
EnergyChem 1, 100008 (2019)

conversion materials, producing lower energy photons upon absorbing higher energy photons. A common example of this type of WLEDs is made by coating a blue-emitting InGaN/GaN diode with a yellow emitting YAG:Ce^{3+} phosphor.[37] Some red-emitting phosphors may also be blended in for light quality optimization, tuning the "cold" white light to "warm" white light.[37,38] The combined emissions from the blue chip and phosphors generate white light of high quality.[36]

When considering a hybrid material for lighting applications, the quality of light produced must be taken into consideration. Light quality is typically evaluated by several parameters, such as internal quantum yield (IQY) and external quantum yield (EQY), the International Commission on Illumination (CIE) colorimetry, correlated color temperature (CCT), and color rendering index (CRI). The quantum yield and the quantum efficiency (QE) may be used interchangeably. The IQY for the commonly used commercial phosphor YAG: Ce^{3+} is as high as 95%,[36] and the CIE coordinates for pure white light is (0.333, 0.333). Color temperature defines the color appearance of a white LED. A warm light is 2700 K or lower, neutral white is at around 4000 K, and cool white is 5000 K or higher temperatures.

Electroluminescence is an optical phenomenon in which a material emits light in response to an electric current or a strong electric field [39] These materials are used to make LED or OLED devices. LEDs based on metal halide perovskite materials have emerged as promising optoelectronic devices, showing great potential for both general lighting and display applications due to their low cost and solution processability.[40-42] Tremendous effort has been focused on improving the performance of these devices, and their quantum efficiency has surpassed 20%.[43] The good performance of the perovskite LEDs is attributed to the intrinsic properties of the perovskite materials, including low defect density, high crystallinity, high absorption, high PLQY, efficient charge transport, etc.[44,45] Strategies in enhancing the performance of perovskite LEDs involves controlling the morphology and crystallization of the films, structural design of perovskite structures of different dimensionality and composition, surface passivation perovskite layers, etc.[46-49] Additionally, several highly luminescent copper halide based molecular clusters have been utilized as emissive layers for OLEDs.[50] The crucial parameters that evaluate the performance of LEDs are the external quantum efficiency (EQE), the power efficiency (PE), the current efficiency (CE), the turn-on voltage (VON), the maximum luminance (Lmax), and the stability.[51] The performance is highly related to the design of the devices and the LED performance can be improved by interfacial engineering.[52-55] The EL performance of perovskite based hybrids and copper halide based hybrid materials will be briefly discussed in this review.

Groups of light-emitting hybrid semiconductor materials

A number of inorganic-organic hybrid semiconductor material classes have been developed for a wide range of applications, and the easiest and most straightforward way to classify them is based on their inorganic components. This review focuses mainly on hybrid materials that are based on binary inorganic semiconductors and that emit light. Five such material groups will be covered. They are (1) IB-VIA, (2) IIB-VIA, (3) IB-VIIA, (4) IVA-VIIA, and (5) VA-VIIA based hybrid materials. Other reported hybrid families with very few luminescent members, such as organosilica and VIB-VIA based hybrids, will not be included in this review.[56,57] Another important class of self-assembled luminescent materials, metal-organic frameworks (MOFs), represent an important class of materials exhibiting significant potential for general lighting applications.[58-60] The extensive work on MOFs has already led to a number of recent comprehensive review articles, and as such they will be excluded from this review.[58,60]

Copper (I) and silver (I) chalcogenide clusters with protecting organic ligands comprise a structurally diverse family with a variety of applications.[61,46,62] The organic ligands play a key role in their formation. The ligands not only maintain the stability of these clusters by acting as protecting reactants, preventing the hybrid from decomposition, but also sometime as a S^{2-} source for the formation of chalcogenides during the reaction.[61] The quantum confinement effect (QCE) and the strong metal-metal interaction of these hybrid materials lead to very interesting optical properties. The stability and photophysical properties of these metal clusters largely depend on their core, ligands, and environments, while their emission properties can be modified by variation of the organic ligands. The stability of these materials could also be improved by using organic ligands that form stronger bonds or extended frameworks. Representative examples of this structural family will be discussed in Section 2.

Another family of crystalline nanostructured inorganic-organic hybrid materials are the IIB-VIA binary semiconductor-based hybrids that were first reported in 2000 [63,64] These materials are typically made of inorganic semiconductor nanomodules and N-containing organic ligands (N-ligands) that are connected via covalent bonds between group IIB (e.g. Zn, Cd) metals and the N-ligands. The inorganic modules can be a 1D chain, a 2D single layer or double layer, etc. The N-ligands used are typically aliphatic amines of different sizes and lengths. By varying the composition and dimensionality of inorganic component and by using different organic amine molecules, a variety of hybrid structures have been synthesized and structurally characterized. Among them, double layered structures exhibit broadband white light emission under UV excitation. These materials are potentially promising for use as single-phase white light phosphors. Their emissions, which are generally band edge emissions, can be tuned by varying ligand length, changing composition or doping Mn ions.[23] More details will be discussed in Section 3.

Hybrid materials based on IB-VIIA binary semiconductors exhibit enormous structural variety.[65] A number of inorganic modules have been found, from discrete inorganic units to extended infinite chains or layers. Such inorganic motifs are interconnected or terminated by different kinds of organic ligands, either aliphatic or aromatic, to form zero dimensional (0D) molecular clusters, one dimensional (1D) chains, and two dimensional (2D) sheets or three dimensional (3D) networks. This large family of compounds can be divided into three types: (i) charge neutral structures where both the inorganic and organic components are neutral and are connected by coordination bonds; (ii) ionic structures where both components are charged and there are no coordination bonds between them; and (iii) all-in-one (AIO) structures where both components are charged and they are connected by coordination bonds.[15] The three different types of structures exhibit very different optical and thermal properties. Their luminescence generally results from charge transfer between the metal/halide and the ligand or metal-metal interactions.[20] Some highly emissive molecular clusters have been developed as emissive layers for OLEDs. Representative examples will be given in Sections 4 and 7.

The IVA-VIIA semiconductor based hybrid structures have excellent performance in photovoltaics (PVs).[54,66-69] Some of the

DOI: 10.1016/j.enchem.2019.100008
EnergyChem 1, 100008 (2019)

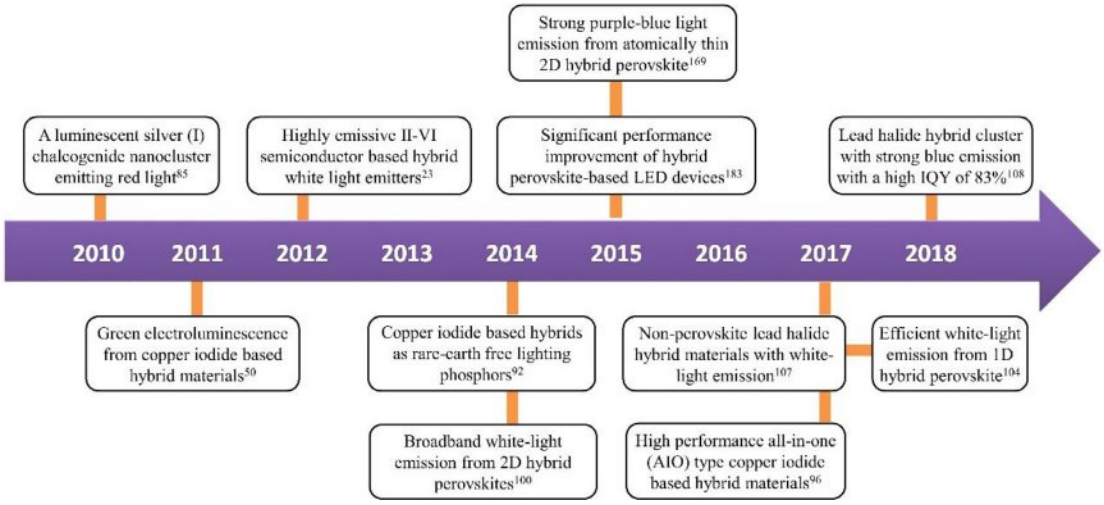

Scheme 1. Timeline of important findings and discoveries in the development of inorganic-organic hybrid materials for lighting applications.

most commonly studied structures are lead or tin halide based hybrid perovskites. These materials exhibit significant promise for high performance and low-cost solar cells due to their unique properties such as extremely high optical absorption, small effective masses for electrons and holes, etc.[70,71] The interactions between inorganic and organic species in perovskite hybrids are primarily ionic, accompanied by relatively weak hydrogen bonds, or in some cases, van der Waals forces.[12] 'Perovskite' is a calcium titanium oxide mineral $CaTiO_3$, and any compounds having the chemical formula ABX_3 and crystallize in the same space group as $CaTiO_3$ are referred to as perovskite structures. When "A" is an organic cation, the structure becomes a "hybrid perovskite". For example, in the case of $CH_3NH_3PbI_3$, the "A" cation is organic $CH_3NH_3^+$, while "B" is Pb^{2+} metal ion and "X" is a halide anion (Cl^-, Br^-, or I^-). Lower-dimensional derivatives of the perovskite structure can be obtained by terminating the 3D network of BX_3 with organic species. The choice of organic ligands is the most important parameters in determining the final structures of the products.[9] The advantages of hybrid perovskites for PV applications along with their high near-unity photoluminescence quantum efficient (PLQE) make them excellent candidates as both phosphors and LED materials.[72-75] Representative compounds will be discussed in Section 5 and 7.

While a limited number of VA-VIIA semiconductor (e.g. antimony or bismuth halides) based hybrid structures have been reported so far, several of them exhibit excellent performance, showing great potential as lighting materials.[54,76] A majority of these structures are molecular clusters, and their inorganic modules form polyhedra such as square pyramid, tetrahedra, and octahedra. Since bismuth represents the only non-toxic heavy metal with low cost, hybrid materials based on bismuth are particularly interesting to scientists.[77] Some important work will be discussed in Section 6. Other organometallic halide hybrid structures are introduced in Section 8.

These inorganic-organic hybrid materials have attracted significant attention, as reflected from numerous review papers on different structure groups.[11,12,15,16,61,65,72,78] Important discoveries and milestones in the research and development of their luminescence properties and applications are highlighted in Scheme 1. Some representative luminescent hybrid materials and their properties are summarized in Table 1 below. This review intends to present a brief overview of luminescent inorganic-organic hybrid semiconductor materials in general, with a well-balanced discussion on each structure group/family. With an emphasis on various types of structures and luminescence properties observed in these structures, our hope is to provide some insight on the structure-property correlation which in turn will help guide future design and development of lighting materials with optimized and enhanced performance.

LUMINESCENT HYBRID MATERIALS BASED ON IB-VIA SEMICONDUCTORS

IB-VIA semiconductor based hybrids are typically in the form of a copper (I) or silver (I) chalcogenide/chalcogenolate inorganic core with adaptable organic ligands.[61,120,121,122] The hybrids formed can be either molecular clusters (in majority cases) or extended frameworks constructed by bridging organic ligands with chalcogenides as their inorganic motifs. The reactants generally contain thiolates acting as the S^{2-} source for the formation of the copper or silver chalcogenides.[123] The ligands also stabilize the chalcogenide clusters. Though there is plenty of literature on copper (I) and silver (I) chalcogenide clusters, most of them are focused on their structures and syntheses, demonstrating their extremely rich structural diversity. The studies on their luminescence properties are relatively rare, mainly because most of them exhibit poor luminescence and are unstable compared to other hybrid materials. However, these structures are fundamentally interesting for photophysical study, since the discrete molecular cluster species are ideal models for understanding molecular size-induced quantum confinement effects.[124] Their emissions mainly originate from ligand-to-metal charge-transfer (LMCT) mixed with metal-metal interactions. Here, we discuss some important work concerning the luminescence of this type of materials.

Light-emitting materials based on Cu(I) chalcogenides

The earliest copper (I) chalcogenide clusters were reported in late 1960s.[125] A well-known example of this type is $[Cu_8(i\text{-}MNT)_6]^{4-}$ (i-MNT = 1,1-dicyanoethylene-2,2-dithiol). This work presents the first structural evidence for a cubic octanuclear cluster of copper atoms. Early studies were mainly focused on the

DOI: 10.1016/j.enchem.2019.100008
EnergyChem 1, 100008 (2019)

Table 1. The excitation energy (λ_{ex}), emission maximum (λ_{em}), emission color, and IQYs of representative luminescent inorganic-organic hybrid structures.

Compounds	λ_{ex} (nm)	λ_{em} (nm)	Emission color	IQY(%)
IB-VIA semiconductor based hybrid materials				
$[Cu_4(\mu\text{-dppm})_4(\mu\text{-S})](PF_6)_2Me_2CO$ [79]	350	579	Orange	–
$[Cu_2(p\text{-S-}C_6H_4\text{-}NMe_2)_2(dppe)_3]$ [80]	366	505	Green	–
$[Cu_2(p\text{-S-}C_6H_4\text{-}NMe_2)_2(dpppt)_2]$ [80]	366	480	Blue	–
$[Cu_4(p\text{-S-}C_6H_4\text{-}NMe_2)_4(PPh_3)_4]$ [80]	366	480	Blue	–
$[Cu_4(p\text{-S-}C_6H_4\text{-}NMe_2)_4(dppm)_2]$ [80]	366	555	Yellow	–
$[Cu_7(p\text{-S-}C_6H_4\text{-}NMe_2)_7(PPh_3)_4]$ [80]	366	560	Yellow	–
$[Cu_2(S\text{-}C_6H_4\text{-}OMe)_2(dpppt)_2]$ [81]	366	465	Blue	–
$[Cu_2(S\text{-}C_6H_4\text{-}NMe_2)_2(dpppt)_2]$ [81]	366	480	Blue	–
$[Cu_{12}S_6(dpppt)_4]$ [82]	350, 500	648	Red	48
$[Cu_{12}S_6(dppo)_4]$ [82]	350, 500	665	Red	67
$[Cu_{12}S_6(dppf)_4]$ [83]	350	638	Red	53
$[Cu_{12}S_6(PPh_2Et)_8]$ [83]	370	673	Red	45
$[Cu_{24}S_{12}(PEt_2Ph)_{12}]$ [83]	540	680	Red	39
$[Ag_4(\mu\text{-dppm})_4(\mu_4\text{-S})]^{2+}$ [84]	360	516	Green	–
$[Ag_{62}S_{13}(SBu^t)_{32}](BF_4)_4$ [85]	365	621	Red	1.4
$(NH_4)_{17}[(\mu_6\text{-S})@Ag_{17}(mba)_{16}]\cdot 22H_2O$ [86]	365	577	Orange	–
$[Ag_{62}S_{13}(SBu^t)_{32}]^{4+}$ (NC-II) [87]	365	605	red	–
IIB-VIA semiconductor based hybrid materials				
2D-$[Cd_2S_2(ba)]$ [88]	365	–	White	4–5
$Zn_2S_2(bza)$ [89]	320	360	UV	–
Mn^{2+} doped $(ZnS)_2\cdot$octylamine[138]	300	597	Orange	–
2D-$[Cd_2Se_2(ba)]$:25 mol% Te [90]	360	–	White	4–5
2D-$[Zn_2S_2(ha)]$ [23]	360	420	Blue	17–18
$[Zn_{1.7}Cd_{0.3}S_2(oa)]$ with 0.08 mol% Mn [23]	365	–	White	31–37
$Zn_{1.5}Cd_{0.5}S_{1.7}Se_{0.3}(ha)$ [22]	360	450, 530	White	–
$[Zn_{1-x}Mn_xSe](DETA)_{0.5}$ [91]	300	585	Yellow	–
IB-VIIA semiconductor based hybrid materials				
1D-$CuI(py)_{1-x}(pm)_x$ [92]	365	480, 570	White	12.5
1D-CuI(5-Br-pm) [92]	450	545	Yellow	13.1
1D-$Cu_2I_2(tpp)_2(bpp)$ [93]	360	458	Blue	91.7
1D-$Cu_2I_2(tpp)_2(4,4'\text{-bpy})$ [93]	360	540	Green-yellow	76.2
2D-$Cu_2I_2(4,4'\text{-dps})_2$ [93]	450	547	Green-yellow	70.8
1D-$Cu_4I_4(bbipe)_2$ [94]	360	560	Yellow	71.8
2D-$Cu_4I_4(bmbipe)_2$ [94]	360	550	Yellow	67.1
3D-$Cu_4I_4(dipe)_2$ [94]	360	580	Yellow	65.6
$(Bu_2DABCO)_{1.5}Cu_3I_6$ [95]	360	548	Yellow	12
$Cu_3I_5(bz\text{-}ted)_2$ [96]	360	560	Yellow	75
$Cu_4I_6(pr\text{-}ted)_2$ [96]	360	535	Green-yellow	92
$Cu_4I_6(tpp)_2(bttmm)_2$ [96]	360	540	Green-yellow	90
$Cu_6I_8(btmdb)_2$ [96]	360	540	Green-yellow	70
$Li(H_2O)(EtOH)_3[Cu_6I_7(tppa)_2]$ [97]	365	485	Blue	27.8
$[N(Et)_4][Cu_6I_7(tppa)_2]$ [97]	365	575	Yellow	79.9
$[N(Pr)_4][Cu_6I_7(tppa)_2]$ [97]	365	580	Yellow	80.6
$[(Ag_4I_4)(bix)]_n$ [98]	380	448, 523	White	–
$[Ag_2(Bmib)Br_2]_\infty$ [99]	366	440	Blue	–
IVA-VIIA semiconductor based hybrid materials				
(N-MEDA)$[PbBr_4]$ [100]	380	–	White	0.5
(N-MEDA)$[PbBr_{2.8}Cl_{1.2}]$ [100]	360	–	White	1.5
(EDBE)$[PbBr_4]$ [101]	365	–	White	9
(CyBMA)$PbBr_4$ [102]	360	–	White	1.5
$C_4N_2H_{14}PbCl_4$ [103]	320 (360)	564 (500)	White	18 (6)
$C_4N_2H_{14}PbBr_4$ [104]	360	–	White	20
$EA_4Pb_3Br_{10-x}Cl_x$ [105]	315	–	White	–
$(2,6\text{-dmpz})_3Pb_2Br_{10}$ [106]	330	585	Yellow	12
$[Pb_2F_2]^{2+}[^-O_2C(CH)_2CO_2^-]$ [107]	327	536	White	1.8
$[Pb_2Cl_2]^{2+}[^-O_2C(CH)_2CO_2^-]$ [107]	327	536	White	11.8
$[Pb_2Br_2]^{2+}[^-O_2C(CH)_2CO_2^-]$ [107]	356	565	White	2.0

(*continued on next page*)

DOI: 10.1016/j.enchem.2019.100008
EnergyChem 1, 100008 (2019)

Table 1 (*continued*)

Compounds	λ_{ex} (nm)	λ_{em} (nm)	Emission color	IQY(%)
$(C_9NH_{20})_7(PbCl_4)Pb_3Cl_{11}$ [108]	348	470	Blue	83
$(C_4N_2H_{14}Br)_4SnBr_3I_3$ [109]	365	582	Orange	85
$HMD_3SnBr_8(CH_3OH)$ [110]	365	590	Orange	65
$HMD_3SnBr_8(CH_2Cl_2)$ [110]	365	601	Orange	86
$(C_9NH_{20})_2SnBr_4$ [111]	365	695	Red	46
VA-VIIA semiconductor based hybrid materials				
$[Bmim]_2SbCl_5$ [76]	370	583	Yellow	86.5
$(C_9NH_{20})_2SbCl_5$ [54]	380	590	Orange	98
[4-methylpiperidinium]$_2SbCl_5$ [112]	373	–	White	1
$(Ph_4P)_2SbCl_5$ [113]	365	648	Red	87
$(TBA)[BiBr_4(bp4mo)]$ [114]	360	540	Green-yellow	85
$[BiBr_3(bp4mo)_2]$ [114]	360	516	Green	11
α-[Bmim][$BiCl_4$(2,2′-bpy)] [115]	397	530	Green-yellow	26.07
β-[Bmim][$BiCl_4$(2,2′-bpy)] [115]	397	530	Green-yellow	36.59
Other luminescent hybrid materials				
$[C_5H_9–NH_3]_4CdBr_6$ [116]	340	–	White	1
$(C_6H_{11}NH_3)_2[CdBr_4]$ [117]	325	–	White	–
$[CdCl_2(Im)_4]$ [118]	365	445	Blue	23.01
$[CdCl_4(HAPI)_2]$ [118]	410	467	Blue	5.84
$[Cd(\mu\text{-}Cl)_2(1\text{-}Mim)_2]_\infty$ [118]	375	450	Blue	27.31
$[CdCl_3(HAPI)]_\infty$ [118]	360	457	Blue	5.71
$[HOOCMim]_2TeCl_6$ [119]	365	610	Red	–
$[HOOCMim]_2TeCl_6$ [119]	465	680	Red	–

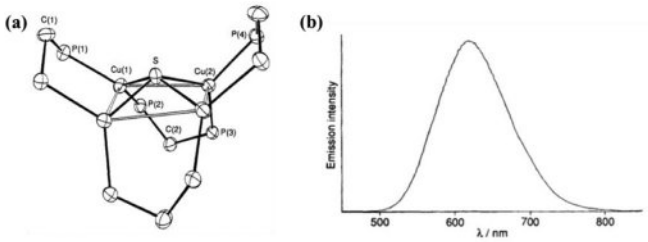

Fig. 2. (a) Structural drawing of the $[Cu_4(\mu\text{-dppm})_4(\mu\text{-S})]^{2+}$ cation. (b) Emission spectrum of $[Cu_4(\mu\text{-dppm})_4(\mu\text{-S})](PF_6)_2Me_2CO$ in degassed MeCN at 298 K. Reproduced from.[79] with permission from The Royal Society of Chemistry.

structures themselves. The photophysical properties of these clusters remained unexplored until the 1990s, with a series of luminescent tetranuclear copper (I) and silver (I) chalcogenide complexes reported by Yam and others.[126]

In 1993, Yam et al. reported a novel tetranuclear copper (I) sulfur cluster, $[Cu_4(\mu\text{-dppm})_4(\mu\text{-S})](PF_6)_2Me_2CO$ [dppm = bis(diphenylphosphino)methane].[79] The four μ-dppm ligands are in a saddle-like configuration (Fig. 2a). The sulfur atom occupies the apex of a distorted square pyramid. The electronic absorption spectrum of this compound shows low energy absorption in the 330–400 nm region. This compound emits intense, long-lived yellow-orange emission (λ_{em} = 579 nm, λ_{ex} > 350 nm) in solid state at room temperature (Fig. 2b). The long excited-state lifetime (3.6 μs) suggests that the emission is most likely associated with a spin-forbidden transition. The authors suggest that the emission is a combination of ligand-to-metal charge transfer [LMCT ($S^{2-} \rightarrow Cu_4$)] and the metal-centered emission from the $3d^94s^1$ state of Cu(I), which has been modified by the copper-copper interaction in the tetramer.

Later in 1996, the same group reported μ$_4$-selenido-bridged copper (I) tetramer, $[Cu_4(\mu\text{-dppm})_4(\mu_4\text{-Se})]^{2+}$.[127] It emits orange light with λ_{em} of 595 nm — a red shift in the emission compared to the sulfur analogue. The luminescence origin is proposed to originate from a ligand-to-metal charge-transfer LMCT[$(Se^{2-}) \rightarrow Cu_4$] triplet excited state, mixed with a metal-centered ($3d^94s^1$) Cu(I) state, which is similar to that of $[Cu_4(\mu\text{-dppm})_4(\mu_4\text{-S})]^{2+}$. When in $(CH_3)_2CO$, the emission red shifted with λ_{em} of 626 nm. Meanwhile, Fackler Jr. et al. reported a tetranuclear copper (I) cluster, $[Cu(S_2P(O^iPr)_2)]_4$, which emits green emission (λ_{em} = 547 nm) under 350 nm excitation.[128] This compound also shows luminescence thermochromism. At 77 K, it displays dual luminescence with emission maxima at 573 and 647 nm.

More recently, a series of highly luminescent copper chalcogenide clusters was reported by Fuhr et al. in 2013.[80] Emission tunability of these structures was demonstrated with a comprehensive study. A total of six luminescent polynuclear copper (I) phenyl thiolate clusters with functional groups in the organic ligands were prepared. All six compounds are copper phenyl thiolate clusters with donor substituents in the para position to the coordinating sulfur atom: $[Cu_2(p\text{-}S\text{-}C_6H_4–NMe_2)_2(dppe)_3]$, $[Cu_2(p\text{-}S\text{-}C_6H_4–NMe_2)_2(dpppt)_2]$, $[Cu_4(p\text{-}S\text{-}C_6H_4\text{-}NMe_2)_4(PPh_3)_4]$, $[Cu_4(p\text{-}S\text{-}C_6H_4NMe_2)_4(dppm)_2]$, $[Cu_7(p\text{-}S\text{-}C_6H_4–NMe_2)_7$

DOI: 10.1016/j.enchem.2019.100008
EnergyChem 1, 100008 (2019)

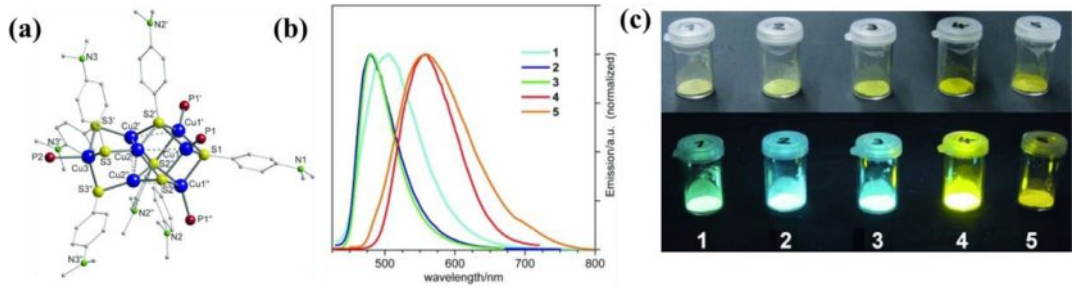

Fig. 3. (a) Molecular structure of $[Cu_7(p\text{-}S\text{-}C_6H_4\text{-}NMe_2)_7(PPh_3)_4]$. (b) Emission (right) spectra of $[Cu_2(p\text{-}S\text{-}C_6H_4\text{-}NMe_2)_2(dppe)_3]$, $[Cu_2(p\text{-}S\text{-}C_6H_4\text{-}NMe_2)_2(dpppt)_2]$, $[Cu_4(p\text{-}S\text{-}C_6H_4\text{-}NMe_2)_4(PPh_3)_4]$, $[Cu_4(p\text{-}S\text{-}C_6H_4\text{-}NMe_2)_4(dppm)_2]$, $[Cu_7(p\text{-}S\text{-}C_6H_4\text{-}NMe_2)_7(PPh_3)_4]$, $[Cu_7(p\text{-}S\text{-}C_6H_4\text{-}OSiMe_3)(SPh)_6(PPh_3)_4]$. (c) Photographs of these hybrids under daylight (top) and UV light ($\lambda = 366$ nm; bottom). Reproduced with permission from.[80] Copyright 2013, Wiley-VCH Verlag GmbH & Co. KGaA.

$(PPh_3)_4]$, $[Cu_7(p\text{-}S\text{-}C_6H_4\text{–}OSiMe_3)(SPh)_6(PPh_3)_4]$, (dppe = bis(diphenylphosphanyl)ethane, dpppt = bis(diphenylphosphanyl)pentane). Their inorganic modules are different, except $[Cu_7(p\text{-}S\text{-}C_6H_4\text{–}NMe_2)_7(PPh_3)_4]$ and $[Cu_7(p\text{-}S\text{-}C_6H_4\text{–}OSiMe_3)(SPh)_6(PPh_3)_4]$ (Fig. 3a). Their optical properties were carefully studied, and the results show strong absorption below 500 nm. The intense luminescence covers the entire visible spectrum (Fig. 3b). The authors concluded that such optical tunability is a result of the influence of the functional groups in the organic ligands and differences in their inorganic modules.

Another work on strongly luminescent copper chalcogenolate complexes was reported by the same group.[81] A total of five compounds are included, based on the formula $[Cu_2(ER)_2(dpppt)_2]$ (ER = *S* or Se based ligands). All of these structures show a planar four-membered ring consisting of two copper and two sulfur or selenium atoms from chalcogenolate ligands with the organic groups in trans orientation. The dpppt ligands also act as bridging ligands between the copper atoms. Strong luminescence was found for all sulfur compounds, which emit blue light in the solid state. Optical tunability was also studied. Since their inorganic modules are identical, the difference in their emission energies suggests that their optical properties could be tuned by changing organic ligands.

It is worth mentioning that two novel clusters with "$Cu_{12}S_6$" cores stabilized by bidentate phosphine ligands were reported by Eichhöfer et al. in 2014.[82] Their formula are $[Cu_{12}S_6(dpppt)_4]$ and $[Cu_{12}S_6(dppo)_4]$ (dpppt = $Ph_2P(CH_2)_5PPh_2$), dppo = $Ph_2P(CH_2)_8PPh_2$) (Fig. 4a and b). They show bright red emission when excited by UV light, with emission maxima at 648 and 665 nm, respectively, in the solid state at room temperature (Fig. 4c). Those two compounds could also be excited by blue-green light at 500 nm) The long decay times of 6.1 and 6.5 μs for $[Cu_{12}S_6(dpppt)_4]$ and $[Cu_{12}S_6(dppo)_4]$ indicate the emissions are from triplet states. Their PLQEs are measured to be 48% and 67%, respectively, using an integrating sphere. These two compounds also show good stability towards oxygen. Such blue light excitable red emitters with high efficiency are very rare and are of great interest. Later, their group reported another series of luminescent phosphine-stabilized copper chalcogenide cluster molecules: $[Cu_{12}Se_6(dppo)_4]$, $[Cu_{12}S_6(dppf)_4]$ (dppf =

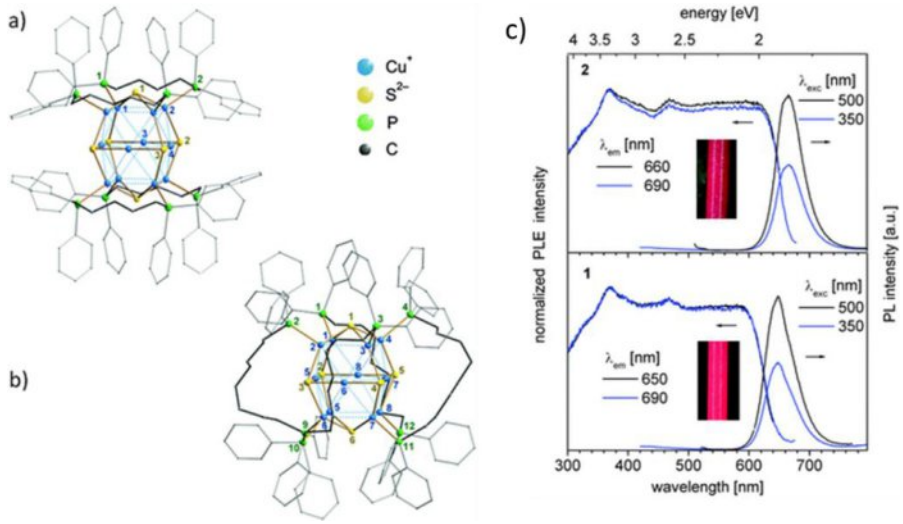

Fig. 4. (a) Molecular structure of (a) $[Cu_{12}S_6(dpppt)_4]$ and (b) $[Cu_{12}S_6(dppo)_4]$. (c) Room temperature photoluminescence excitation (PLE) and emission (PL) spectra of a suspension of freshly prepared microcrystals in toluene of $[Cu_{12}S_6(dpppt)_4]$ (bottom) and $[Cu_{12}S_6(dppo)_4]$ (top) measured in the integrating sphere. The inset shows the colors of the suspensions of microcrystal under white LED light. Reproduced from.[82] with permission from The Royal Society of Chemistry. (For interpretation of the references to color in this figure legend, the reader is referred to the web version of this article.).

DOI: 10.1016/j.enchem.2019.100008
EnergyChem 1, 100008 (2019)

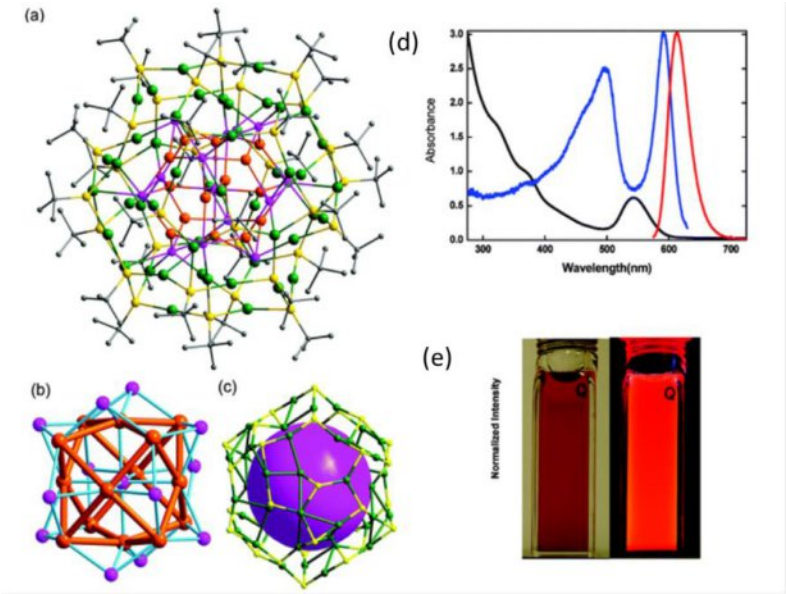

Fig. 5. (a) Structural plot of $[Ag_{62}S_{13}(SBu^t)_{32}](BF_4)_4$. (b) The $[Ag_{14}S_{13}]$ core configuration. (c) The $Ag_{48}(SBu^t)_{32}$ shell structure. The $[Ag_{14}S_{13}]$ core and the tert-butyl groups have been omitted for clarity, and the artificial large purple sphere shows the inner space occupied by the $[Ag_{14}S_{13}]$ core. Color legend: orange, Ag (core); green, Ag (shell); purple, S^{2-}; yellow, S (thiolate); gray, C. (d) Electronic absorption (black trace), excitation (blue trace), and emission (red trace) spectra of $[Ag_{62}S_{13}(SBu^t)_{32}](BF_4)_4$. (d) Photos of emissions from $[Ag_{62}S_{13}(SBu^t)_{32}](BF_4)_4$ in MeOH at room temperature under ambient light and 365 nm excitation. Reproduced with permission from.[85] Copyright 2010, American Chemical Society. (For interpretation of the references to color in this figure legend, the reader is referred to the web version of this article.).

$Ph_2PCpFeCpPPh_2$), $[Cu_{12}S_6(PPh_2Et)_8]$, $[Cu_{12}S_6(PEt_3)_8]$, $[Cu_{24}S_{12}(PEt_2Ph)_{12}]$, $[Cu_{20}S_{10}(PPh_3)_8]$, and $[Cu_{20}S_{10}(P^tBu_3)_8]$.[83] Their luminescence properties have been evaluated in depth. The above complexes show high PLQYs, up to 63% at room temperature. At lower temperatures, the quantum yield would increase. Most of these compounds emit in the red light region and exhibit high photo-stability.

Light-emitting materials based on silver (I) chalcogenides

Silver (I) chalcogenide based hybrids have developed across a similar timeline as their copper chalcogenide analogues with almost identical luminescence mechanisms proposed. However, silver based compounds are much less investigated due to their optical instability towards light. In 1996, Yam et al. reported the first series of luminescent hybrid structures based on silver (I) chalcogenide clusters, with the formula of $[Ag_4(\mu\text{-dppm})_4(\mu_4\text{-}E)]^{2+}$ ($E = S$, Se, Te).[84] In these structures, the silver (I) metals in the tetranuclear cluster were bridged by a chalcogenide atom with short Ag(I)-Ag(I) distances. The optical properties were investigated, and these structures emit green to orange emission in the solid state. Experimental results show that the emission could be tuned by changing chalcogenides. Relative red shifts are observed when comparing S (516 nm) to Se (527 nm) to Te (574 nm) containing hybrids. The emission was assigned to a combination of LMCT $[(E^{2-}) \rightarrow Ag_4]$ excited state and a metal-centered (d-s/d-p) Ag(I) state.[129,130]

Wang et al. reported a luminescent Ag-S nanocluster $[Ag_{62}S_{13}(SBu^t)_{32}](BF_4)_4$,[85] synthesized by heating a mixture of $AgBF_4$, H_2NNH_2, and $AgSBu^t$. Its structure was solved by single crystal X-ray diffraction analysis, and the results show that it consists of tetracationic spherical clusters containing 62 silver (I) centers with four BF_4^- serving as counter ions (Fig. 5a). The inorganic core can be depicted as a core-shell configuration with a $[Ag_{14}S_{13}]$ core (Fig. 5b) and a $Ag_{48}(SBu^t)_{32}$ shell (Fig. 5c). This hybrid structure is stable in the air and is soluble in several organic solvents. Photophysical study shows that this compound emits bright red light in the solid state under irradiation of UV or visible light at room temperature with emission band peaked at 621 nm (Fig. 5d). It also luminesces in solution, with an emission peak at 613 nm (Fig. 5e). The quantum yield was measured to be 1.4% with rhodamine B in absolute ethanol as the standard.

Several other luminescent silver (I) chalcogenide clusters were reported after that. Zheng et al. reported an anionic heptadecanuclear silver (I) cluster $(NH_4)_{17}[(\mu_6\text{-}S)@Ag_{17}(mba)_{16}]\cdot 22H_2O$; H_2mba = 2-mercaptobenzoic acid) with orange-red emission at room temperature.[86] Single crystal analysis shows that the structure is a ball-shaped skeleton comprised of 17 Ag ions, 16 mba^{2-} ligands, and 1 $\mu_6\text{-}S^{2-}$ ion sitting inside the silver cluster (Fig. 6a). The orange-red emission peaks at 577 nm under 365 nm excitation (Fig. 6b). Its emission origin can be assigned to a ligand-to-metal charge-transfer excited state, mixed with a cluster-based metal-centered (4d-5 s/5p) excited state perturbed by Ag···Ag interactions. In addition, Su et al. reported a sandwich-like $Ag_{20}S_{10}$ luminescent nanocluster $[Ag_{20}(S^tBu)_{10}(CF_3COO)_2]^{8+}$ in 2013 (Fig. 6c).[131] It shows intense blue emission in methanol solution with an emission band maximum at 410 nm (Fig. 6d). Later in 2014, Zhu et al. reported $[Ag_{62}S_{12}(SBu^t)_{32}]^{2+}$ (NC-I) and $[Ag_{62}S_{13}(SBu^t)_{32}]^{4+}$ (NC-II).[87] Their results show that the PL of NC-I was quenched compared to that of NC-II. Such quenching of photoluminescence is caused by the free valence electrons in the NC-1, which dramatically change the ligand to metal charge transfer (S 3p to Ag 5 s).

In 2017, a study by Zang et al. demonstrated that the stability of the silver (I) chalcogenide clusters could be significantly improved by incorporating them into extended frameworks.[132] A silver (I) chalcogenolate inorganic-organic

DOI: 10.1016/j.enchem.2019.100008
EnergyChem 1, 100008 (2019)

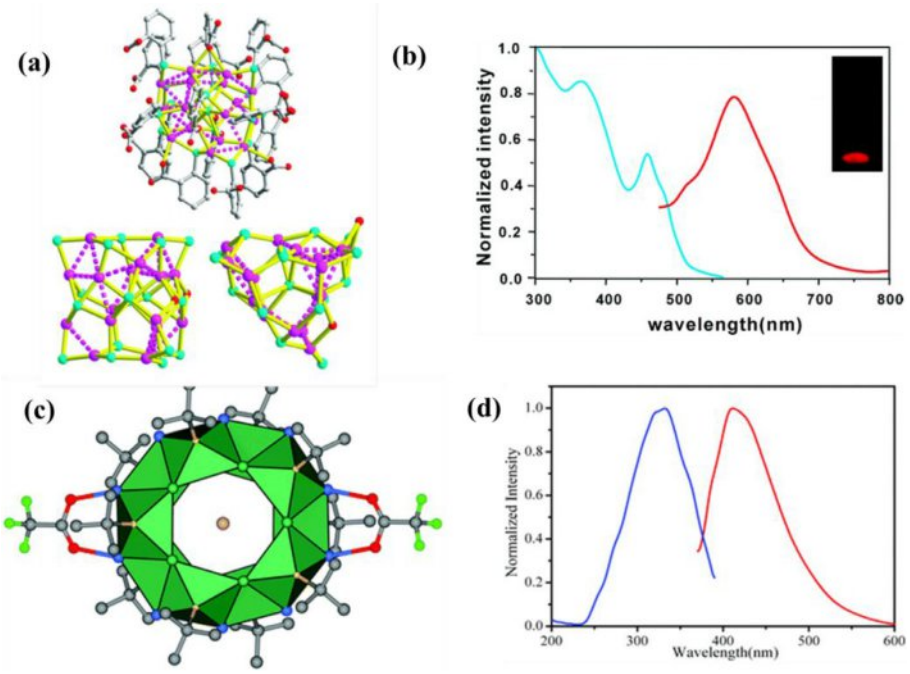

Fig. 6. (a) Representation of the molecule structure of the $[(\mu_6\text{-S})@Ag_{17}(mba)_{16}]^{17-}$ cluster. Color legend: purple, Ag; cyan, S; red, O; gray, C. (b) Excitation (cyan trace) and emission (red trace) spectra of $[(\mu_6\text{-S})@Ag_{17}(mba)_{16}]^{17-}$ in the solid state. Inset: photograph of the emission from $[(\mu_6\text{-S})@Ag_{17}(mba)_{16}]^{17-}$ in the solid state at room temperature under 365 nm excitation. (c) Polyhedral/ball-and-stick representation of $[Ag_{20}(S^tBu)_{10}(CF_3COO)_2]^{8+}$. Color code: Ag, sea green and light blue; C, gray-50%; S, gold; O, red; F, bright green; Cl, lavender. (d) Excitation (blue trace) and emission (red trace) spectra of $[Ag_{20}(S^tBu)_{10}(CF_3COO)_2]^{8+}$ in CH_3OH solution. Reproduced with permission from.[86] Copyright 2011, American Chemical Society. (For interpretation of the references to color in this figure legend, the reader is referred to the web version of this article.).

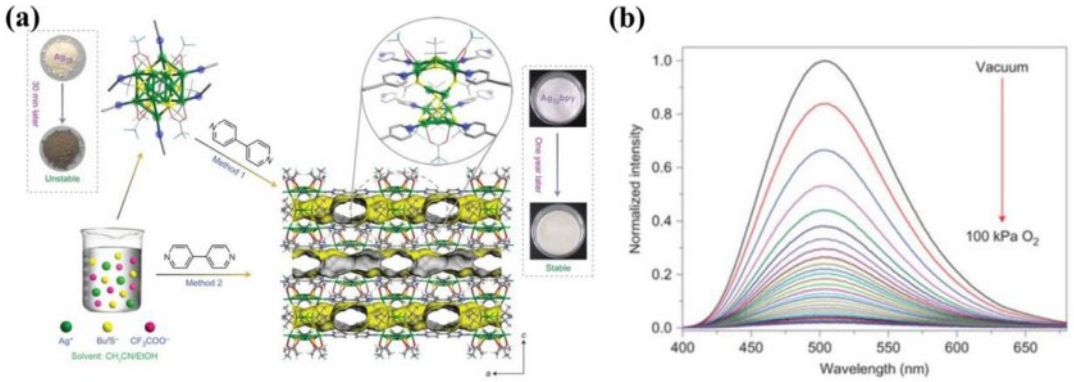

Fig. 7. (a) Schematic representation of the ligand-exchange strategy used to obtain $Ag_{12}bpy$ crystals. (b) Emission spectra at different O_2 pressures (excited at 365 nm) from vacuum to 100 kPa O_2. Reprinted with permission from.[132] Copyright 2017, Nature Publishing Group.

framework $[(Ag_{12}(StBu)_8(CF_3COO)_4(bpy)_4)]_n$ ($Ag_{12}bpy$) was synthesized and structurally characterized. In the novel structure, bridging ligands were used to inter-connect silver (I) chalcogenolate clusters into a 3D framework (Fig. 7a). It exhibits significantly enhanced stability compared to previously reported clusters. Ag_{12} emits weak red emission ($\lambda_{em} = 620$ nm, QY = 0.2%) in air, which quickly disappeared due to deterioration, while the emission of $Ag_{12}bpy$ could not be observed in the air due to quenching induced by oxygen (Fig. 7b). The $Ag_{12}bpy$ crystals emit bright green light ($\lambda_{em} = 507$ nm) in vacuum with a PLQY up to 12.1%. This emission peak is independent of temperature and excitation wavelength, with an enhanced QY when compared to the original structure. The photoluminescence of $Ag_{12}bpy$ originates from a metal-to-ligand excited state with ligand-to-ligand (S, O to bpy) charge transfer character. In addition, the high QY of $Ag_{12}bpy$ should be attributed to the ordered arrangement of chromophores and the structural rigidity of the coordination framework, which effectively restrict non-radiative decay.

■ LUMINESCENT MATERIALS BASED ON IIB-VIA SEMICONDUCTORS

IIB-VIA (IIB: Zn, Cd; VIA: S, Se, Te) binary semiconductor based hybrids represent another unique family of crystalline nanostructured inorganic-organic hybrid materials, first discovered by us. These materials are typically made of 1D or 2D inorganic nanomodules (e.g. ZnS, CdSe) and N-containing

DOI: 10.1016/j.enchem.2019.100008
EnergyChem 1, 100008 (2019)

organic alkylamines (N-ligands, e.g. butylamine, ethylenediamine) via coordinate bonds between group IIB metals and N-ligands.[8,13,63,64,133–135] By varying the composition and dimensionality of the inorganic component and by using different organic amine molecules, hybrid semiconductors of different dimensionalities (from 1D to 3D) have been synthesized and structurally characterized. Their optical properties have been investigated, and most of them exhibit strong structure-induced quantum confinement effect (QCE) as a result of the modular nature of perfectly ordered and alternating inorganic and organic motifs at the nanometer or subnanometer scale.[64] The insulating organic amine molecules serve as passivating agents and prevent interactions between the neighboring inorganic modules. Since the organic molecules bond to the inorganic nanostructural motifs in a periodically ordered fashion, the QCE takes place within a macroscopic crystalline particle, giving rise to a very large increase in their band gaps.[64,133] These attractive features make them promising candidates for various optoelectronic applications. Interestingly, some members from this family exhibit direct broadband white light emission under UV light excitation at room temperature, and they can be used as single-phase white-light-emitting phosphors.[22,23,88,90] This family of hybrid structures can be broadly divided into two subgroups: MQ (M = Zn, Cd; Q = S, Se, Te) based hybrids and substituted MQ (M = Zn, Cd; Q = S, Se, Te) hybrids. These two subgroups are discussed in the following two subsections.

MQ (M = Zn, Cd; q = S, Se, Te) based hybrids

We reported the first group of MQ (M = Zn, Cd; Q = S, Se, Te) based inorganic-organic hybrid structures in 2000.[63] They are $[\alpha\text{-ZnTe(en)}_{1/2}]$ (I), $[\beta\text{-ZnTe(en)}_{1/2}]$ (II), and $[\text{ZnTe(pda)}_{1/2}]$(III) (en = ethylenediamine, pda = 1,3-propanediamine). The inorganic module is a ZnTe single atomic layer formed by alternating, three-coordinated Zn and Te, and such a layer may also be regarded as a "slice" from the zinc blende or wurtzite structure of ZnTe. The layers are further linked together by organic diamine molecules to form 3D networks. Blue shifts with respect to their binary semiconductor parent ZnTe were observed in their band gaps as a result of QCE. Later in 2007, we developed a series of related hybrid structures built of M_2Q_2 double atomic layers, with the formula $[(M_2Q_2)(L)]$ (M = Zn, Cd; Q = S, Se; and L = ethylamine, n-propylamine, n-butylamine, n-amylamine, n-hexylamine) (Fig. 8a and b).[133] The main difference between these double-layer and the above-mentioned single-layer structures is the thickness of the inorganic layer, which are roughly doubled in $[(M_2Q_2)(L)]$. The degree of their band gap increase is less than that of the single-layer 2D-$[(MQ)(L)]$ systems due to the smaller extent of QCE (Fig. 8c).

Early studies were not focused on the luminescence of these hybrid structures. In 2008, we discovered that the double-layered 2D-$[Cd_2S_2(ba)]$ structure emits direct white light with an IQY of ~ 4–5%, which was the first semiconductor bulk material generating white light (Fig. 9a and b).[88] Since these materials were processed in bulk form, there were no issues related to particle size, as in the case for nanocrystals.[136] The broad emission covers the entire visible spectrum, and the band edge emission is significantly reduced, leading to a well-balanced white-light spectrum (Fig. 9c). A prototype WLED bulb was assembled by coating this material onto a UV LED chip (Fig. 9d). Mn^{2+} was used to enhance the luminescence efficiency of these materials and to tune the white color of the bulbs. The highest PL intensity was achieved at a dopant level of 0.5 mol%. The enhancement of the luminescence is due to the efficient energy transfer from

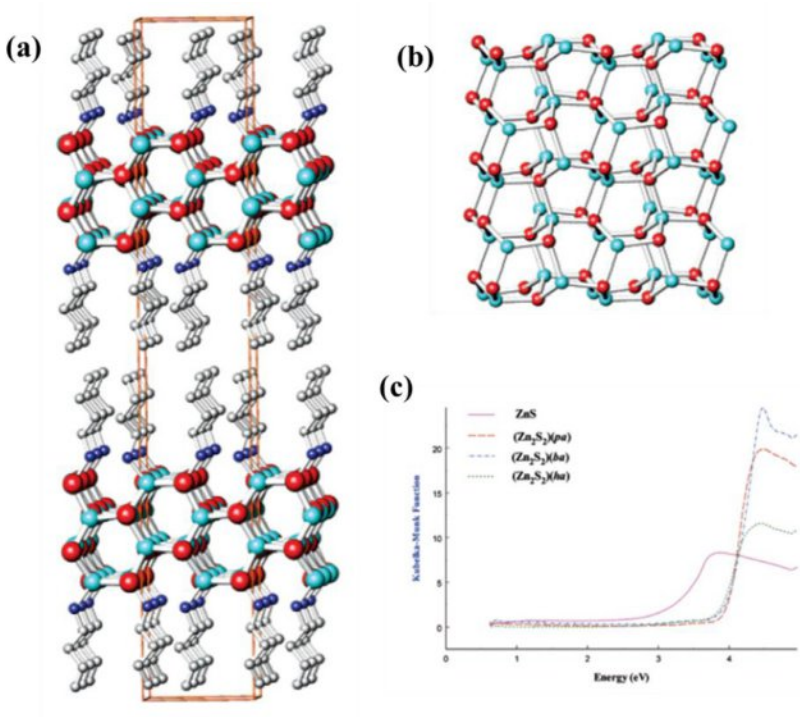

Fig. 8. (a) Crystal structure of double-layer 2D-$[(Zn_2Se_2)(ba)]$ viewed along the b-axis. The light blue balls are Zn; red balls, Se; blue balls, N; gray balls, C. (b) Double atomic layer of $[Zn_2Se_2]$ of shown along the ab plane (c) Optical absorption spectra of ZnS and $Zn_2S_2(L)$. Reproduced with permission from.[133] Copyright 2007, American Chemical Society.

DOI: 10.1016/j.enchem.2019.100008
EnergyChem 1, 100008 (2019)

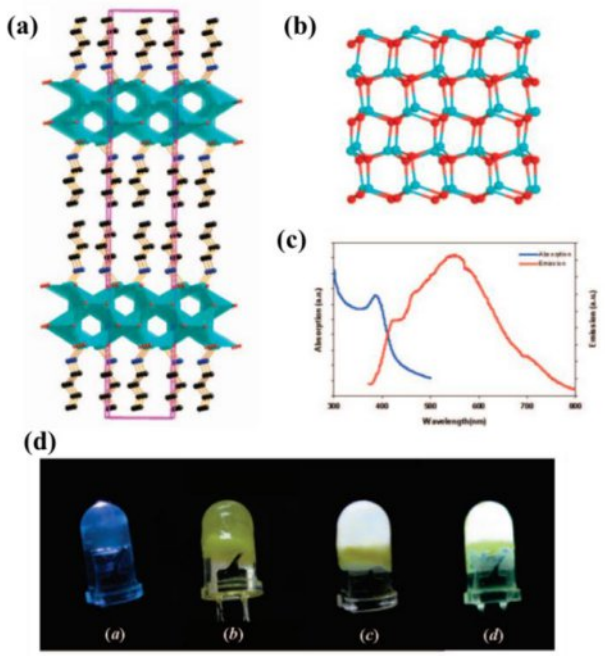

Fig. 9. (a) Side view of the double-layer 2D-$[Cd_2S_2(ba)]$ based crystal structure. Cd: teal; S: red; N: blue; C: black spheres. (b) The double layer of CdS in 2D-$[Cd_2S_2(ba)]$. (c) Room temperature absorption and emission spectra of 2D-$[Cd_2S_2(ba)]$ ($\lambda_{ex} = 360$ nm). Reproduced with permission from.[88] Copyright 2007, American Chemical Society.

the CdS host to the Mn^{2+} ions.[137] Higher Mn^{2+} concentrations result in a decrease in the PL intensity, due to appreciable Mn^{2+}-Mn^{2+} interactions resulting from the close proximity of these ions (Fig. 9d).

Continued effort led to five new two-dimensional double-layered structures reported in 2014. They were synthesized employing monoamines with different aromatic or heterocyclic aliphatic rings: $Zn_2S_2(bza)$, $Zn_2S_2(mbza)$, $Zn_2S_2(fbza)$, $Zn_2S_2(pca)$, and $Zn_2S_2(thfa)$ (bza = benzylamine, mbza = 4-methoxybenzylamine, fbza = 4-flurobenzylamine, pca = 3-picolylamine, and thfa = tetrahydrofurfurylamine).[89] Their structures were identified by powder X-ray diffraction analysis. The photoluminescence emission spectra of these compounds were recorded, and the results show that all compounds emits in the UV or blue light region (Fig. 10).

Mn^{2+} doped $(ZnS)_2$·octylamine was reported by Wei et al. in 2015, which was the first study making use of luminescence from these materials for sensing.[138] The 5% Mn^{2+}-doped hybrid compound exhibited an intense orange luminescence peaking at 597 nm under 300 nm excitation (Fig. 11). Thin films were fabricated by the drop-casting method. It was used as sensor for detecting several environmental contaminant species: n–butyl xanthate (BX), crystal violet (CV), and reaction black 5 (RB5).

substituted MQ (M = Zn, Cd; q = S, Se, Te) hybrids

Due to the potential applications in general lighting applications, many efforts have been directed towards enhancing the emission efficiency of MQ based hybrids. However, the limited luminescence efficiency and white-light quality of unsubstituted MQ hybrids remained a problem. Results show that ZnS based $[Zn_2S_2(L)]$ compounds exhibit higher quantum efficiencies compared the CdQ (Q = S, Se) based hybrid structures, and

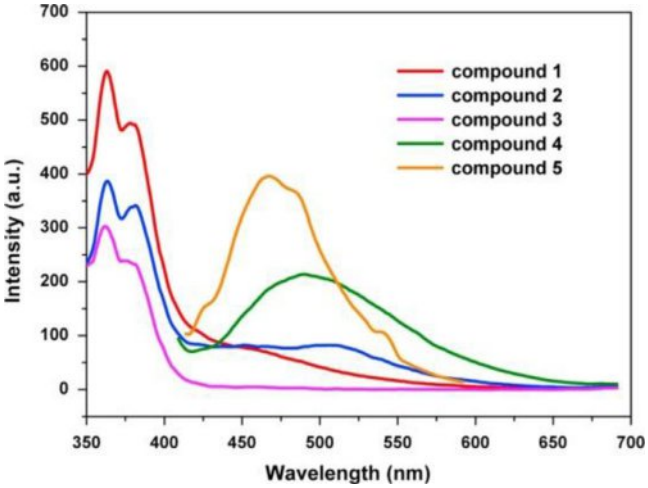

Fig. 10. Emission spectra for compounds $Zn_2S_2(bza)$ (red), $Zn_2S_2(mbza)$ (blue), $Zn_2S_2(fbza)$ (pink), $Zn_2S_2(pca)$ (green) and $Zn_2S_2(thfa)$ (orange) recorded at room temperature. Reproduced with permission from.[89] Copyright 2014, Elsevier B. V.

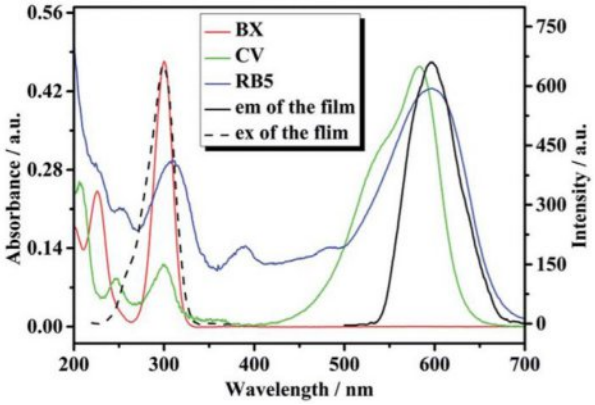

Fig. 11. The photoluminescence excitation (dash black) and emission (solid black) spectra of the Mn^{2+} doped $(ZnS)_2$·octylamine hybrid film and the optical absorption spectra of the three selected environmental contaminants BX (red curve, 31.86 μM), CV (green curve, 7.35 μM) and RB5 (blue curve, 10.08 μM). Reproduced from [138] with the permission of the Royal Society of Chemistry.

their emissions are typically in the blue light region. A strategy using metal and chalcogenides substitution in $[M_2Q_2(L)]$ has been developed to optimize the efficiency and quality of the light emissions. As a concept-proving case for chalcogenide substitution, a substituted double layered semiconductor 2D-$[Cd_2Se_2(ba)$:Te] was reported in 2010.[90] Experimental results showed the band gap and photoluminescence properties can be systematically tuned by changing the composition of Te in $Cd_2Se_2(ba)$. An optimal condition was found at 25 mol% of Te, corresponding to the CIE coordinates of (0.29, 0.35), which is closest to the white point (0.33, 0.33) (Fig. 12) among similar compounds. The broadening of emission spectrum was attributed to the fact that the recombination of charge carriers trapped by Te states leads to emission in the long-wavelength region. The IQY was measured to be 4–5%.

Significant quantum yield enhancement in these materials was achieved by metal substitution along with Mn ion doping. In 2012, we reported white-light emitting double-layered

DOI: 10.1016/j.enchem.2019.100008
EnergyChem 1, 100008 (2019)

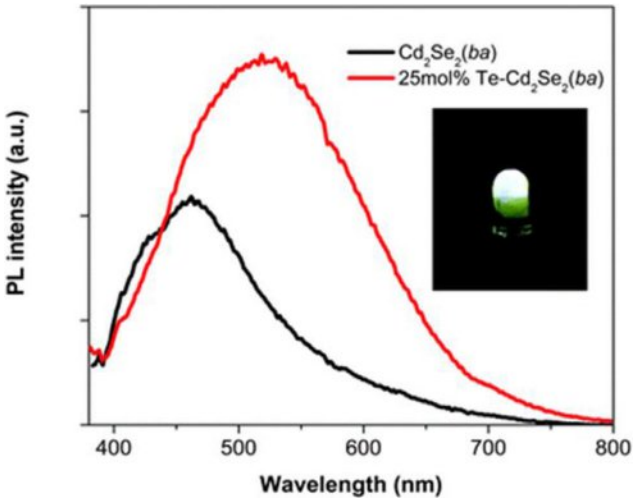

Fig. 12. Room temperature photoluminescence of the double-layer 2D-$[Cd_2Se_2(ba)]$ (black, $\lambda_{ex} = 360$ nm) and 2D-$[Cd_2Se_2(ba)]$:25 mol% Te structure (red, $\lambda_{ex} = 360$ nm) (inset: demonstration of white light emission from a thin layer of 2D-$[Cd_2Se_2(ba)]$:25mol% Te coated on a commercial UV-LED). Reproduced with permission from.[90] Copyright 2010, American Chemical Society.

substituted MQ hybrids which show significantly enhanced quantum efficiency compared to unsubstituted analogues.[23] Various types of inorganic modules are plotted (Fig. 13a–e). 2D-$[Zn_2S_2(ha)]$ emits strongly in the green-blue region with its emission peak centered at approximately 420 nm. In order to enhance the IQY and to achieve well-balanced white light, substituted hybrid structures were designed, such as $[Zn_{1.7}Cd_{0.3}S_2(ha)]$. Its emission covers the entire visible light region, with an IQY of 17–18% using both relative/comparative and absolute methods on solution and solid samples. The IQY was further improved by doping Mn ion in low concentrations. The highest IQY was achieved for $[Zn_{1.7}Cd_{0.3}S_2(oa)]$ (oa = octylamine) with 0.08 mol% Mn doping (Fig. 13f), which yielded a IQY of 31–37%, an 8-fold increase compared to previously reported unsubstituted 2D-$[Cd_2S_2(ba)]$. These materials are highly solution processable and can be easily coated onto LED chips to make LED devices (Fig. 13g).

A follow-up study was carried out to investigate substitution effect of both metal and chalcogen ions.[22] Ternary $Zn_{2-2x}Cd_{2x}S_2(ha)$ hybrid compounds were prepared that exhibit two PL emission peaks, one of which was attributed to band gap emission, and the other resulting from Cd doping and surface sites (Fig. 14). The relative emission intensity of the two bands could be tuned by adjusting the concentration of Cd. In addition, the quaternary $Zn_{2-2x}Cd_{2x}S_{2-2y}Se_{2y}(ha)$ compounds were prepared, showing that the substitution of Se may also tune the emission. Detailed analysis revealed that the PL emission properties of the ternary and quaternary hybrid semiconductors originate from their unique double-layered nanostructures that combine strong QCE and a large number of surface sites. This work provides a thorough and in-depth luminescence study of the substituted MQ (M = Zn, Cd; Q = S, Se, Te) hybrids.

In addition to chalcogenide substitution, Mn substitution for 1D $ZnSe(L)_{0.5}$ hybrid nanobelts was reported by Yu et al.[91] 1D $[Zn_{1-x}Mn_xSe](DETA)_{0.5}$ (DETA = diethylenetriamine, $x = 0 - 0.3$) inorganic-organic hybrid nanobelts were synthesized by a solvothermal reaction. Their structures are plotted in Fig. 15a. The room-temperature PL spectra

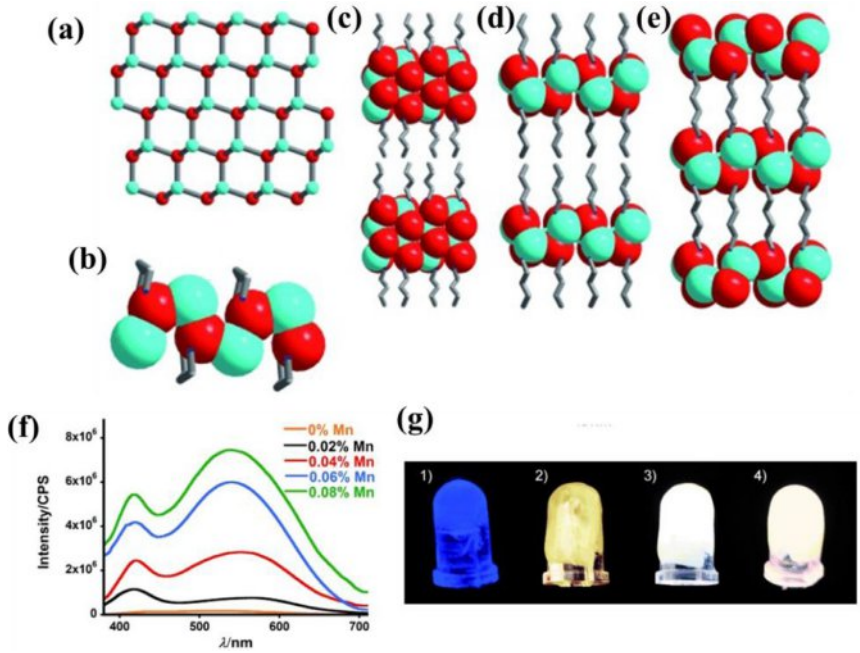

Fig. 13. (a) Single layer of honeycomb-like net of ZnS in the $[M_nQ_n(L)_x]$ type hybrid structure (M = Zn, Cd; Q = S, Se, Te; L = mono- or diamine); (b) Single-chain 1D-[MQ(L)] structure; (c) double-layer 2D-$[M_2Q_2(L)]$ structure; (d) single-layer 2D-[MQ(L)] structure; (e) Single-layer 3D-$[MQ(L)_{0.5}]$ structure. Blue M, red Q_n in (b)–(d) the stick model corresponds to L; (f) White-light emission spectra of $[Zn_{1.7}Cd_{0.3}S_2(ha)]$:Mn] at various Mn concentrations ($\lambda_{ex} = 365$ nm); (g) white-light LED aggregates made by coating a thin layer of sample on the surface of a 5 mm reference UV LED. Reproduced with permission from.[23] Copyright 2012, Wiley-VCH Verlag GmbH & Co. KGaA.

DOI: 10.1016/j.enchem.2019.100008
EnergyChem 1, 100008 (2019)

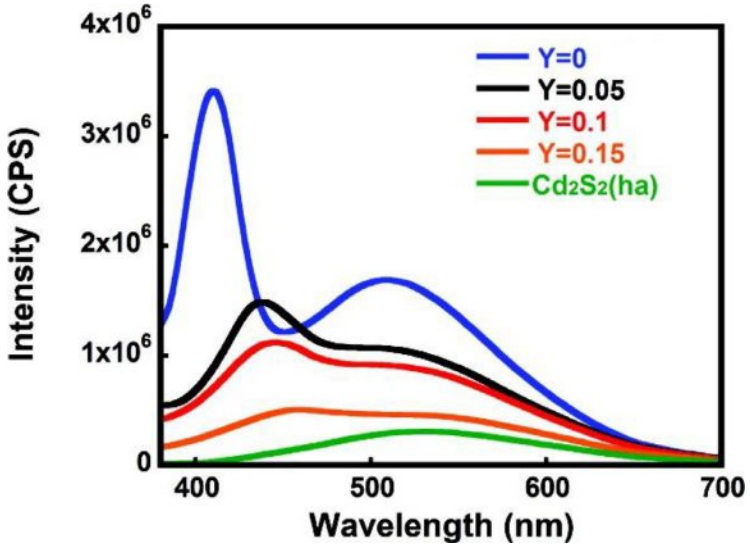

Fig. 14. Room temperature PL emission spectra of the $Zn_{1.6}Cd_{0.4}S_{2-2y}Se_{2y}$(ha) ($y = 0$, 0.05, 0.10, and 0.15) compounds, along with that of Cd_2S_2(ha) ($\lambda_{ex} = 360$ nm). Reproduced from.[22] Copyright 2012, American Chemical Society.

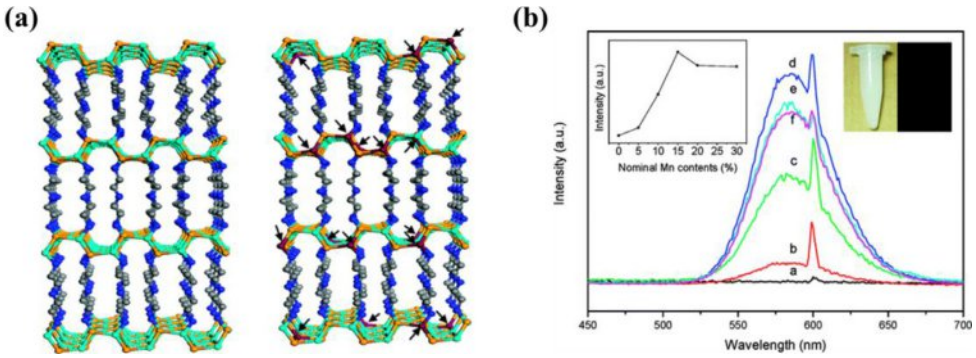

Fig. 15. (a) Schematic illustrations of the crystal structures of $[ZnSe](DETA)_{0.5}$ and $[Zn_{1-x}Mn_xSe](DETA)_{0.5}$ nanobelts. The light-blue cylinders are Zn, the saffron cylinders represent Se, and the blue and gray cylinders are N and C, respectively. The introduced Mn are shown with brown cylinders and marked with arrows. (b) Room-temperature PL spectra of synthesized $[ZnSe](DETA)_{0.5}$ and $[Zn_{1-x}Mn_xSe](DETA)_{0.5}$ nanobelts with different Mn contents. The excitation wavelength is 300 nm. Curves from (a) to (f) correspond to the nominal Mn content $x = 0$, 0.05, 0.10, 0.15, 0.20, and 0.30, respectively. Inset (left) shows the pattern of the PL integrated intensity versus Mn contents, and inset (right) shows the color of the sample before and after illumination at $\lambda = 365$ nm. Reproduced from.[91] Copyright 2009, American Chemical Society. (For interpretation of the references to color in this figure legend, the reader is referred to the web version of this article.).

show a distinct emission band centered at 585 nm for all the products, originating from the Mn^{2+} internal $d-d$ ($^4T_1 \rightarrow {}^6A_1$) transition. The emission intensities and energies vary based on the Mn substitution amount (Fig. 15b), and the maximum intensity is observed when Mn content is 15%. These compounds also exhibit temperature and pressure dependent photoluminescence.

LUMINESCENT MATERIALS BASED ON IB-VIIA SEMICONDUCTORS

Inorganic-organic hybrid materials based on IB-VIIA binary compound have been studied for decades because of their unique photophysical and photochemical properties originating from the d^{10} electronic configuration of the IB metal atoms, leading to a variety of applications for light emitting devices, sensing devices, solar cells, and artificial photosynthesis.[16,139–146] Though the luminescence of the parent IB-VIIA semiconductors is not very strong, it can be enhanced significantly when coordinated to organic ligands.[147] Such hybrid materials are generally constructed of inorganic modules interacting with organic ligands through either coordinate/covalent bonds or ionic bonds. A variety of inorganic modules have been found, from discrete inorganic units (0D) to extended infinite chains (1D) or layers (2D). These inorganic motifs combine with different types of organic ligands, mostly N-containing species, either aliphatic or aromatic, to form molecular clusters, chains, sheets/layers, and extended networks.[15,65] They can also be classified into neutral, ionic, and AIO-type structures. Their luminescence mechanisms include metal-to-ligand-charge-transfer (MLCT), halide-to-ligand-charge-transfer (XLCT), metal-center change transfer (CC), or some combination thereof.[20,148] Their development as lighting materials started in the 2010s, and the general design strategies are based on two central hypotheses: first, that through rational inorganic module selection and ligand functionalization, the optical properties and emission efficiencies of the hybrids could

DOI: 10.1016/j.enchem.2019.100008
EnergyChem 1, 100008 (2019)

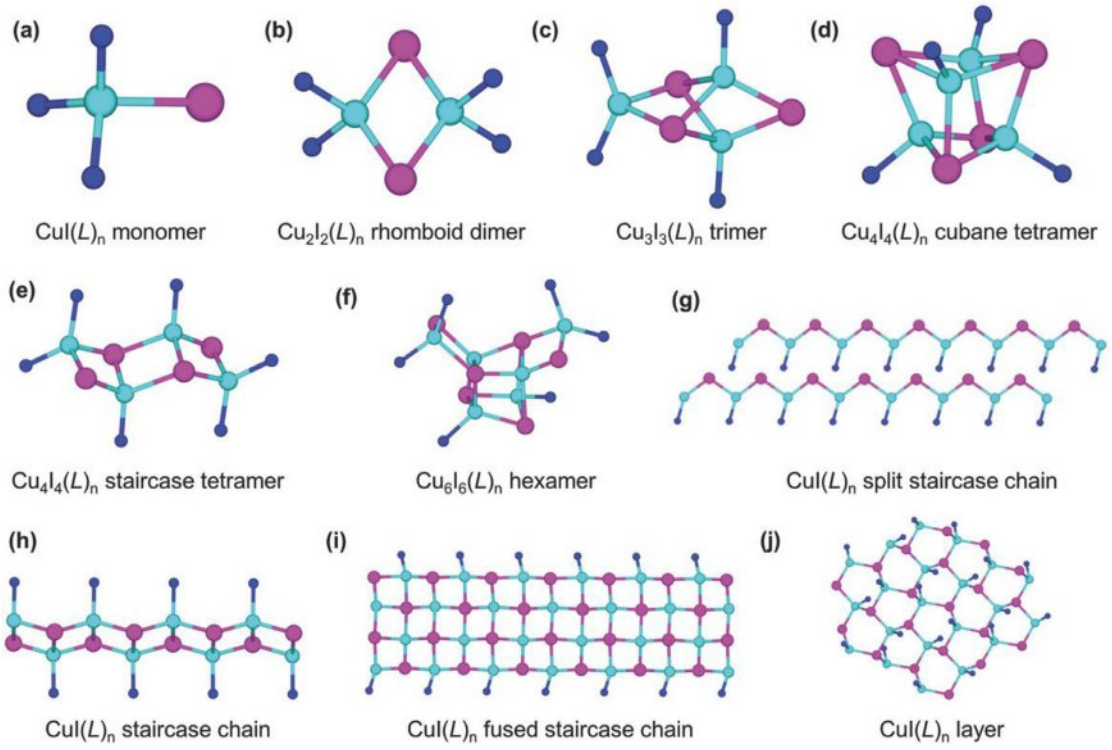

Fig. 16. (a–j) Examples of common CuI inorganic motifs. Color scheme: Cu, cyan; I, purple; organic ligands, blue. Reproduced with permission from.[15] Copyright 2018, Wiley-VCH Verlag GmbH &Co. KGaA. (For interpretation of the references to color in this figure legend, the reader is referred to the web version of this article.).

be systematically tuned and optimized; and second, that the stability of the hybrids could be enhanced with proper structural design approaches.

Light-emitting materials based on Cu(I) halides

The investigation of copper halide hybrids started as early as the 1970s and has evolved with the introduction of X-ray diffraction crystallography. The most well-studied compound, 0D-$Cu_4I_4(py)_4$, was first identified as cubane tetramer in 1976 by White et al.[149] After then, a large number of structures with different composition and structural types have been synthesized and structurally identified (Fig. 16).[15,65]

In 2014, the Li group began developing them as phosphor materials for general lighting applications.[92] A series of neutral 1D-CuI(L) staircase chain based structures were synthesized. Density Function Theory (DFT) calculation results show that the valence band maximum (VBM) of these materials is composed primarily of the inorganic module, while the conduction band minimum (CBM) is generally made up of the LUMO orbital of the organic ligands. Their PL emissions are also in trend with their band gap values, and the emission wavelengths of obtained structures range from violet to red (Fig. 17a). These results confirm that, in general, the emission wavelengths of these hybrid compounds can be tuned systematically by tailoring their band gaps, which can in turn be achieved by selecting organic ligands with the desired electronic properties. Their IQYs range from 10% to 37% under 365 nm excitation. White light could be achieved by doping pyrimidine into 1D-CuI(py), which afforded 1D-$CuI(py)_{1-x}(pm)_x$ (Fig. 17b).

Further exploration led to a family of highly luminescent Cu_2I_2 rhomboid dimer based hybrid structures that display tunable emissions and high IQYs that are ideal as lighting emitting materials.[93] DFT calculations confirm that they display similar band structure patterns as staircase chain based structures. The luminescence mechanism of these structures is generally MLCT and XLCT.[150] These materials were prepared using a precursor approach. The starting material is a Cu_2I_2 precursor, and the Cu_2I_2 dimer motif is maintained in the final products. The IQYs of most of these structures exceed 70%, and can be as high as 92%. Blue-excitable yellow-emitting phosphors were obtained, such as 2D-$Cu_2I_2(4,4'\text{-dps})_2$. White light was achieved by blending a blue phosphor with a yellow phosphor; for example, 1D-$Cu_2I_2(tpp)_2(bpp)$ can be combined with 1D-$Cu_2I_2(tpp)_2(4,4'\text{-bpy})$ (Fig. 18). Relevant work on the strong luminescence and optical tunability of Cu_2I_2 dimer based hybrid structures has also been reported and reviewed by Tusge et al.[150,151]

The Cu_4I_4 cubane tetramer based structures are the most well-known group of copper complexes. A series of stable Cu_4I_4 cubane tetramer based hybrids with strong luminescence and high IQYs were synthesized using a precursor approach.[94] PL emission spectra show that all compounds emit bright yellow-orange color (Fig. 19a). The strong luminescence originates from the strong Cu-Cu interactions resulting from the shorter distance of Cu-Cu atoms (less than 2.80 Å) in the cubane core.[20,148] Their mechanochromic and thermochromic luminescence were thoroughly investigated by Perruchas et.al.[152,153] The reversible thermochromic phenomenon was attributed to distortions in the crystal packing leading to modifications of the intermolecular interactions and thus of the Cu_4I_4 cluster core geometry. The IQYs of these compounds were measured at room temperature, ranging from 56% to 96% under UV excitation. Long PL lifetimes of these structures indicate that the observed emission can be attributed to phosphorescence. Stability measurements show that members of this family are very robust (Fig. 19b), with some

DOI: 10.1016/j.enchem.2019.100008
EnergyChem 1, 100008 (2019)

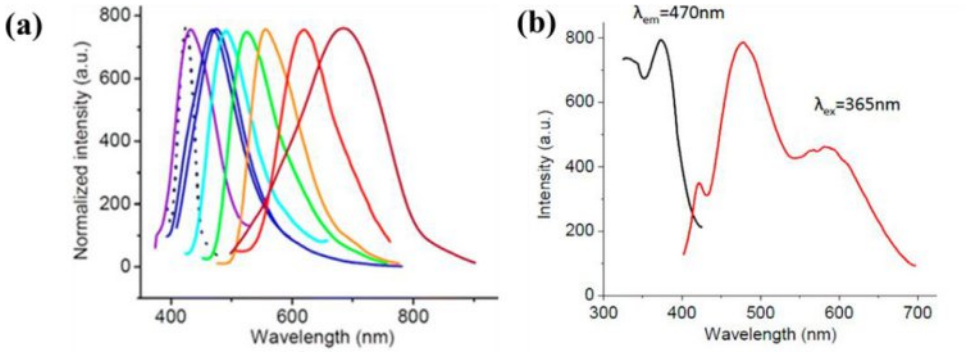

Fig. 17. (a) Emission spectra of CuI semiconductor and selected 1D-CuI(L) hybrid structures (λ_{ex} 365 nm). (b) Excitation spectrum (black, λ_{em} 470 nm) and PL emission spectrum (red, λ_{ex} 365 nm) of 1D-CuI(py)$_{1-x}$(pm)$_x$. Reproduced from.[92] Copyright 2014, American Chemical Society.

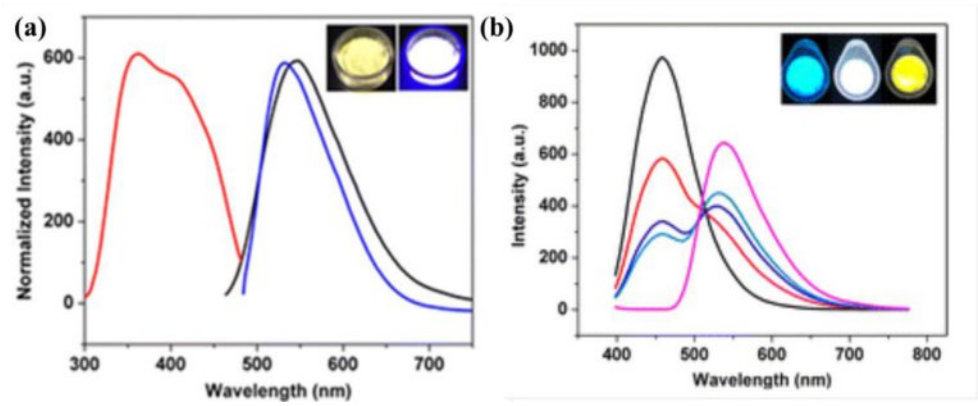

Fig. 18. (a) Excitation (red, $\lambda_{em} = 543$ nm) and emission (black, $\lambda_{ex} = 455$ nm) spectra of 2D-Cu_2I_2(4,4′-dps)$_2$ compared with emission spectrum of YAG:Ce^{3+} (blue, $\lambda_{ex} = 455$ nm). Inset: powder sample of 2D-Cu_2I_2((4,4′-dps)$_2$ under natural light (left) and blue light (right, 455 nm). (b) Luminescence spectra of the two-component phosphors with the following weight percentage of 1D-Cu_2I_2(tpp)$_2$(4,4′-bpy): 0 wt% (black), 5 wt% (red), 15 wt% (blue), 25 wt% (green), 100 wt% (pink). Reproduced from.[93] Copyright 2015, American Chemical Society.

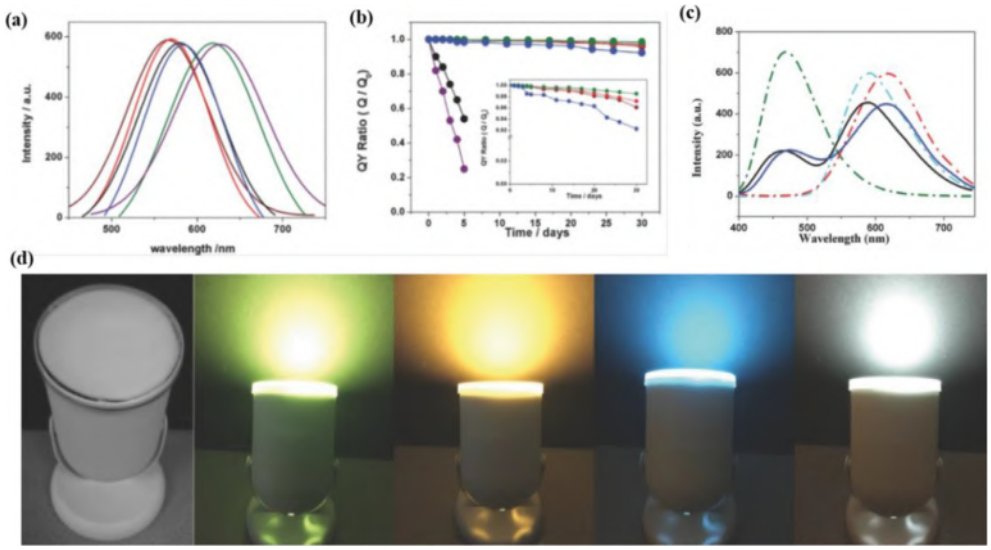

Fig. 19. (a) Photoluminescence spectra ($\lambda_{ex} = 360$ nm) of selected compounds. (b) Plot of QY ratios (Q_0 and Q are QY values measured before and after heating at each selected temperature for 24 h in air) (c) Luminescence spectra of white light blends of different composition. (d) A prototype LED lamp at "off" (left) and "on" stages coated with the phosphors. Reproduced with permission from.[94] Copyright 2017, Wiley-VCH Verlag GmbH &Co. KGaA.

DOI: 10.1016/j.enchem.2019.100008
EnergyChem 1, 100008 (2019)

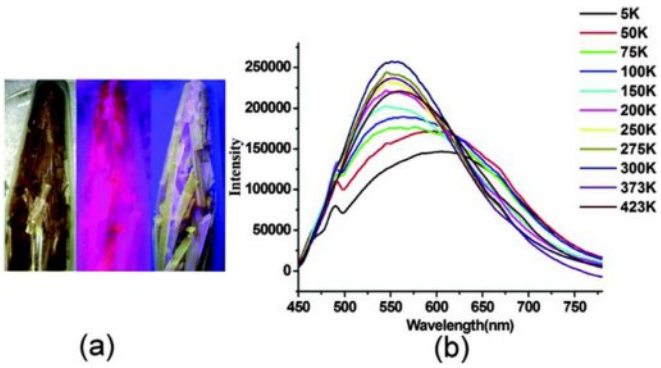

Fig. 20. (a) Photos of crystals $(Bu_2DABCO)_{1.5}Cu_3I_6$ without UV irradiation (left), just taken out of liquid nitrogen (middle) and room temperature (right) under 365 nm UV lamp irradiation. (b) Temperature-dependent luminescence spectra from 5–423 K in the solid state. Reproduced from [95] with the permission of the Royal Society of Chemistry.

structures stable up to 350°C. White emitting phosphor blends were prepared by combining a commercial blue phosphor BAM ($BaMgAl_{10}O_{17}:Eu^{2+}$) with a yellow hybrid phosphor (Fig. 19c). LED devices have been fabricated using a remote model in which the phosphor coating layer was not in direct contact with the excitation source (Fig. 19d).

Light-emitting materials based on $Cu_kX_l^{m-}$

CuX based hybrid materials in form of $Cu_kX_l^{m-}$ include pure ionic structures, in which there are no coordinate bonds between the inorganic component and the organic ligand, and AIO type structures, in which anionic inorganic components and cationic organic ligands are also connected by coordinate bond.[15] Select compounds of both types are discussed below.

An organic-ligand-free ionic copper iodide trinuclear cluster $(Bu_2DABCO)_{1.5}Cu_3I_6$ was reported in 2015.[95] This compound represents the first organic-ligand-free cuprous iodide trinuclear cluster showing thermochromic luminescence. At room temperature, this compound emits single-band yellow emission peaked at 548 nm (Fig. 20). The lifetime is 15.8 μs, and the quantum yield is 12% at room temperature. The reversible thermochromic luminescence from darkish red (77 K) to bright yellow (423 K) can be distinguished by the naked eye or recorded by a digital camera (Fig. 20). Luminescence solvatochromism was also found for this compound. Since ligand-free ionic compounds generally have very poor luminescence, the relatively high IQY of this compound is fundamentally interesting.

After that, Yu et al. reported another type of copper iodide based ionic structures. These are $Li(H_2O)(EtOH)_3[Cu_6I_7(tppa)_2]$ (1-Li), $Na(H_2O)(EtOH)_3[Cu_6I_7(tppa)_2]$ (1-Na), $NH_4(H_2O)(EtOH)_3[Cu_6I_7(tppa)_2]$ (1-NH_4), $K(H_2O)_2(MeOH)_2[Cu_6I_7(tppa)_2]\cdot MeCN$ (1-K), $[N(Et)_4][Cu_6I_7(tppa)_2]$ (1-TEA), and $[N(Pr)_4][Cu_6I_7(tppa)_2]$ (1-TPA) (tppa = *N*,N′,N″-tris(3-pyridinyl)phosphoric triamide), with similar 2D structures based on the identical $Cu_6I_7^-$ anionic clusters, but different counter-ions (Fig. 21a–e).[97] It was determined that the cations play important roles not only for the formation of the ionic structures, but also as a tool in tuning their optical properties. All compounds displayed strong and broad single-band emissions with similar profiles. Their luminescence can be tuned by exclusively changing the monovalent cations between the layers (Fig. 21f and g). Their IQYs range from 24.2–80.6%, and all show excellent photostability. White light phosphors are made by combining BAM: Eu^{2+} and a yellow hybrid phosphor.

In 2017, we designed a unique type of AIO structures which combine both ionic and coordinate bonds within a molecular cluster. Such a combination greatly enhances structural stability while maintaining the molecular identity of the cluster and its high luminescence.[96] The novel AIO structures are composed of various anionic $(Cu_mI_{m+n})^{n-}$ clusters and cationic N-ligands (Fig. 22a). They are strongly emissive, with IQYs greater than 60%, and as high as 92%. They also show significantly improved chemical, thermal and moisture stability, and excellent solution processability. The AIO structures can be divided into two subgroups. Structures in subgroup I are made of aliphatic ligands and structures in subgroup II are made of aromatic ligands. Their optical properties and luminescence mechanism is different. Sub-group II structures all have lower band gaps that could be excited by blue light, as they are all blue-excitable yellow emitting phosphors. The exceptional solution processability makes it possible to fabricate high quality lighting devices using these phosphor materials (Fig. 22b).

Light-emitting materials based on Ag(I) halides

The closed-shell d^{10} electronic configuration of Ag(I) can adopt 2-, 3-, 4-, and 5-coordinated geometries. The inorganic modules of silver-based hybrids can be clusters, chain or layers. Examples include the AgX monomeric unit, the rhomboid Ag_2X_2 dimer, Ag_4X_4 cubane tetramer, the hexagonal prism-shaped Ag_6X_6 cluster, the AgX split staircase chain, the AgX staircase chain, the Ag_2X_2 helical chain, and the wavelike Ag_4X_4 chain, similar as the inorganic modules of copper halide based hybrids (Fig. 16).[98,154-156] Extensive research has been focused on copper (I) based compounds, while Ag(I) and Au(I) based hybrid compounds have been relatively less investigated. Silver halide based inorganic-organic hybrid compounds have similar structure types and photophysical properties to copper halide based hybrid structures.[16,20]

A representative white-light emitting $[(Ag_4I_4)(bix)]_n$ [bix = 1, 4-bis (imidazole-1-ylmethyl)benzene] was reported by Hong et al. in 2012.[98] Its inorganic module forms wave-like silver iodide chains arranged in parallel with an ABAB…type periodicity (Fig. 23a). The infinite wave-like chains are further connected by the bridge ligands forming a two dimensional network. Because of the compound's two domains, its exhibits

DOI: 10.1016/j.enchem.2019.100008
EnergyChem 1, 100008 (2019)

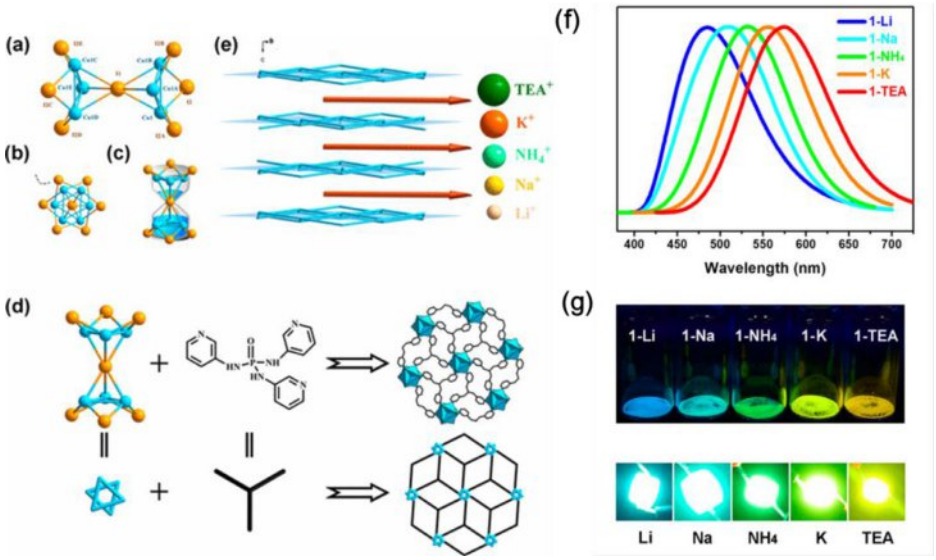

Fig. 21. Structure presentation of $Cu_6I_7^-$ cluster viewed from side (a) and top (b) as well as its sandglass shape (c), the (3,6)-connected kgd layer structure of the compounds (d), and schematic stacking diagram with different monovalent cations occupying the interlayer space (e). Symmetry code: A (1 – *x* + *y*, 2 – x, z), B (2 – y, 1 + *x* – y, z), C (2 – x, 2 – y, 1 – z), D (y, 1 – *x* + *y*, 1 – z), E (1 + *x* – y, x, 1 – z). (f) Photoluminescence of the five compounds (g) solid-state luminescence image under the 365 nm UV light and LED lamps displayed at working condition. Reproduced from.[97] Copyright 2017, American Chemical Society.

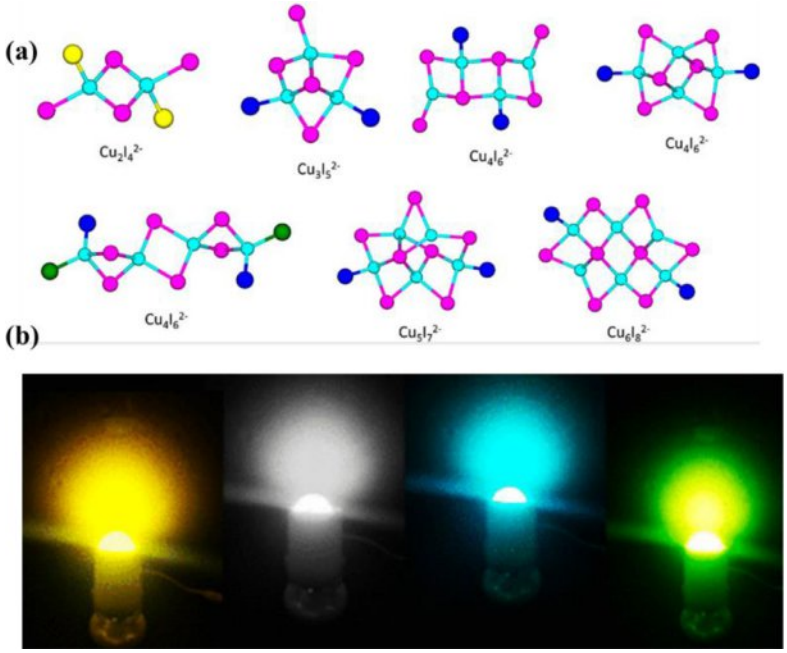

Fig. 22. Examples of inorganic anionic cluster motifs obtained for compounds. C and H atoms are omitted for clarity purpose. Color scheme: Cu, cyan; I, purple; N, blue; P, green; S, yellow. (b) Illuminating LED light bulbs (110 V, 2 W) coated by selective AIO phosphors. Reproduced from.[96] Copyright 2017, American Chemical Society. (For interpretation of the references to color in this figure legend, the reader is referred to the web version of this article.).

multiple emission processes, with two main emission peaks at 448 nm and 523 nm (Fig. 23b).

Excepting white light emitting compounds, the luminescence tunability of silver halide based hybrids has been demonstrated by Fang and Huang et al.[99] Two silver halide based hybrid structures with the flexible organic ligand 1,4-bis(2-methylimidazol-1-yl)butane (Bmib) $[Ag_2(Bmib)Br_2]_\infty$ (IAM16-1) and $[Ag_2(Bmib)I_2]_\infty$(IAM16-2) were reported with monochromic emissions (Fig. 24). The inorganic modules are AgX staircase chains, and both structures exhibit excitation-wavelength-dependent photoluminescence (EWDP). Calculations and experimental results show that the emissive excited states of those two structures are primarily attributed to cluster-centered halogen-metal to ligand (XMLCT) charge transfer.

DOI: 10.1016/j.enchem.2019.100008
EnergyChem 1, 100008 (2019)

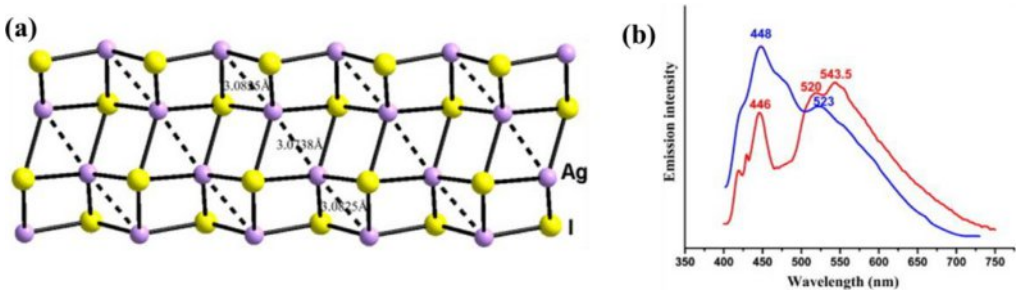

Fig. 23. A wave-like inorganic chain constructed by Ag and I atoms. (b) The emission spectra of $[(Ag_4I_4)(bix)]_n$ in solid state at room temperature (blue) and 10 K (red). Reproduced with permission from.[98] Copyright 2012, Wiley-VCH Verlag GmbH &Co. KGaA.

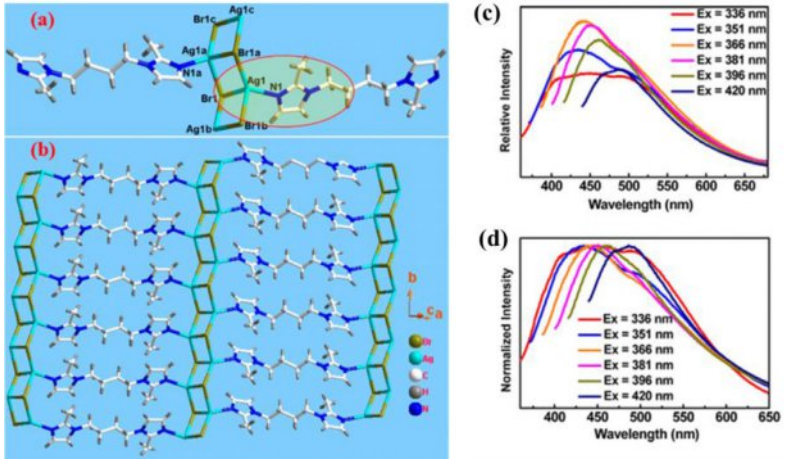

Fig. 24. (a) For IAM16-1: perspective view of the coordination environments of Ag and Bmib ligand, with the crystallographic minimum asymmetric unit highlighted; (b) perspective view of the 2-D infinite layer with the 1-D corrugated double stranded stair-like inorganic $[AgBr]_n$ chains. (c) and (d) Solid-state emission spectra IAM16-1 (c = measured, d = normalized) at various excitation wavelengths from 336 to 420 nm at ambient temperature. Reproduced from.[99] Copyright 2016, American Chemical Society.

■ LUMINESCENT MATERIALS BASED ON IVA-VIIA SEMICONDUCTORS

Inorganic-organic hybrid perovskites based on lead halide and tin halide semiconductors show interesting optical features, including small exciton binding energy, high charge carrier mobility, and strong light absorption, which has led to the development of highly efficient photovoltaic (PV) devices based on these materials.[157–159] The tunability of this structural family enables scientists to construct a variety of structures of different types and dimensionality.[9] By choosing appropriate organic and inorganic components, the connectivity of the metal halide polyhedra can be tuned to form 0D, 1D, 2D and 3D structures surrounded by the organic ligands. Apart from their use in PV devices, their excellent photoluminescence properties have also attracted tremendous attention.[160–162] In addition to having PLQEs approaching unity, these materials also possess unique properties such as high conductivity, long carrier lifetimes, optical tunability and ease of fabrication.[161,163] The emission color of the materials can be easily adjusted from blue to green or red by simply changing the halide anion from Cl^- to Br^-, or I^-.[101,105,162,164] The research of this field has grown rapidly, and relevant work has been summarized in a number of review papers.[44,160,162,165] Recently, some non-perovskite IVA-VIIA semiconductor based hybrid structures have also been reported with interesting luminescence properties.[107,166] Representative cases are briefly discussed here.

Light-emitting materials based on Pb(II) halides

Broadband white-light emission is the most important feature for several luminescent lower dimensional perovskites. In 2014, Karunadasa and co-workers reported two 2D lead bromide layered perovskite structures: (N-MPDA)$[PbBr_4]$ and (N-MEDA)$[PbBr_4]$ [N^1-methylethane-1,2-diammonium(N-MEDA) and N^1-methylpropane-1,3-diammonium (N-MPDA)].[100] The inorganic sheets of layered perovskites can be derived from the three-dimensional perovskite structure by slicing along specific crystallographic planes (Fig. 25a). The two materials were prepared by solution-state synthetic routes. Their broadband emissions span over the entire visible spectrum and can be tuned though halide substitution to adjust the white light from "cold" to "warm" (Fig. 25b). The PLQY of (N-MEDA)$[PbBr_4]$ was measured to be 0.5% and can be improved by chloride substitution, with (N-MEDA)$[PbBr_{2.8}Cl_{1.2}]$ exhibiting a PLQE of 1.5%. Further studies show that the emission is from the bulk material and not from surface sites. Later in 2014, the same group reported other layered hybrid perovskites with enhanced PLQY.[101] Structures with the general formula of (EDBE)$[PbX_4]$ (EDBE =, X = Cl, Br, I) were prepared and exhibit broadband white light emission in the solid state, and the Pb-Br perovskite has an improved PLQE of 9% (Fig. 25c and d). Mechanistic studies indicate that the emission has contributions from strong electron-phonon coupling in a

DOI: 10.1016/j.enchem.2019.100008
EnergyChem 1, 100008 (2019)

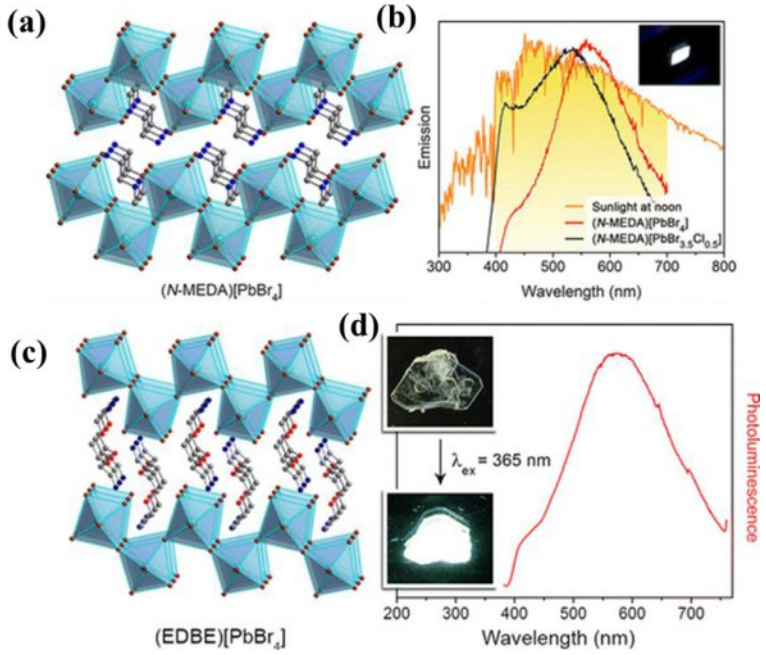

Fig. 25. (a) Structure plot of (N-MEDA)[$PbBr_4$]. (b) Solar spectrum (orange) with the visible region shaded in yellow and emission spectra of (N-MEDA)[$PbBr_4$] (red, excited at 380 nm) and (N-MEDA)[$PbBr_{3.5}Cl_{0.5}$] (black, excited at 360 nm). Reproduced from.[100] Copyright 2014, American Chemical Society. (c) Structure plot of (EDBE)[$PbBr_4$]. (d) Emission spectra for (EDBE)[$PbBr_4$], λ_{ex} = 365 nm; Inset: Photographs showing photoluminescence from (EDBE)[$PbBr_4$]. Reproduced from.[101] Copyright 2014, American Chemical Society.

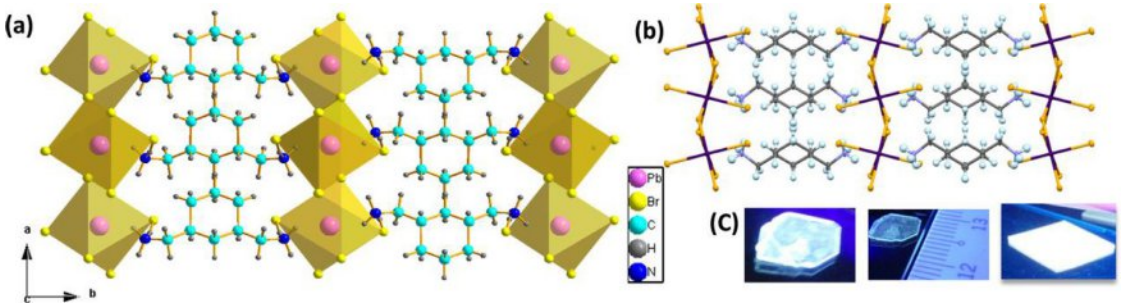

Fig. 26. (a) Crystal packing diagram for (CyBMA)$PbBr_4$ showing propagation of $[PbBr_6]^{4-}$ octahedron along the ac-plane, (b) packing along the bc-plane revealing twist of the Pb—Br chains, (c) photographs of a (CyBMA)$PbBr_4$ crystal with scale bar and spin-coated film illuminated under UV lamp. Reproduced from.[102] Copyright 2017, Wiley-VCH Verlag GmbH &Co. KGaA.

deformable lattice and from a distribution of intrinsic trap states. (EDBE)[PbX_4] remained stable after 3 months of continuous irradiation. This work also shows that the emission is tunable by changing halogen atoms in the hybrid structures.

Other white-light-emitting 2D perovskites include (CyBMA)$PbBr_4$ with a cyclohexane-bis(methylamonium) cation as the organic ligand, which was reported by Mhaisalkar et al.[102] It has a broadband emission in the range 380–750 nm with CIE coordinates of (0.23, 0.29) at room temperature. TG analysis show that this compound has very high thermal stability (T_D = 319 °C). The broad emission has been attributed to self-trapped states of various trapping depths. The authors propose that the flexibility and softness of the cyclohexane core of CyBMABr can initiate strong exciton-phonon interactions, leading to trapping of excitons inside the self-created potential barriers. Also the deformations of the (CyBMA)$PbBr_4$ inorganic lattice can favor self-trapping by acting as potential sites for self-localization. The IQY of this compound is measured to be 1.5% (Fig. 26). Another 2D layered perovskite $(C_6H_5C_2H_4NH_3)_2PbBr_xCl_{4-x}$ $(0 < x < 4)$ with tunable and optimized white light quality and efficiency was reported.[167] Its optical properties could be tuned by varying the amount of Br and Cl. By increasing concentrations of Br, the IQYs of the hybrids increase from 0.2 to 16.9%. The CCT could also been tuned from 4000 K to 7000 K. These structures have a high CRI of 87–91.

Broadband white light emissions were also observed for 1D perovskites reported by Ma et al.[104] A one-dimensional lead bromide perovskite $C_4N_2H_{14}PbBr_4$ with efficient bluish white-light emission was reported. This novel structure has 1D edge sharing octahedral lead bromide chains $[PbBr_4^{2-}]_\infty$ that surrounded by the organic cations $C_4N_2H_{14}^{2+}$ to form the bulk assembly of core-shell quantum wires (Fig. 27a and b). It emits broadband white light in the solid state (Fig. 27c). The IQYs measured are 20% for the bulk single crystals and 12% for the microscale crystals. Further studies reveal that the structure's emission originates from strong quantum confinement with the formation of self-trapped excited states.

DOI: 10.1016/j.enchem.2019.100008
EnergyChem 1, 100008 (2019)

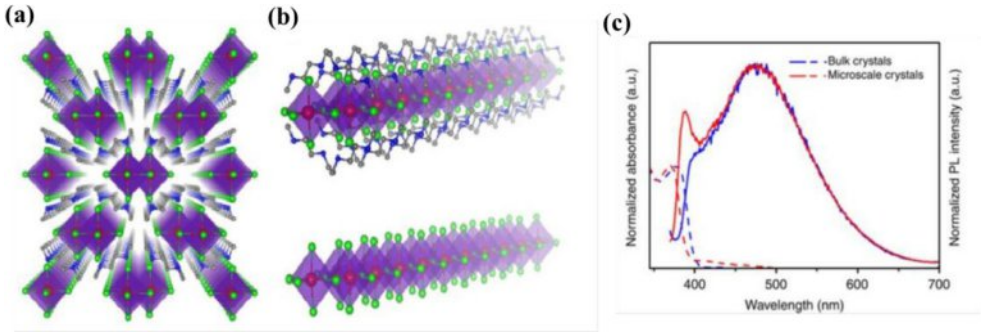

Fig. 27. (a) Structure of 1D perovskite $C_4N_2H_{14}PbBr_4$ (red spheres: lead atoms; green spheres: bromine atoms; blue spheres: nitrogen atoms; grey spheres: carbon atoms; purple polyhedrons: $PbBr_6^{4-}$ octahedrons; hydrogen atoms were hidden for clarity). (b) View of an individual lead bromide quantum wire wrapped by the organic cations. (c) Absorption (dash lines) and emission (solid lines, excited at 360 nm) spectra of the bulk and microscale perovskite crystals at room temperature. Reproduced from.[104] Copyright 2017, Nature Publishing Group.

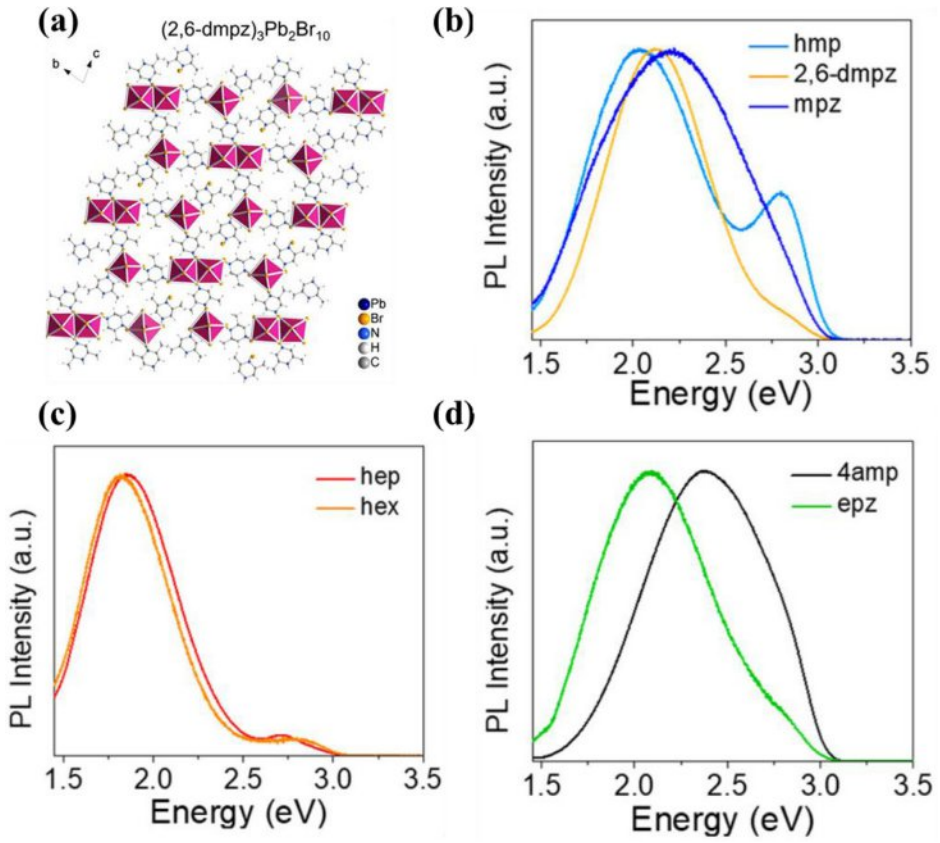

Fig. 28. Steady-state PL (excited at 330 nm) at room temperature for (a) $(hmp)PbBr_4$, $(2,6\text{-}dmpz)_3Pb_2Br_{10}$, and $(mpz)_2Pb_3Br_{10}$; (b) $(hep)PbBr_3$ and $(hex)PbBr_3$; (c) $(4amp)PbBr_4$ and $(epz)PbBr_4$. Reproduced from.[106] Copyright 2018, American Chemical Society.

Another 1D white-light-emitting perovskite $(C_9H_{10}N_2)PbCl_4$ was reported by Abid et al.[168] This structure is built up from an infinite 1D chain of edge-sharing $PbCl_6$ octahedra surrounded by 3-aminoquinoline (AQ) organic molecules. Experimental results illustrate that the strong photoluminescence is the result of a resonant energy transfer mechanism between inorganic wires and organic molecules, leading to the conversion of Wannier excitons localized in $PbCl_4$ chains to Frenkel excitons localized in organic molecules.

Dong et al. determined that broadband emissions from 1D perovskite $C_4N_2H_{14}PbCl_4$ is excitation-dependent, and may change from bluish-green to yellow depending on the excitation wavelength.[103] The results show that this structure has two emission centers, corresponding to the self-trapped excitons (STEs) and vacancy-bound excitons. The excitation-dependent emission is a result of different populations of these two types of excitons generated at different excitation wavelengths. The IQYs of this compound under 320 nm excitation and 365 nm excitation are 18% and 6%, respectively.

The correlation between structure and white light emissions has been carefully studied by the Kanatzidis group.[105,106,164] In 2017, they reported a multilayered 2D perovskite $EA_4Pb_3X_{10}$ (X = Cl and Br, EA = ethylammonium) exhibiting tunable white-light emission.[105] $EA_4Pb_3Cl_{10}$ has

DOI: 10.1016/j.enchem.2019.100008
EnergyChem 1, 100008 (2019)

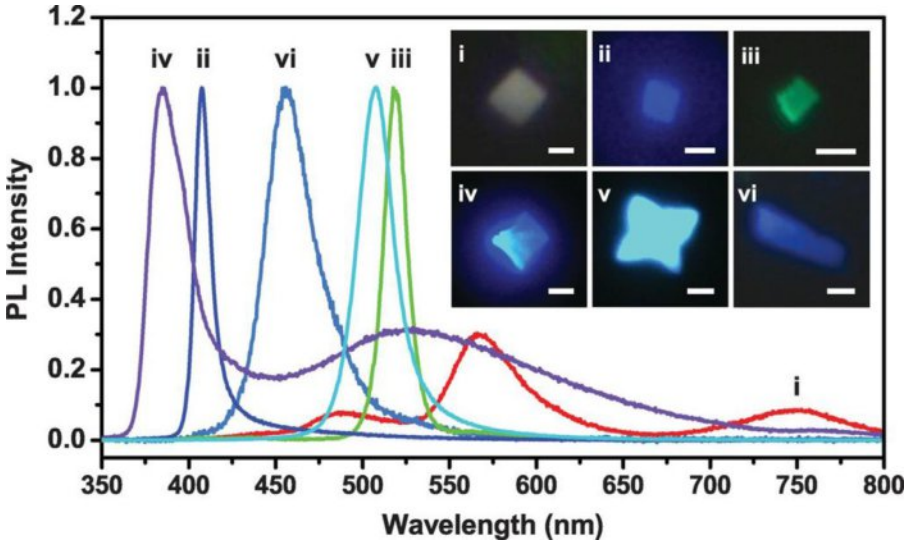

Fig. 29. Photoluminescence of different 2D hybrid perovskites. $(C_4H_9NH_3)_2PbCl_4$ (i), $(C_4H_9NH_3)_2PbBr_4$ (ii), $(C_4H_9NH_3)_2PbI_4$ (iii), $(C_4H_9NH_3)_2PbCl_2Br_2$ (iv), $(C_4H_9NH_3)_2PbBr_2I_2$ (v), and $(C_4H_9NH_3)_2(CH_3NH_3)Pb_2Br_7$ (vi) 2D sheets demonstrate that the solution-phase direct growth method is generalizable. The corresponding optical PL images are shown in the inset. Scale bars, 2 μm for (i) to (v) and 10 μm for (vi). Reproduced with permission from.[169] Copyright 2015, AAAS.

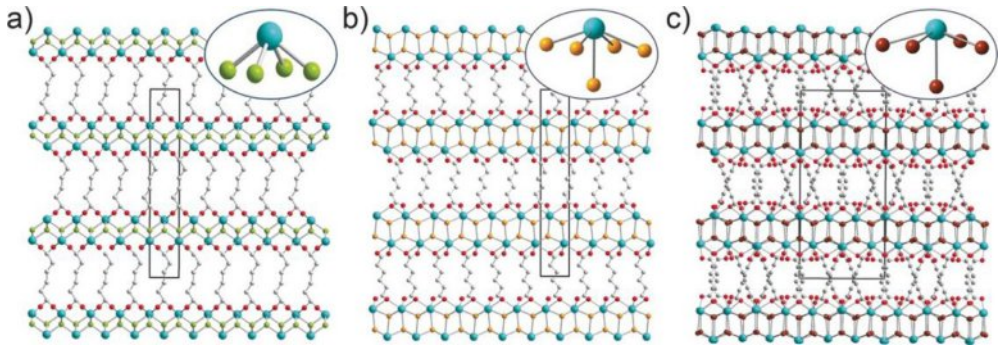

Fig. 30. Crystallographic view of $[Pb_2X_2]^{2+}[^-O_2C(CH)_2CO_2^-]$ $X = F$ (a), Cl (b), Br (c) . Insets show the asymmetric Pb-X coordination environments. Pb cyan, F green, Cl orange, Br brown, O red, and C gray. H atoms are omitted for clarity. Black boxes highlight the unit cells. Reproduced with permission from.[107] Copyright 2017, Wiley-VCH Verlag GmbH &Co. KGaA.

a broadband white-light emission, while $EA_4Pb_3Br_{10}$ has a narrow blue emission. The emission could be systematically tuned by varying the composition of Cl and Br. They also discovered that the larger the octahedral distortion of the inorganic layer, the broader the bandwidth of the PL emission.[164] In 2018, they synthesized a series of new light emitting lead bromide based hybrid compounds with different dimensionalities.[106] These include $(hep)PbBr_3$, $(hex)PbBr_3$, $(2,6\text{-dmpz})_3Pb_2Br_{10}$, $(4amp)PbBr_4$, $(epz)PbBr_4$, $(mpz)_2Pb_3Br_{10}$, and $(hmp)PbBr_4$ (mpz = 1-methylpiperazine, epz = 1-ethylpiperazine, 4amp = 4-(aminomethyl)piperidine, 2,6-dmpz = 2,6-dimethylpiperazine, hmp = homopiperazine, hex = hexamethylenimine, hep = heptamethylenimine), all emitting in the visible light region. The compounds crystallize in a variety of structural types, and their structures and optical properties have been comprehensively studied. Except for $(hep)PbBr_3$ and $(hex)PbBr_3$, the rest of the compounds exhibit white-light emission at room temperature (Fig. 28). The 1D compound $(2,6\text{-dmpz})_3Pb_2Br_{10}$ has the highest PLQY of 12%, while the other's IQYs are lower than 1%.

The emission colors of 2D hybrid perovskites could also been tuned by the thickness of the inorganic sheet as demonstrated by Yang et al.[169] Single-and few-unit-cell-thick single-crystalline 2D hybrid perovskites of $(C_4H_9NH_3)_2PbBr_4$ have been synthesized. These materials exhibit strong and tunable blue photoluminescence (Fig. 29). Both the bulk materials and the sheets show similar strong purple-blue light emission. The slightly increased optical band gap for the ultrathin 2D sheets is probably induced by the lattice expansion. The emission colors of the hybrids could be tuned by changing the thickness of the inorganic sheet or the composition of the hybrid materials.

Non-perovskite lead halide hybrid materials have also attracted much attention and exhibit great promise. A family of novel cationic lead halide layered hybrid materials $[Pb_2X_2^{2+}][^-O_2C(CH_2)_4CO_2^-]$ ($X = F$, Cl, and Br) was reported by Fei et al.[107] Single-crystal X-ray crystallography reveals that all three materials form a highly unusual $[PbX]^+$ layered architecture connected by organic ligands (Fig. 30). They all exhibit broadband white light emissions with a QY up

DOI: 10.1016/j.enchem.2019.100008
EnergyChem 1, 100008 (2019)

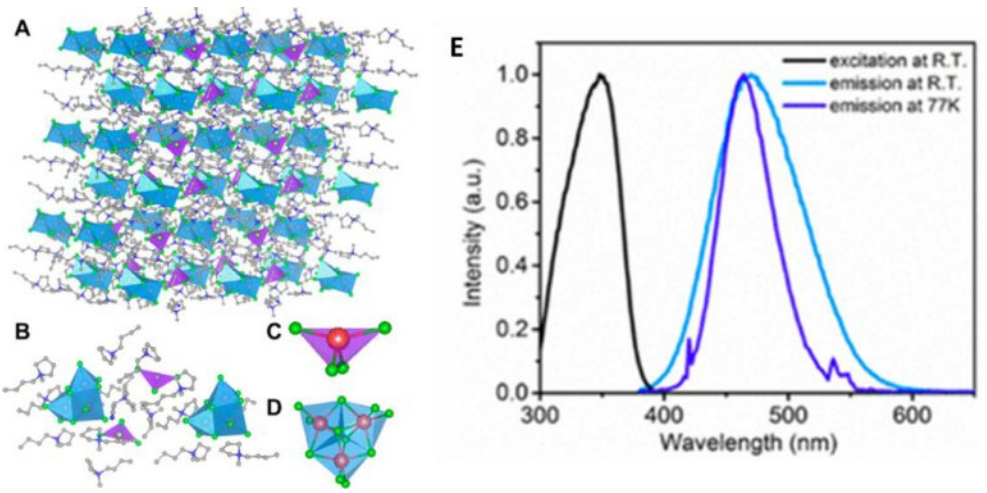

Fig. 31. (a-d) Structural plot of $(C_9NH_{20})_7(PbCl_4)Pb_3Cl_{11}$. (e) Excitation and emission spectra of the single crystals at room temperature and 77 K. Reproduced with permission from.[108] Copyright 2018, American Chemical Society.

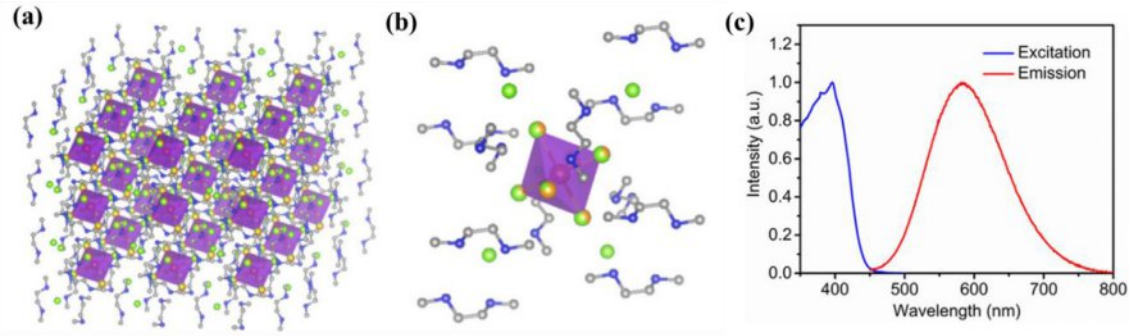

Fig. 32. (a) Single-crystal structure of the Sn mixed-halide perovskite $(C_4N_2H_{14}Br)_4SnBr_xI_{6-x}$ $(x = 3)$ (red spheres: tin atoms; green spheres: bromine atoms; orange spheres: iodine atoms; blue spheres: nitrogen atoms; and gray spheres: carbon atoms; hydrogen atoms were hidden for clarity). (b) Individual Sn mixed-halide octahedron completely surrounded by organic ligands. (c) Excitation (blue line) and emission (red line) spectra of bulk Sn mixed-halide perovskite crystals at room temperature. Reproduced with permission from.[109] Copyright 2017, American Chemical Society.

to 11.8% for $[Pb_2Br_2^{2+}][^-O_2C(CH_2)_4CO_2^-]$. Such cationic materials exhibit high chemical and thermal stability.

A strongly luminescent blue emitting lead halide cluster $(C_9NH_{20})_7(PbCl_4)Pb_3Cl_{11}$ was reported by Ma et al.[108] This 0D cluster can be considered to be lead chloride tetrahedrons ($PbCl_4^{2-}$) and face-sharing lead chloride trimer clusters ($Pb_3Cl_{11}^{5-}$) cocrystallizing with organic cations ($C_9NH_{20}^+$) (Fig. 31a–d). This cluster emits strong blue emission peaked at 470 nm under UV excitation with a high QY of 83% (Fig. 31e).

Light-emitting materials based on Sn(II) halides

Since the lead halide perovskites cause environmental concerns due to the toxicity of Pb^{2+}, developing other lead-free hybrid metal halides has attracted increasing attention.[78,170,171] The effort to develop tin halide based hybrid structures as alternatives for lead halide hybrids is mainly based on this concern.[165]

A highly efficient broadband yellow light emitter based on 0D tin mixed-halide perovskite $(C_4N_2H_{14}Br)_4SnBr_xI_{6-x}$ $(x = 3)$ was reported by Hong et al.[109] The octahedral SnX_6^{4-} contains equal amounts of bromine and iodine, whereas all four halide ions associated with the organic ligand are bromines (Fig. 32a and b). It emits yellow light peaked at 582 nm, with a high PLQE of ~85% (Fig. 32b) and was blended with a commercial europium-doped barium magnesium aluminate blue phosphor BAM ($BaMgAl_{10}O_{17}:Eu^{2+}$) to generate white light with high CRI of 85 under UV excitation.

The layered tin bromide based perovskite HMD_3SnBr_8 (HMD = hexamethylene diamine) was reported by Ning et al. (Fig. 33a).[110] There are two forms synthesized in different solvents: $HMD_3SnBr_8(CH_3OH)$ and $HDM_3SnBr_8(CH_2Cl_2)$. Both of them emit intense orange emission with peaks at 590 nm and 601 nm, respectively (Fig. 33b), and their QYs are as high as 86%. Experiments show that the distortion of the octahedral structure under excitation results in the formation of self-trapped excitons, which is responsible for the broadband emission of HMD_3SnBr_8. Lighting devices have been fabricated using these phosphors.

Luminescent tin halide structures not based on perovskite have also been investigated. A luminescent seesaw-shaped 0D cluster $(C_9NH_{20})_2SnBr_4$ was reported by Ma et al.[111] In the structure, $SnBr_4^{2-}$ are surrounded by the organic cations ($C_9NH_{20}^+$) to form a 0D cluster (Fig. 34a and b). This material exhibits strong deep-red emission peaked at about 695 nm at solid state with a PLQE of 46%. The Stokes shift of 332 nm is one of the highest values reported to date for any solid-state light-emitting material (Fig. 34c).

DOI: 10.1016/j.enchem.2019.100008
EnergyChem 1, 100008 (2019)

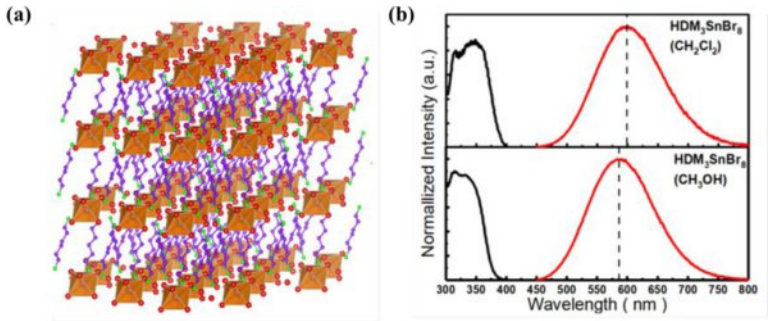

Fig. 33. (a) View of the crystal structure of HMD_3SnBr_8 (Sn, blue; Br, red; N, green; C, purple; orange octahedra $[SnBr_6]^{4-}$, hydrogen atoms, and solvent molecules were omitted for clarity). (b) Excitation and emission spectra of $HMD_3SnBr_8(CH_3OH)$ and $HDM_3SnBr_8(CH_2Cl_2)$, respectively. Reproduced with permission from.[110] Copyright 2018, American Chemical Society.

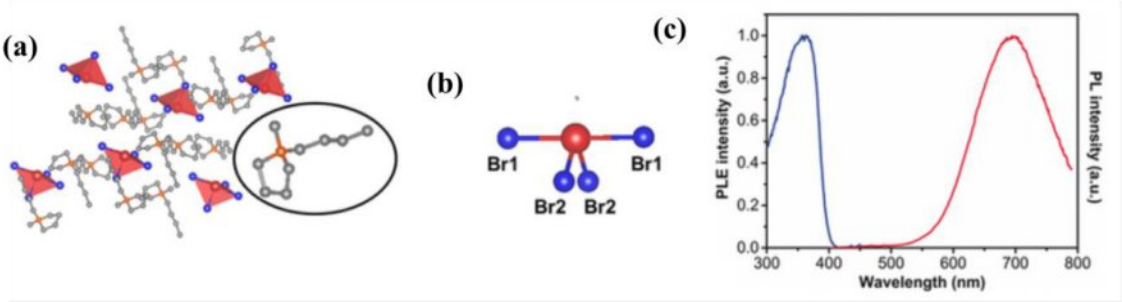

Fig. 34. (a) Views of individual $SnBr_4^{2-}$ ions isolated from each other and surrounded by the $C_9NH_{20}^+$ ions; the inset shows a $C_9NH_{20}^+$ cation. (b) Ball and stick model of an individual $SnBr_4^{2-}$ anion. (c) Excitation and emission spectra of $(C_9NH_{20})_2SnBr_4$ bulk crystals. Reproduced with permission from.[111] Copyright 2018, Wiley-VCH Verlag GmbH &Co. KGaA.

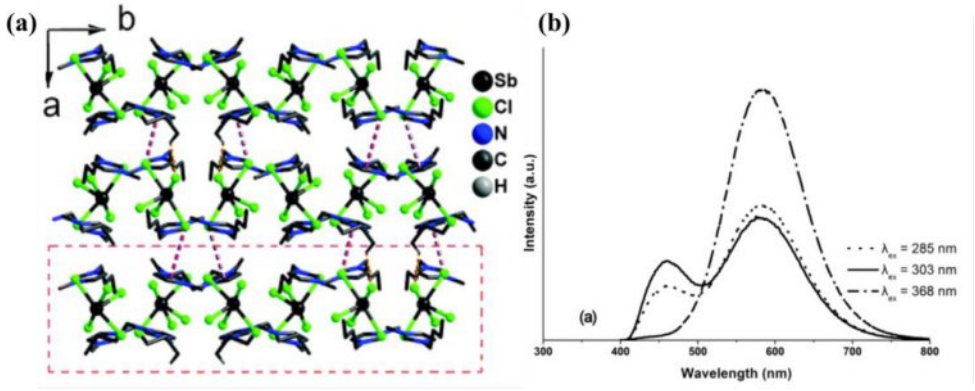

Fig. 35. Packing of the structure of $[Bmim]_2SbCl_5$ viewed along the c-axis; (b) Emission spectra of $[Bmim]_2SbCl_5$ at different excitation wavelengths. Reproduced from [76] with the permission of the Royal Society of Chemistry.

LUMINESCENT MATERIALS BASED ON VB-VIIA SEMICONDUCTORS

Antimony or bismuth halide based inorganic-organic hybrid materials have attracted significant attention recently due to the fact that they can be non-toxic alternatives for lead halide structures for PV and lighting applications.[78,165] Some members of this group, especially Sb based compounds, exhibit very impressive luminescence, with QYs up to 98%, showing great potential for highly efficient lighting phosphors.[54,76] Some representative materials are briefly described below.

Light-emitting materials based on Sb(III) halides

A highly luminescent antimony-based hybrid structure $[Bmim]_2SbCl_5$ was reported by Huang and coworkers in 2015.[76] In the structure, each Sb(III) ion is coordinated with five Cl^- ions in the form of a quadrangular pyramid, and every pyramid-like anion is surrounded by six imidazole rings (Fig. 35a). Each discrete $[SbCl_5]^{2-}$ anion interacts with neighboring $[Bmim]^+$ cations via inter-molecular C–H···Cl hydrogen bonds, resulting in a 2D infinite layer. It exhibits bright yellow light when exposed to 365 nm excitation at room temperature. As it also exhibits

DOI: 10.1016/j.enchem.2019.100008
EnergyChem 1, 100008 (2019)

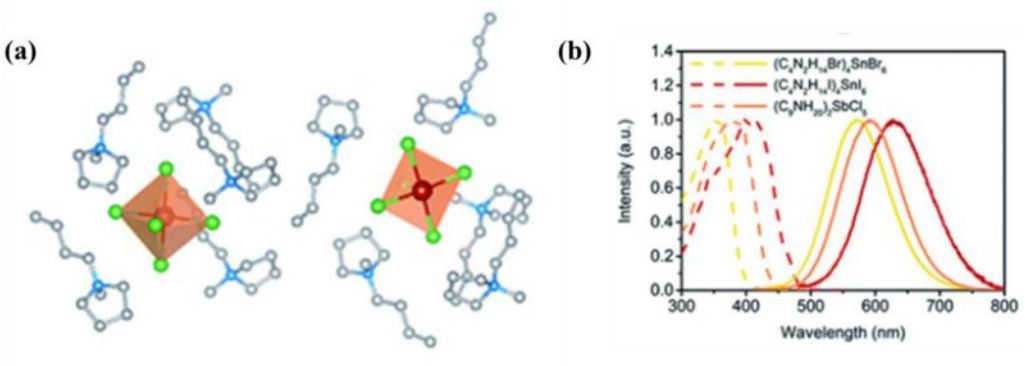

Fig. 36. (a) Two isolated $SbCl_5^{2-}$ quadrangular pyramids surrounded by $C_9NH_{20}^+$ ligands. (b) Excitation (dashed lines) and emission (solid lines) spectra of 0D organic metal halide hybrids at room temperature. Reproduced from [54] with the permission of the Royal Society of Chemistry.

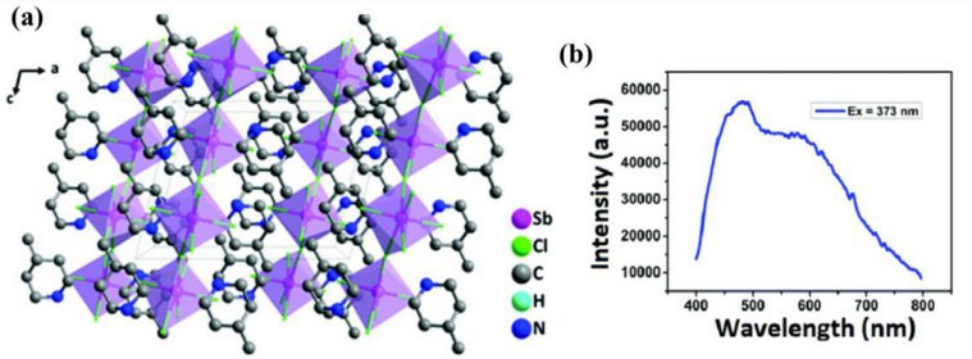

Fig. 37. (a) The packing structure of 4-MPSC viewed along the b-axis direction. (b) Emission spectra at room temperature (excited at 373 nm). Reproduced from [112] with the permission of the Royal Society of Chemistry.

excitation-dependent luminescence, when exposed to higher energy UV light at 303 nm, another emission band peaking at 460 nm shows up, generating white light (Fig. 35b). This compound exhibits a high quantum yield of 86.3% in solid state.

A new 0D Sb(III) halide based inorganic-organic hybrid structure with an exceptionally high PLQE was reported by Ma et al.[54] $(C_9NH_{20})_2SbCl_5$, along with other two Sn halide based hybrids, were reported. The inorganic module of $(C_9NH_{20})_2SbCl_5$ is a quadrangular pyramid (SbX_5^{2-}) (Fig. 36a). This metal halide hybrid emits in the orange light region peaked at 590 nm and has extremely high PLQEs at room temperature, which is 98±2% (Fig. 36b). Such a high IQY value for orange emission is very rare.

Direct white-light-emitting materials from this family have also been developed. A new Sb(III) halide based hybrid material, $[4\text{-methylpiperidinium}]_2SbCl_5$ (4-MPSC), was reported by Luo et al.[112] It represents a new lead-free single-component hybrid with the potential to serve as a white light-emitting material. The inorganic modules of this hybrid are one-dimensional inorganic chains of corner-sharing $SbCl_6$ octahedra (Fig. 37a). It emits broadband white light emission with CIE coordinates of (0.33, 0.32), which is extremely close to pure white light (Fig. 37b). There are two peaks in the emission spectra; one is the narrow peak at 480 nm, and the second is located at 580 nm. The IQY of this compound is ~1%.

Red-light-emitting materials have also been reported, such as $(Ph_4P)_2SbCl_5$, a very efficient red phosphor reported by Ma et al. (Fig. 38a).[113] This compound can be prepared easily by cocrystallizingof tetraphenylphosphonium (Ph_4P^+) and antimony (Sb^{3+}) chloride salts. It emits in the red region with a peak at 648 nm and a PLQE of around 87% (Fig. 38b). Another yellow-emitting, kinetically favored metastable product can be formed within minutes, and will convert to the red-emitting, thermodynamically stable product slowly at room temperature or with thermal treatment.

Light-emitting materials based on Bi(III) halides

Bismuth represents the only non-toxic heavy metal with low cost; therefore, hybrid materials based on bismuth have attracted much attention.[172-175] Their structural variety and properties have been summarized in a recent review by Sokolov et al.[176] Some of these structures are luminescent, showing potential for use in lighting applications.[114,115]

Mercier et al. reported two bismuth compounds, $(TBA)[BiBr_4(bp4mo)]$ (TBA = tetrabutylammonium) and $[BiBr_3(bp4mo)_2]$.[114] $(TBA)[BiBr_4(bp4mo)]$ emits green-yellow emission at 540 nm with a high IQY of 85% (Fig. 39a), while $[BiBr_3(bp4mo)_2]$ emits green light 516 nm with a IQY of 11% (Fig. 39b). Their luminescence was quenched in solution. These two materials also exhibit mechanochromic behavior, and represent the first examples of mechanochromic phosphors based on bismuth(III).

Two Bi(III) halide based hybrid compounds composed of a bismuth(III) chloride anion and an imidazolium cation, namely α- and β-$[Bmim][BiCl_4(2,2'\text{-bpy})]$ (Bmim = 1–butyl–3-methyl imidazolium; 2,2′-bpy=2,2′-bipyridine) (Figs. 40a and 40b) were reported by Shen et al.[115] They were synthesized in ionic liquid and exhibit green-yellow phosphorescence with quantum yields of 26.07% and 36.59%, respectively (Fig. 40c).

DOI: 10.1016/j.enchem.2019.100008
EnergyChem 1, 100008 (2019)

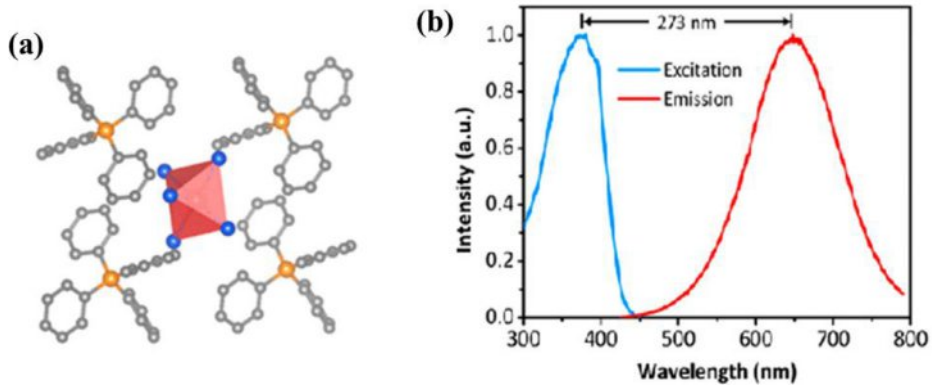

Fig. 38. (a) View of an individual $SbCl_5^{2-}$ anion and nearest neighbor Ph_4P^+ cations. (b) Excitation and emission spectra of bulk $(Ph_4P)_2SbCl_5$ crystals. Reproduced with permission from.[113] Copyright 2018, American Chemical Society.

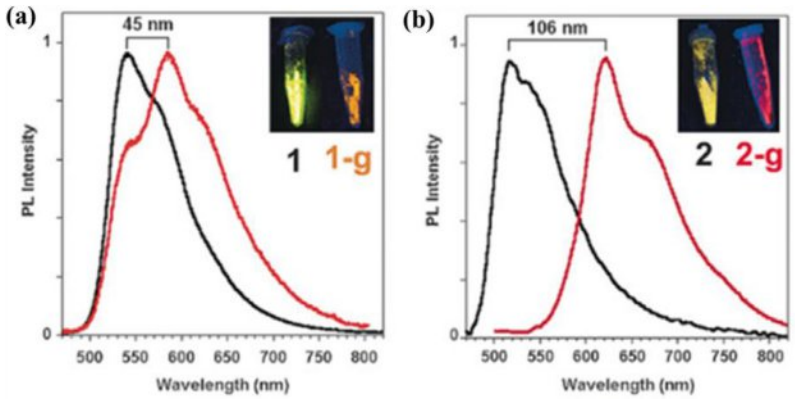

Fig. 39. (a) PL spectra of (TBA)[$BiBr_4$(bp4mo)] and (TBA)[$BiBr_4$(*bp4mo*)]-g (left) and [$BiBr_3$(bp4mo)$_2$] and [$BiBr_3$(bp4mo)$_2$-g (right). Inset: photographs under UV light. (-*g* = after grinding). Reproduced with permission from.[114] Copyright 2016, Wiley-VCH Verlag GmbH &Co. KGaA.

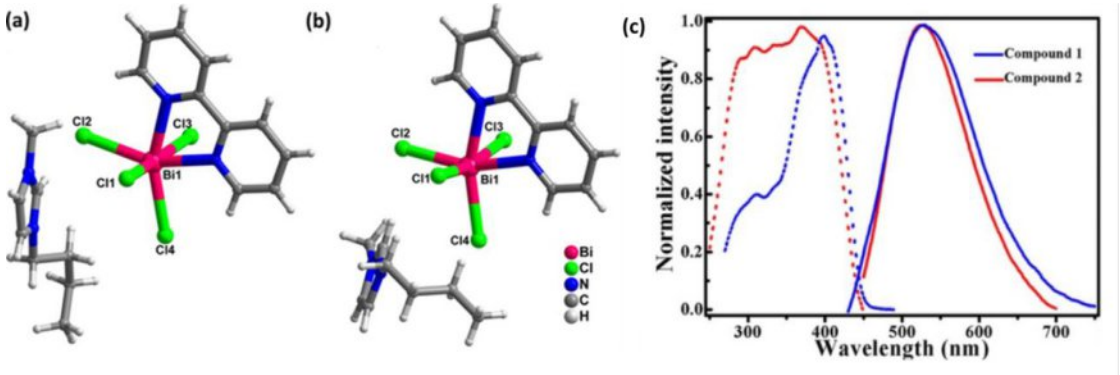

Fig. 40. The crystallographic asymmetric units of compounds (a) α-[B*mim*][$BiCl_4$(2,2′-bpy)] and (b) β-[B*mim*][$BiCl_4$(2,2′-bpy)]. (c) Excitation (dashed lines) and emission spectra (solid lines) of compounds α-[B*mim*][$BiCl_4$(2,2′-bpy)] (blue lines) and β-[B*mim*][$BiCl_4$(2,2′-bpy)] (red lines); for α-[B*mim*][$BiCl_4$(2,2′-bpy)], $\lambda_{ex} = 397$ nm, $\lambda_{em} = 530$ nm; for β-[B*mim*][$BiCl_4$(2,2′-bpy)], $\lambda_{ex} = 372$ nm, $\lambda_{em} = 524$ nm. Reproduced with permission from.[115] Copyright 2017, Wiley-VCH Verlag GmbH &Co. KGaA.

DOI: 10.1016/j.enchem.2019.100008
EnergyChem 1, 100008 (2019)

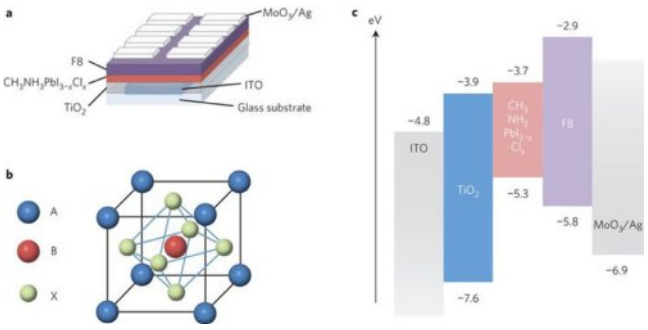

Fig. 41. (a) Device architecture of the $CH_3NH_3PbI_{3-x}Cl_x$ PeLED. (b) Single unit cell of an ABX_3 perovskite crystal, where A is methylammonium, B is Pb and X is I, Br or Cl. (c) Energy-level diagram of different layers of materials in the infrared PeLED, showing conduction and valence band levels with respect to vacuum. Reproduced with permission from.[181] Copyright 2014 Nature Publishing Group.

■ ELECTROLUMINESCENT MATERIALS FOR LIGHT-EMITTING-DIODES

Electroluminescent materials for inorganic-organic hybrid materials primarily fall into one of two structural groups. These are either lead or tin halide perovskites, which have emerged as a highly promising class of semiconductor for LEDs,[10,177,178] or copper halide hybrid complexes, typically used as the emissive layer in OLEDs.[50,179] Representative examples from both groups are introduced in this section.

Perovskite based hybrid electroluminescent materials

IVB-VIIB semiconductor based hybrid perovskites have emerged as a highly promising class of semiconductor for optoelectronic device applications. The recent development of halide perovskite as electroluminescent materials for LEDs has been a very hot research topic and has been discussed in several review papers.[10,11,72,165] Here, we only discuss a few representative works.

Light-emitting diodes based on layered perovskites were first investigated in the 1990s. An important work by Mitzi et al. demonstrates that electroluminescence was realized for hybrid organic-inorganic perovskite as the emission layer.[180] A specially modified quaterthiophene dye was incorporated within infinite lead halide perovskite sheets, and 0.1 lm/W of green emission peaked at 530 nm with low turn-on voltages of 5.5 V was achieved with a device using a 3000Å-thick emission layer.

Another important work in this area was reported later by Friend et al. in 2014.[181] They showed strong room-temperature electroluminescence in perovskite light-emitting diodes. The emission of the electroluminescence could be also be tuned by changing halide composition in the perovskite. They developed green, red, and near-infrared (NIR) LEDs using $CH_3NH_3PbBr_3$ ($MAPbBr_3$), $CH_3NH_3PbBr_2I$, and $CH_3NH_3PbI_{3-x}Cl_x$ ($MAPbI_{3-x}Cl_x$), respectively, as the emissive layer in two device structures of ITO/PEDOT:PSS/$MAPbBr_3$/F8/Ca/Ag and ITO/TiO_2/$MAPbI_{3-x}Cl_x$/F8/MoO_3/Ag (Fig. 41a). The energy-level diagram of the different layers is shown in Fig. 41c. The EQE of the two devices are measured to be 0.1% and 0.76%, respectively.

The efficiency of the perovskite-based LED was improved by Huang et al. in 2015, who developed an interfacial engineering approach to achieve high-performance perovskite light-emitting diodes.[182] In this approach, materials of different band energies were applied to improve charge injection, transport, and confinement. A multifunctional polyethyleneimine (PEI) interlayer was incorporated in the LED structure between the oxide electron-transporting layer and the perovskite emissive layer, facilitating the formation of high-quality perovskite film and reducing the work function of ZnO for improved electron injection (Fig. 42). The maximum radiance and EQE for NIR LEDs based on $MAPbI_{3-x}Cl_x$ was 28 W sr^{-1} m^{-2} and 3.5% at 2.2 V, respectively. A $MAPbBr_3$ device of the same structure produced an EQE and brightness of 0.8% and 20,000 cd m^{-2} at 2.8 V.

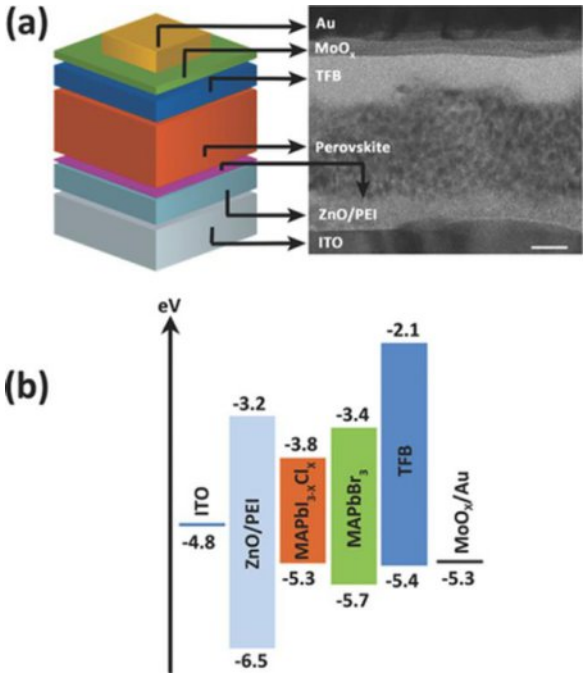

Fig. 42. Multi-layered PeLED. (a) Schematic illustration and a cross-sectional TEM image (scale bar: 20 nm) showing the device architecture: ITO/PEI-modified ZnO (20 nm)/perovskite (50 nm)/TFB (25 nm)/MoO_x (8 nm)/Au. In this TEM image, the perovskite layer is a $CH_3NH_3PbI_{3-x}Cl_x$ film. (b) Flat-band energy level diagram ($MAPbI_{3-x}Cl_x$: $CH_3NH_3PbI_{3-x}Cl_x$, $MAPbBr_3$: $CH_3NH_3PbBr_3$). The energy level values for ITO and PEI treated ZnO were obtained by UPS and optical measurements. Reproduced with permission from.[182] Copyright 2015, Wiley-VCH Verlag GmbH &Co. KGaA.

The work by Lee et al. boosted the efficiency and EQE of perovskite LEDs to 42.9 cd A^{-1} and 8.53% by making two modifications.[183] First, a small excess of MABr was applied to prevent exciton quenching from Pb atoms. Second, a "nanocrystal pinning" process was introduced to spatially confine the excitons in $CH_3NH_3PbBr_3$ nanograins (Fig. 43). These two approaches improved the device performance significantly.

Copper halide based hybrid electroluminescent materials

The copper halide (mostly CuI) complexes can also be utilized as emissive layers in organic light-emitting diodes.[50,179,184] The ligand material in this case serves a dual role as both a ligand for forming the emissive complex and as a host matrix for the formed emitter.[50] Such an approach generally involves *in situ* codeposition of CuI and the emissive organic ligands, forming highly emissive CuI based molecular clusters. Thompson

DOI: 10.1016/j.enchem.2019.100008
EnergyChem 1, 100008 (2019)

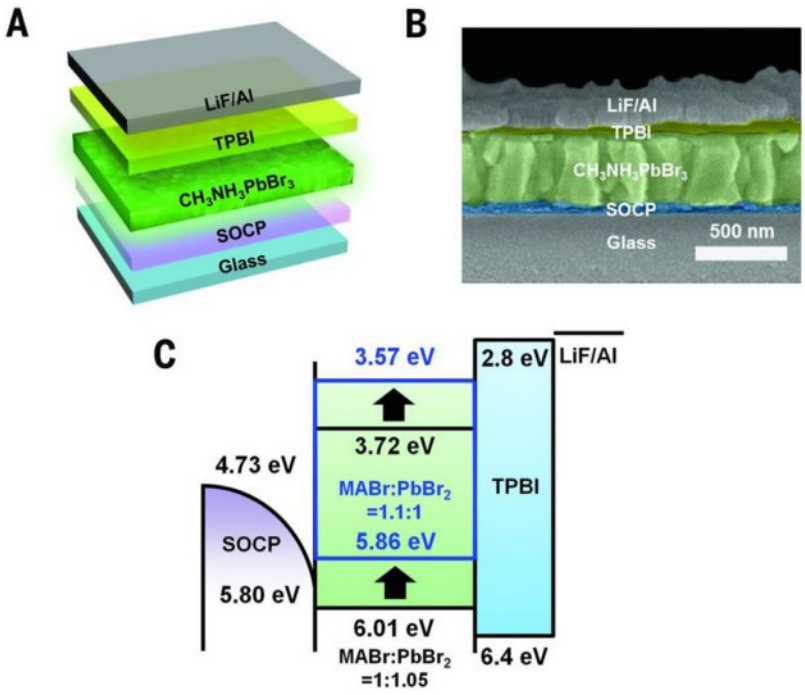

Fig. 43. (a) The device structure. (b) Cross-sectional SEM image of PeLEDs. (c) Energy band diagram of PeLEDs, showing a decrease in IE with increasing MABr molar proportion. Reproduced with permission from.[183]

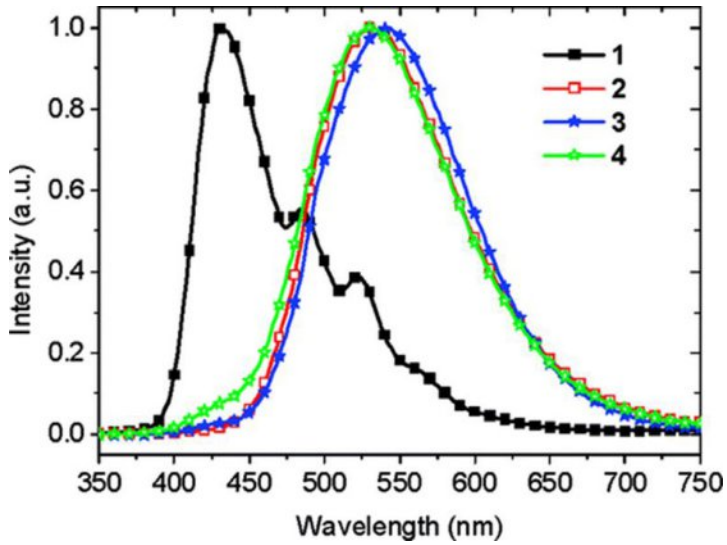

Fig. 44. EL spectra of ITO/NPD/EML/BCP/LiF/Al devices at 8 V, where EML denotes neat mCPy (device 1), 1:4 CuI:mCPy (device 2), 1:6 CuI:mCPy (device 3), or 1:10 CuI:mCPy (device 4). Reproduced with permission from.[50] Copyright 2011, American Chemical Society.

et al. demonstrated this approach by codeposition of CuI and 3,5-bis(carbazol-9-yl)pyridine (mCPy).[50] Green electroluminescence at 530 nm from the CuI based complex was observed in a simple three-layer device structure. Different ratios of CuI to ligand were tested, showing different luminescence efficiency (Fig. 44). A maximum luminance and EQE of 9700 cd/m^2 and 4.4%, respectively, were achieved.

Bian et al. produced the following four compounds via codeposition, and used them to form a luminescent CuI based complex doped film *in situ*: 4-[3,6-*di*(*carbazol-9-yl*)*carbazol-9-yl*]isoquinoline (TCIQ), 3-[3,6-*di*(*carbazol-9-yl*)*carbazol-9-yl*]pyridine (TCPy), 4-(carbazol-9-yl)isoquinoline (4CIQ), and 3-(carbazol-9-yl)pyridine (CPy).[179] These complexes could be utilized as the emissive layer in OLEDs (Fig. 45). The ratio of CuI to ligand could be varied to adjust the performance of the device. A total of 10 OLEDs were fabricated, and their performance has been summarized.[179] It was determined that TCIQ could serve as a blue emitter for white light OLEDs.

An interesting pair of red emitting OLEDs based on CuI complexes was reported by Ni et.al. in 2015 using a similar codeposition approach.[184] Two isoquinolyl carbazole (CIQ) compounds 9-(8-(carbazol-9-yl)isoquinolin-5-yl)-carbazole (DCIQ)

DOI: 10.1016/j.enchem.2019.100008
EnergyChem 1, 100008 (2019)

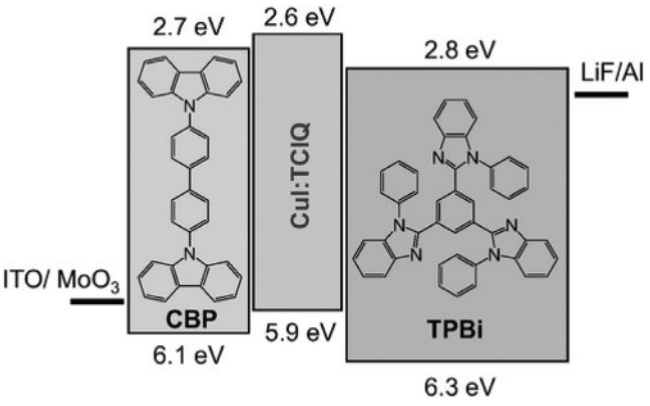

Fig. 45. The schematic device structure, chemical structure, and energy level diagrams of the molecules used in OLEDs. Reproduced with permission from.[179] Copyright 2014, Wiley-VCH Verlag GmbH &Co. KGaA.

and 9-(4-(5-(4-(carbazol-9-yl)phenyl)isoquinolin-8-yl)phenyl)-carbazole (DCDPIQ) were synthesized and codeposited with CuI to form a red emissive CuI dimer based complex doped film in situ. This film could be utilized directly as the emissive layer in OLEDs. After a systematic study and optimization of the CuI composition, red OLEDs were achieved, showing a maximum emission band, an EQE, a luminance of 643 nm, 3.5%, 3290 cd m^{-2} for DCIQ, and 635 nm, 3.6%, 853 cd m^{-2} for DCDPIQ, respectively (Fig. 46).

OTHER LUMINESCENT HYBRID MATERIALS

In addition to the lead or tin organometal halide perovskites that have drawn much attention recently, organometal halides comprise other important class of luminescent hybrid materials have also been point of interests. Representative examples include inorganic-organic hybrid cadmium and tellurium halides.[116–118,185–192] A single-component white-light emitting inorganic-organic semiconductor, $[C_5H_9–NH_3]_4CdBr_6$ was reported by Luo et al. in 2017.[116] It is the first example of broadband white light emission from a perovskite that is not based on lead or tin. The photoluminescence spectra of $[C_5H_9–NH_3]_4CdBr_6$ exhibits two emission peaks located at 420 nm (a narrow peak) and 690 nm (a broad peak) (Fig. 47a). The two emission peaks have different maximum excitation wavelengths, with the emission at 420 nm having a maximum excitation wavelength of 315 nm, while the 690 nm emission displays a maximum excitation wavelength of 365 nm. Upon varying the excitation wavelengths from 315 nm to 365 nm, the emission spectra changes accordingly, showing tunable emission from blue-violet to orange (Fig. 47b). The compound showed a white-light emission with ideal CIE chromaticity coordinates of (0.33, 0.33) when exited by 340 nm, with a quantum yield of approximately 1%. The CRI of the white-light emission is as high as 92.5.

Another white-light emitting Cd-based 2D hybrid perovskite $(C_6H_{11}NH_3)_2[CdBr_4]$ was reported by Yangui et al. in 2018.[117] The inorganic module is 2D $[CdBr_4]^{2-}$ layer (Fig. 47c). The compound's optical absorption spectrum shows a sharp absorption peak at 3.24 eV, arising from the two-dimensional excitons confined into the $[CdBr_4]^{2-}$layers. The origin of two emission bands has been analyzed. The higher energy band is attributed to excitons confined in the $[CdBr_4]^{2-}$ inorganic layers, while the lower energy band is attributed to the emission of the cyclohexylammonium cations. This compound emits a broadband white light emission under UV irradiation.

A series of cadmium chloride hybrid structures with monochromic emissions were reported by Huang et al. in 2017.[118] A total of four new hybrid structures were reported: $[CdCl_2(Im)_4]$ (Im = imidazole), $[CdCl_4(HAPI)_2]$ (API = *N*-(3-Aminopropyl)-imidazole), $[Cd(\mu\text{-}Cl)_2(1\text{-}Mim)_2]_\infty$ (1-Mim = 1-methyl imidazole) and $[CdCl_3(HAPI)]_\infty$. The first two structures are 0D molecular clusters of different inorganic motifs, while the latter two form 1D infinite chains constructed from different subunits and connection modes (Fig. 48). Photophysical measurement results show that all compounds display strong blue emission. The emission quantum yields are measured to be 23.01%, 5.84%, 27.31%, 5.71%, respectively, for these four hybrid structures. The difference in quantum yield may be attributed to the different substituents on the imidazole rings.

Similar to Sn^{2+}, Pb^{2+}, Sb^{3+}, and Bi^{3+}, the external electron shell of the Te^{4+} possesses a s^2 configuration and exhibits luminescent properties. A series of tellurium chloride based hybrid structures were reported by Huang et al.[119] A total of six new structures were reported: α-$[Bmim]_2TeCl_6$ (Bmim = 1–butyl–3-methyl imidazolium), β-$[Bmim]_2TeCl_6$, $[HOOCMim]_2TeCl_6$ (HOOCMim = 1-carboxymethyl-3-methyl imidazolium), $[Bzmim]_2TeCl_6$ (Bzmim = 1-benzyl-3-methyl imidazolium), $[EPy]_2TeCl_6$ (EPy = 1-ethylpyridinium), $[Bmmim]_2TeCl_6$ (Bmmim = 1–butyl–2,3-dimethyl imidazolium). Their inorganic modules are isolated $[TeCl_6]^{2-}$ octahedra anions. Among them, $[HOOCMim]_2TeCl_6$ and $[HOOCMim]_2TeCl_6$ display intense red luminescence at both room temperature and 77 K (Fig. 49a

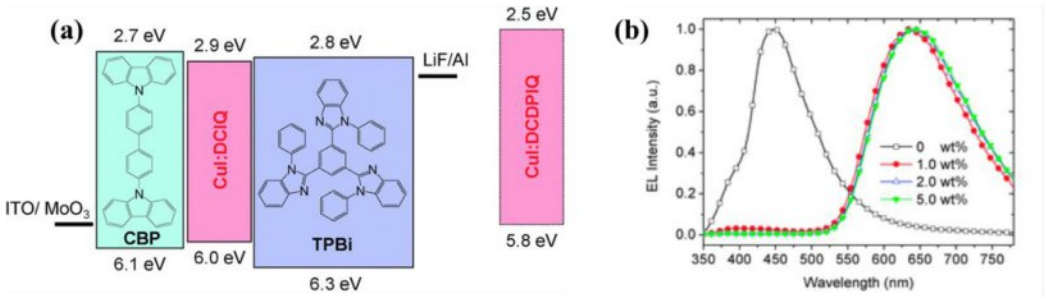

Fig. 46. (a) The schematic device structure, chemical structure, and energy level diagrams of the molecules used in OLEDs. (b) EL spectra of OLED devices of different CuI compositions. Reproduced from [184] with the permission of the Royal Society of Chemistry.

DOI: 10.1016/j.enchem.2019.100008
EnergyChem 1, 100008 (2019)

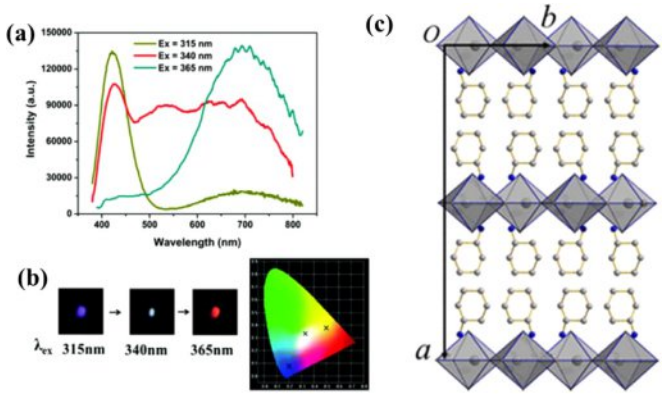

Fig. 47. (a) Emission spectra of $[C_5H_9–NH_3]_4CdBr_6$ at different excitation wavelengths. (b) CIE coordinates of the emission colors and the corresponding photoluminescence images of $[C_5H_9–NH_3]_4CdBr_6$ at different excitation wavelengths. Reproduced from [116] with the permission of the Royal Society of Chemistry. (c) Projection of the compound $(C_6H_{11}NH_3)_2[CdBr_4]$ structure along c-axis at room temperature. Reproduced with permission from.[117] Copyright 2018, American Chemical Society. (For interpretation of the references to color in this figure legend, the reader is referred to the web version of this article.).

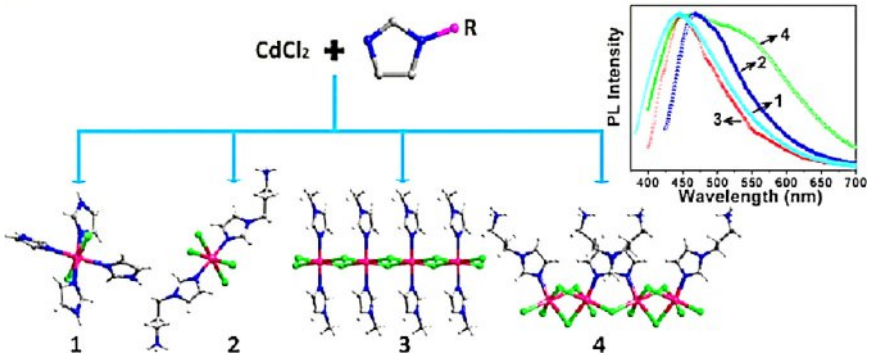

Fig. 48. The structures plots of the$[CdCl_2(Im)_4]$, $[CdCl_4(HAPI)_2]$, $[Cd(\mu\text{-}Cl)_2(1\text{-}Mim)_2]_\infty$ (and $[CdCl_3(HAPI)]_{\infty H}$ and their emission spectra. Reproduced with permission from.[118] Copyright 2017, Elsevier.

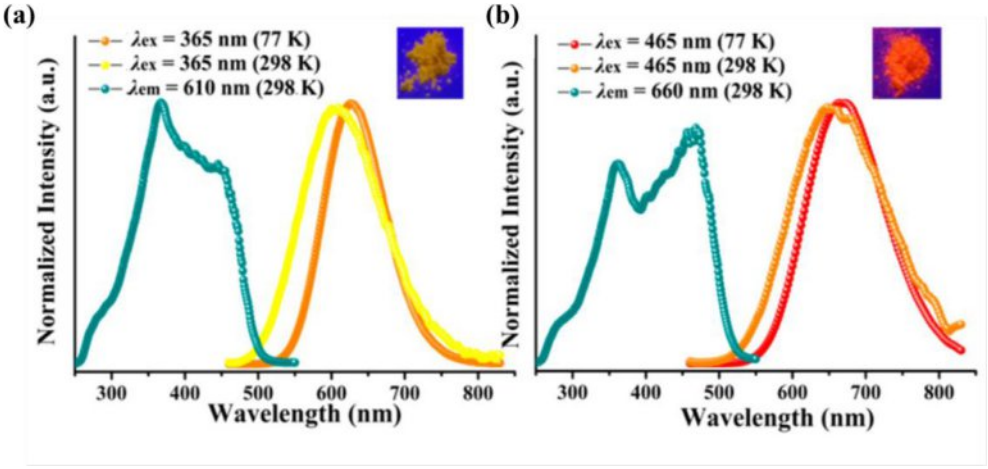

Fig. 49. Excitation and emission spectra of compound $[HOOCMim]_2TeCl_6$ (a) and $[HOOCMim]_2TeCl_6$ (b) at 77 and 298 K; for $[HOOCMim]_2TeCl_6$ $\lambda_{ex} = 365$ nm, λ_{em} (77 K) = 630 nm, λ_{em} (298 K) = 610 nm; for $[HOOCMim]_2TeCl_6$ $\lambda_{ex} = 465$ nm, λ_{em} (77 K) = 680 nm, λ_{em} (298 K) = 660 nm. Inset: photographs of powders under ultraviolet light irradiation. Reproduced with permission from.[119] Copyright 2018, American Chemical Society.

DOI: 10.1016/j.enchem.2019.100008
EnergyChem 1, 100008 (2019)

and b). Such luminescence may originate from the discrete TeX_6 units under minor distortion.

CONCLUSIONS AND OUTLOOK

In summary, we have provided a brief review on the recent development of luminescent inorganic-organic semiconductor materials. Five hybrid structure groups are presented with representative work discussed. A variety of materials, including single-phase direct white-light-emitting phosphors, white-light-emitting composite blends, and blue excitable yellow phosphors, are selected as examples. While some of these materials show very interesting luminescence behavior and relatively high luminescence efficiency, their performance level needs further improvement to be comparable to commercial phosphors. The IQY for the benchmark yellow phosphor YAG:Ce is 95%, while the IQYs of most of the hybrid phosphors are significantly lower. Although organic ligands are vital for the tunability, flexibility, solution processability, etc. of the hybrid structure, enhancing the stability of structures involving them is a crucial aspect in order to meet the stringent requirement for commercialization. Many studies have revealed that several approaches can be applied to effectively improve the stability of hybrid structures. These include selecting ligands that form extended networks or forming stronger bonds between the inorganic and organic components. While some of the organic ligands used in hybrid structures are expensive, those in perovskite hybrids are generally inexpensive and thus, serve as good examples for potential lost-cost devices.

Designing and synthesizing next-generation lighting materials that are energy-efficient, environmental-friendly and better-performing remain a very important yet challenging task. An ideal lighting material should be made of earth abundant, cost-effective elements, have strong resistance to atmosphere and heat, near-unity quantum efficiency, and high photostability. As current WLEDs generally give "cold" white light, there is ever-increasing demand for high efficiency red emitting phosphors. A combination of the state-of-the-art experimental and theoretical methods is essential in guiding the future design and optimization of the hybrid phosphors that outperform the commercial phosphors currently on the lighting market.

ACKNOWLEDGMENT

Financial support from the National Science Foundation (grant no. DMR-1507210) and from Hoffmann Institute of Advanced Materials is gratefully acknowledged.

AUTHOR CONTRIBUTIONS

The manuscript was written with contributions from all authors. All authors have given approval to the final version of the manuscript.

Wei Liu: Data curation, Investigation, Writing - original draft, Writing - review & editing. **William P. Lustig:** Writing - original draft. **Jing Li:** Conceptualization, Data curation, Funding acquisition, Investigation, Writing - original draft, Writing - review & editing.

CONFLICT OF INTEREST

The authors declare no conflict of interest.

REFERENCES

1. Zhou, N., Khanna, N., Feng, W., Ke, J., Levine, M. Scenarios of energy efficiency and CO2 emissions reduction potential in the buildings sector in China to year 2050. *Nat. Energy* **3**, 978–984 (2018).
2. Pattison, P. M., Tsao, J. Y., Brainard, G. C., Bugbee, B. LEDs for photons, physiology and food. *Nature* **563**, 493–500 (2018).
3. Qiu, Y., Kahn, M. E. Better sustainability assessment of green buildings with high-frequency data. Nat. Sustain. **1**, 642–649 (2018).
4. Attari, S. Z Misperceived energy use and savings. *Nat. Energy* **3**, 1029–1030 (2018).
5. Liang, J., Ying, L., Huang, F., Cao, Y. Recent advances in high performance solution processed WOLEDs for solid-state lighting. *J. Mater. Chem. C* **4**, 10993–11006 (2016).
6. Huang, X. Y., Li, J., Zhang, Y., Mascarenhas, A From 1D chain to 3D network: tuning hybrid II-VI nanostructures and their optical properties. *J. Am. Chem. Soc.* **125**, 7049–7055 (2003).
7. Kagan, C. R., Mitzi, D. B., Dimitrakopoulos, C. D. Organic-Inorganic hybrid materials as semiconducting channels in thin-film field-effect transistors. Science **286**, 945–947 (1999).
8. Li, J., Zhang, R. in *Prog. Inorg. Chem.* (ed. Karlin, K. D.) 445–504 (John Wiley & Sons, Inc., Hoboken, 2011).
9. Mitzi, D.B. in *Prog. Inorg. Chem.* (ed. Karlin, K. D.) 11–21 (John Wiley & Sons, Inc., Hoboken, 2007).
10. Zhao, X., Ng, J. D. A., Friend, R. H., Tan, Z.-K. Opportunities and challenges in perovskite light-emitting devices. ACS Photonics **5**, 3866–3875 (2018).
11. Shan, Q., Song, J., Zou, Y., Li, J., Xu, L., Xue, J., Dong, Y., Han, B., Chen, J., Zeng, H. High performance metal halide perovskite light-emitting Diode: from material design to device optimization. *Small* **13**, 1701770 (2017).
12. Saparov, B., Mitzi, D. B. Organic–Inorganic Perovskites: structural versatility for functional materials design. *Chem. Rev.* **116**, 4558–4596 (2016).
13. Li, J., Zhang, R. in *Comprehensive Inorganic Chemistry* (ed. Jan Reedijk, J., Poeppelmeier, K.) 375–415 (Elsevier, Amsterdam, 2012).
14. Wang, M.-S., Guo, G.-C. Inorganic–organic hybrid white light phosphors. *Chem. Commun.* **52**, 13194–13204 (2016).
15. Liu, W., Fang, Y., Li, J. Copper iodide based hybrid phosphors for energy-efficient general lighting technologies. *Adv. Funct. Mater.* **28**, 1705593 (2018).
16. Yam, V. W.-W., Au, V. K.-M., Leung, S. Y.-L. Light-Emitting self-assembled materials based on d8 and d10 transition metal complexes. *Chem. Rev.* **115**, 7589–7728 (2015).
17. de Silva, A. P., Gunaratne, H. Q. N., Gunnlaugsson, T., Huxley, A. J. M., McCoy, C. P., Rademacher, J. T., Rice, T. E. Signaling recognition events with fluorescent sensors and switches. *Chem. Rev.* **97**, 1515–1566 (1997).
18. Sariciftci, N. S., Smilowitz, L., Heeger, A. J., Wudl, F. Photoinduced electron transfer from a conducting polymer to buckminsterfullerene. Science **258**, 1474–1476 (1992).
19. Adachi, C., Baldo, M. A., Thompson, M. E., Forrest, S. R. Nearly 100% internal phosphorescence efficiency in an organic light-emitting device. *J. Appl. Phys.* **90**, 5048–5051 (2001).
20. Ford, P. C., Cariati, E., Bourassa, J. Photoluminescence properties of multinuclear Copper(I) compounds. *Chem. Rev.* **99**, 3625–3648 (1999).
21. Allendorf, M. D., Bauer, C. A., Bhakta, R. K., Houk, R. J. T. Luminescent metal–organic frameworks. *Chem. Soc. Rev.* **38**, 1330–1352 (2009).
22. Fang, X., Roushan, M., Zhang, R., Peng, J., Zeng, H., Li, J. Tuning and enhancing white light emission of II–VI based inorganic–organic hybrid semiconductors as single-phased phosphors. *Chem. Mater.* **24**, 1710–1717 (2012).
23. Roushan, M., Zhang, X., Li, J. Solution-Processable white–light-emitting hybrid semiconductor bulk materials with high

DOI: 10.1016/j.enchem.2019.100008
EnergyChem 1, 100008 (2019)

photoluminescence quantum efficiency. *Angew. Chem.* **124**, 451–454 (2012).
Highly emissive II-VI semiconductor based hybrid white light emitters.
24. Zhang, C., Lin, J Defect-related luminescent materials: synthesis, emission properties and applications. *Chem. Soc. Rev.* **41**, 7938–7961 (2012).
25. Hu, T., Smith, M. D., Dohner, E. R., Sher, M.-J., Wu, X., Trinh, M. T., Fisher, A., Corbett, J., Zhu, X. Y., Karunadasa, H. I, et al. Mechanism for broadband white-light emission from two-dimensional (110) hybrid perovskites. *J. Phys. Chem. Lett.* **7**, 2258–2263 (2016).
26. Jia, J.-H., Chen, X.-L., Liao, J.-Z., Liang, D., Yang, M.-X., Yu, R., Lu, C.-Z. Highly luminescent copper(i) halide complexes chelated with a tetradentate ligand (PNNP): synthesis, structure, photophysical properties and theoretical studies. *Dalton Trans* **48**, 1418–1426 (2019).
27. Kepenekian, M., Even, J. Rashba and dresselhaus couplings in halide Perovskites: accomplishments and opportunities for spintronics and spin–orbitronics. *J. Phys. Chem. Lett.* **8**, 3362–3370 (2017).
28. Amnuyswat, K., Thanomngam, P. Roles of spin-orbit coupling in tetragonal hybrid halide perovskite for photovoltaics light-absorber. Mater. Today Proc. **5**, 14857–14861 (2018).
29. Even, J., Pedesseau, L., Jancu, J.-M., Katan, C. Importance of spin–orbit coupling in hybrid organic/inorganic perovskites for photovoltaic applications. *J. Phys. Chem. Lett.* **4**, 2999–3005 (2013).
30. Du, M.-H. Density functional calculations of native defects in CH3NH3PbI3: effects of spin–orbit coupling and self-interaction error. *J. Phys. Chem. Lett.* **6**, 1461–1466 (2015).
31. Dirac Paul Adrien, M., Fowler Ralph, H.. The quantum theory of the electron. In: Proceedings of the Royal Society of London. Series A, Containing Papers of a Mathematical and Physical Character, 117. p. 610–24.
32. Manchon, A., Belabbes, A.. In: Robert E., Camley & Robert L., editors. Solid State Physics, 68. Academic Press. p. 1–89. Stamps.
33. Marian, C.M. Spin–orbit coupling and intersystem crossing in molecules. 2, 187–203 (2012).
34. Bergmann, L., Hedley, G. J., Baumann, T., Bräse, S., Samuel, I. D. W. Direct observation of intersystem crossing in a thermally activated delayed fluorescence copper complex in the solid state. *Sci. Adv.* **2**, e1500889 (2016).
35. Chen, X.-L., Yu, R., Wu, X.-Y., Liang, D., Jia, J.-H., Lu, C.-Z. A strongly greenish-blue-emitting Cu4Cl4 cluster with an efficient spin–orbit coupling (SOC): fast phosphorescence versus thermally activated delayed fluorescence. *Chem. Commun.* **52**, 6288–6291 (2016).
36. McKittrick, J., Shea-Rohwer, L. E. Review: down conversion materials for solid-state lighting. *J. Am. Ceram. Soc.* **97**, 1327–1352 (2014).
37. Huang, X Red phosphor converts white LEDs. *Nat. Photonics* **8**, 748 (2014).
38. Zhu, H., Lin, C. C., Luo, W., Shu, S., Liu, Z., Liu, Y., Kong, J., Ma, E., Cao, Y., Liu, R.-S, et al. Highly efficient non-rare-earth red emitting phosphor for warm white light-emitting diodes. Nat Commun **5**, 4312 (2014).
39. Bhushan, S. Electroluminescent materials. Nucl Tracks Radiat Meas **10**(1985), 215–224 (1982).
40. Yuan, M., Quan, L. N., Comin, R., Walters, G., Sabatini, R., Voznyy, O., Hoogland, S., Zhao, Y., Beauregard, E. M., Kanjanaboos, P, et al. Perovskite energy funnels for efficient light-emitting diodes. Nat. Nanotechnol. **11**, 872 (2016).
41. Xiao, Z., Kerner, R. A., Zhao, L., Tran, N. L., Lee, K. M., Koh, T.-W., Scholes, G. D., Rand, B. P. Efficient perovskite light-emitting diodes featuring nanometre-sized crystallites. *Nat. Photonics* **11**, 108 (2017).
42. Stranks, S. D., Snaith, H. J. Metal-halide perovskites for photovoltaic and light-emitting devices. Nat. Nanotechnol. **10**, 391 (2015).
43. Lin, K., Xing, J., Quan, L. N., de Arquer, F. P. G., Gong, X., Lu, J., Xie, L., Zhao, W., Zhang, D., Yan, C, et al. Perovskite light-emitting diodes with external quantum efficiency exceeding 20 per cent. Nature **562**, 245–248 (2018).
44. Van Le, Q., Jang, H. W., Kim, S. Y. Recent advances toward high-efficiency halide perovskite light-emitting diodes: review and perspective. Small Method. **2**, 1700419 (2018).
45. Wang, N., Cheng, L., Ge, R., Zhang, S., Miao, Y., Zou, W., Yi, C., Sun, Y., Cao, Y., Yang, R, et al. Perovskite light-emitting diodes based on solution-processed self-organized multiple quantum wells. *Nat. Photonics* **10**, 699 (2016).
46. Chang, J., Zhang, S., Wang, N., Sun, Y., Wei, Y., Li, R., Yi, C., Wang, J., Huang, W. Enhanced performance of red perovskite light-emitting diodes through the dimensional tailoring of perovskite multiple quantum wells. *J. Phys. Chem. Lett.* **9**, 881–886 (2018).
47. Salado, M., Jodlowski, A. D., Roldan-Carmona, C., de Miguel, G., Kazim, S., Nazeeruddin, M. K., Ahmad, S. Surface passivation of perovskite layers using heterocyclic halides: improved photovoltaic properties and intrinsic stability. *Nano Energy* **50**, 220–228 (2018).
48. Yang, X., Zhang, X., Deng, J., Chu, Z., Jiang, Q., Meng, J., Wang, P., Zhang, L., Yin, Z., You, J. Efficient green light-emitting diodes based on quasi-two-dimensional composition and phase engineered perovskite with surface passivation. *Nat. Commun.* **9**, 570 (2018).
49. Bonabi Naghadeh, S., Luo, B., Abdelmageed, G., Pu, Y.-C., Zhang, C., Zhang, J. Z. Photophysical properties and improved stability of organic–inorganic perovskite by surface passivation. *J. Phys. Chem. C* **122**, 15799–15818 (2018).
50. Liu, Z., Qayyum, M. F., Wu, C., Whited, M. T., Djurovich, P. I., Hodgson, K. O., Hedman, B., Solomon, E. I., Thompson, M. E. A codeposition route to cui—Pyridine coordination complexes for organic light-emitting diodes. *J. Am. Chem. Soc.* **133**, 3700–3703 (2011).
Green electroluminescence from copper iodide based hybrid materials.
51. Adjokatse, S., Fang, H.-H., Loi, M. A. Broadly tunable metal halide perovskites for solid-state light-emission applications. *Mater. Today* **20**, 413–424 (2017).
52. Zou, Y., Ban, M., Yang, Y., Bai, S., Wu, C., Han, Y., Wu, T., Tan, Y., Huang, Q., Gao, X, et al. Boosting perovskite light-emitting diode performance via tailoring interfacial contact. *ACS Appl. Mat. Inter.* **10**, 24320–24326 (2018).
53. Zhang, L., Yang, X., Jiang, Q., Wang, P., Yin, Z., Zhang, X., Tan, H., Yang, Y., Wei, M., Sutherland, B. R, et al. Ultra-bright and highly efficient inorganic based perovskite light-emitting diodes. *Nat. Commun.* **8**, 15640 (2017).
54. Xi, C., Chengjun, Q., Wei, D., Jingwen, L., Xiaoming, M., Yulu, Z., Tao, L., Xiaoma, T., Hongmei, C., Yifang, O. Boosted electroluminescence of perovskite light-emitting diodes by pinhole passivation with insulating polymer. *J. Phys. D: Appl. Phys.* **51**, 405103 (2018).
55. Chunyan, L., Ping, C., ZiYang, X., Debei, L., Gang, W., Yan, M., Qunliang, S. Interfacial engineering with ultrathin poly (9,9-di-n-octylfluorenyl-2,7-diyl) (PFO) layer for high efficient perovskite light-emitting diodes. Nanotechnology **29**, 075203 (2018).
56. Park, S. S., Santha Moorthy, M., Ha, C.-S. Periodic mesoporous organosilicas for advanced applications. *Npg Asia Mater* **6**, e96 (2014).
57. Zhang, X., Hejazi, M., Thiagarajan, S. J., Woerner, W. R., Banerjee, D., Emge, T. J., Xu, W., Teat, S. J., Gong, Q., Safari, A, et al. From 1D chain to 3D Network: a new family of inorganic–organic hybrid semiconductors MO3(L)x (M = Mo, W; l = organic Linker) built on Perovskite-like structure modules. *J. Am. Chem. Soc.* **135**, 17401–17407 (2013).

DOI: 10.1016/j.enchem.2019.100008
EnergyChem 1, 100008 (2019)

58. Lustig, W. P., Li, J. Luminescent metal–organic frameworks and coordination polymers as alternative phosphors for energy efficient lighting devices. *Coord. Chem. Rev.* **373**, 116–147 (2018).
59. Vellingiri, K., Boukhvalov, D. W., Pandey, S. K., Deep, A., Kim, K.-H. Luminescent metal-organic frameworks for the detection of nitrobenzene in aqueous media. *Sensors Actuat. B: Chem.* **245**, 305–313 (2017).
60. Cui, Y., Yue, Y., Qian, G., Chen, B. Luminescent functional metal–organic frameworks. *Chem. Rev.* **112**, 1126–1162 (2012).
61. Fuhr, O., Dehnen, S., Fenske, D. Chalcogenide clusters of copper and silver from silylated chalcogenide sources. *Chem. Soc. Rev.* **42**, 1871–1906 (2013).
62. Yan, C., Tian, Q., Yang, S. Recent advances in the rational design of copper chalcogenide to enhance the photothermal conversion efficiency for the photothermal ablation of cancer cells. *RSC Adv* **7**, 37887–37897 (2017).
63. Huang, X., Li, J., Fu, H. The first covalent organic—inorganic networks of hybrid Chalcogenides: structures that may lead to a new type of quantum wells. *J. Am. Chem. Soc.* **122**, 8789–8790 (2000).
64. Huang, X., Li, J., Zhang, Y., Mascarenhas, A From 1D chain to 3D Network: tuning hybrid II-VI nanostructures and their optical properties. *J. Am. Chem. Soc.* **125**, 7049–7055 (2003).
65. Peng, R., Li, M., Li, D. Copper(I) halides: a versatile family in coordination chemistry and crystal engineering. *Coord. Chem. Rev.* **254**, 1–18 (2010).
66. Perovskite fever. *Nat. Mater.* **13**, 837 (2014).
67. Snaith, H. J. Present status and future prospects of perovskite photovoltaics. *Nat. Mater.* **17**, 372–376 (2018).
68. Rong, Y., Hu, Y., Mei, A., Tan, H., Saidaminov, M. I., Seok, S. I., McGehee, M. D., Sargent, E. H., Han, H. Challenges for commercializing perovskite solar cells. *Science* **361**, eaat8235 (2018).
69. Turren-Cruz, S.-H., Hagfeldt, A., Saliba, M. Methylammonium-free, high-performance and stable perovskite solar cells on a planar architecture. Science, eaat3583 (2018).
70. Jeon, N. J., Noh, J. H., Kim, Y. C., Yang, W. S., Ryu, S., Seok, S. I. Solvent engineering for high-performance inorganic–organic hybrid perovskite solar cells. *Nat. Mater.* **13**, 897 (2014).
71. Grätzel, M. The light and shade of perovskite solar cells. *Nat. Mater.* **13**, 838 (2014).
72. Quan, L. N., García de Arquer, F. P., Sabatini, R. P., Sargent, E. H. Perovskites for light emission. *Adv. Mater.* **30**, 1801996 (2018).
73. Liu, F., Zhang, Y., Ding, C., Kobayashi, S., Izuishi, T., Nakazawa, N., Toyoda, T., Ohta, T., Hayase, S., Minemoto, T, et al. Highly luminescent phase-stable CsPbI3 perovskite quantum dots achieving near 100% absolute photoluminescence quantum yield. ACS Nano **11**, 10373–10383 (2017).
74. Kim, Y.-H., Cho, H., Heo, J. H., Kim, T.-S., Myoung, N., Lee, C.-L., Im, S. H., Lee, T.-W. Multicolored organic/inorganic hybrid perovskite light-emitting diodes. *Adv. Mater.* **27**, 1248–1254 (2015).
75. Shang, Y., Li, G., Liu, W., Ning, Z. Quasi-2D inorganic CsPbBr3 perovskite for efficient and stable light-emitting diodes. *Adv. Funct. Mater.* **28**, 1801193 (2018).
76. Wang, Z.-P., Wang, J.-Y., Li, J.-R., Feng, M.-L., Zou, G.-D., Huang, X.-Y. [Bmim]2SbCl5: a main group metal-containing ionic liquid exhibiting tunable photoluminescence and white-light emission. *Chem. Commun.* **51**, 3094–3097 (2015).
77. Bothwell, J. M., Krabbe, S. W., Mohan, R. S. Applications of bismuth(iii) compounds in organic synthesis. *Chem. Soc. Rev.* **40**, 4649–4707 (2011).
78. Shi, Z., Guo, J., Chen, Y., Li, Q., Pan, Y., Zhang, H., Xia, Y., Huang, W. Lead-Free organic–inorganic hybrid perovskites for photovoltaic Applications: recent advances and perspectives. *Adv. Mater.* **29**, 1605005 (2017).
79. Yam, V. W.-W., Lee, W.-K., Lai, T.-F. Synthesis and luminescent properties of a novel tetranuclear copper(I) cluster containing a μ4-sulfur moiety. X-Ray crystal structure of [Cu4(μ-dppm)4(μ4-S)](PF6)2·2Me2CO [dppm = bis(diphenylphosphino)methane]. *J. Chem. Soc., Chem. Commun.*, 1571–1573 (1993).
80. Langer, R., Yadav, M., Weinert, B., Fenske, D., Fuhr, O. Luminescence in functionalized copper thiolate clusters – Synthesis and structural effects. *Eur. J. Inorg. Chem.*(2013), 3623–3631 (2013).
81. Hu, B., Su, C.-Y., Fenske, D., Fuhr, O. Synthesis, characterization and optical properties of a series of binuclear copper chalcogenolato complexes. *Inorg. Chim. Acta* **419**, 118–123 (2014).
82. Yang, X.-X., Issac, I., Lebedkin, S., Kühn, M., Weigend, F., Fenske, D., Fuhr, O., Eichhöfer, A Red-luminescent biphosphine stabilized 'Cu12S6' cluster molecules. *Chem. Commun.* **50**, 11043–11045 (2014).
83. Eichhöfer, A., Buth, G., Lebedkin, S., Kühn, M., Weigend, F. Luminescence in phosphine-stabilized copper chalcogenide cluster Molecules—A comparative study. *Inorg. Chem.* **54**, 9413–9422 (2015).
84. Yam, V. W.-W., Lo, K. K.-W., Wang, C.-R., Cheung, K.-K. The first series of luminescent (μ4-Chalcogenido)silver(I) clusters. *Inorg. Chem.* **35**, 5116–5117 (1996).
85. Li, G., Lei, Z., Wang, Q.-M. Luminescent molecular Ag—S nanocluster [Ag62S13(SBut)32](BF4)4. *J. Am. Chem. Soc.* **132**, 17678–17679 (2010).
A luminescent silver chalcogenide nanocluster emitting red light.
86. Sun, D., Liu, F.-J., Huang, R.-B., Zheng, L.-S. Anionic heptadecanuclear Silver(I) cluster constructed from in situ generated 2-Mercaptobenzoic acid and a sulfide anion. *Inorg. Chem.* **50**, 12393–12395 (2011).
87. Jin, S., Wang, S., Song, Y., Zhou, M., Zhong, J., Zhang, J., Xia, A., Pei, Y., Chen, M., Li, P, et al. Crystal structure and optical properties of the [Ag62S12(SBut)32]2+ nanocluster with a complete face-centered cubic kernel. *J. Am. Chem. Soc.* **136**, 15559–15565 (2014).
88. Ki, W., Li, J A semiconductor bulk material that emits direct white light. *J. Am. Chem. Soc.* **130**, 8114–8115 (2008).
89. Wang, S., Li, J. Two-dimensional inorganic–organic hybrid semiconductors composed of double-layered ZnS and monoamines with aromatic and heterocyclic aliphatic rings: syntheses, structures, and properties. *J. Solid State Chem.* **224**, 40–44 (2015).
90. Ki, W., Li, J., Eda, G., Chhowalla, M. Direct white light emission from inorganic–organic hybrid semiconductor bulk materials. *J. Mater. Chem.* **20**, 10676–10679 (2010).
91. Zhang, M., Shi, C., Zhang, T.-K., Feng, M., Chang, L., Yao, W.-T., Yu, S.-H. Mn-Substituted [Zn1—xMnxSe](DETA)0.5 (x = 0—0.3) inorganic—organic hybrid Nanobelts: synthesis, electron paramagnetic resonance Spectroscopy, and their Temperature- and Pressure-Dependent optical properties. *Chem. Mater.* **21**, 5485–5490 (2009).
92. Zhang, X., Liu, W., Wei, G. Z., Banerjee, D., Hu, Z., Li, J. Systematic approach in designing rare-earth-free hybrid semiconductor phosphors for general lighting applications. *J. Am. Chem. Soc.* **136**, 14230–14236 (2014).
Copper iodide based hybrids as rare-earth free lighting phosphors.
93. Liu, W., Fang, Y., Wei, G. Z., Teat, S. J., Xiong, K., Hu, Z., Lustig, W. P., Li, J. A family of highly efficient cui-Based lighting phosphors prepared by a Systematic, Bottom-up synthetic approach. *J. Am. Chem. Soc* **137**, 9400–9408 (2015).
94. Fang, Y., Liu, W., Teat, S. J., Dey, G., Shen, Z., An, L., Yu, D., Wang, L., O'Carroll, D. M., Li, J. A systematic approach to achieving high performance hybrid lighting phosphors with excellent Thermal- and Photostability. *Adv. Funct. Mater.* **27**, 1603444 (2017).
95. Li, S.-L., Zhang, F.-Q., Zhang, X.-M. An organic-ligand-free thermochromic luminescent cuprous iodide trinuclear cluster: evidence for cluster centered emission and configuration distortion with temperature. *Chem. Commun.* **51**, 8062–8065 (2015).

DOI: 10.1016/j.enchem.2019.100008
EnergyChem **1**, 100008 (2019)

96. Liu, W., Zhu, K., Teat, S. J., Dey, G., Shen, Z., Wang, L., O'Carroll, D. M., Li, J. All-in-One: achieving Robust, strongly luminescent and highly dispersible hybrid materials by combining ionic and coordinate bonds in molecular crystals. *J. Am. Chem. Soc.* **139**, 9281–9290 (2017).
High performance all-in-one (AIO) type copper iodide based hybrid materials.
97. Yu, M., Chen, L., Jiang, F., Zhou, K., Liu, C., Sun, C., Li, X., Yang, Y., Hong, M. Cation-Induced strategy toward an hourglass-shaped Cu6I7– Cluster and its color-tunable luminescence. *Chem. Mater.* **29**, 8093–8099 (2017).
98. Chen, L., Ma, J., Chen, Q., Feng, R., Jiang, F., Hong, M. A 2D silver-iodide-organic framework with both fluorescent and phosphorescent emissions. *Inorg. Chem. Commun.* **15**, 208–211 (2012).
99. Yang, D., Xu, W., Cao, X., Zheng, S., He, J., Ju, Q., Fang, Z., Huang, W. Two silver coordination network compounds with colorful photoluminescence. *Inorg. Chem.* **55**, 7954–7961 (2016).
100. Dohner, E. R., Hoke, E. T., Karunadasa, H. I. Self-Assembly of broadband white-light emitters. *J. Am. Chem. Soc.* **136**, 1718–1721 (2014).
Broadband white-light emission from 2D hybrid perovskites.
101. Dohner, E. R., Jaffe, A., Bradshaw, L. R., Karunadasa, H. I. Intrinsic white-light emission from layered hybrid perovskites. *J. Am. Chem. Soc.* **136**, 13154–13157 (2014).
102. Neogi, I., Bruno, A., Bahulayan, D., Goh, T. W., Ghosh, B., Ganguly, R., Cortecchia, D., Sum, T. C., Soci, C., Mathews, N, et al. Broadband-Emitting 2 D hybrid organic–inorganic perovskite based on Cyclohexane-bis(methylamonium) cation. ChemSusChem **10**, 3765–3772 (2017).
103. Wu, G., Zhou, C., Ming, W., Han, D., Chen, S., Yang, D., Besara, T., Neu, J., Siegrist, T., Du, M.-H, et al. A one-dimensional organic lead chloride hybrid with excitation-dependent broadband emissions. *ACS Energy Lett* **3**, 1443–1449 (2018).
104. Yuan, Z., Zhou, C., Tian, Y., Shu, Y., Messier, J., Wang, J. C., van de Burgt, L. J., Kountouriotis, K., Xin, Y., Holt, E, et al. One-dimensional organic lead halide perovskites with efficient bluish white-light emission. *Nat. Commun.* **8**, 14051 (2017).
Efficient white-light emission from 1D hybrid perovskite.
105. Mao, L., Wu, Y., Stoumpos, C. C., Traore, B., Katan, C., Even, J., Wasielewski, M. R., Kanatzidis, M. G. Tunable white–light emission in single-cation-templated three-layered 2D perovskites (CH3CH2NH3)4Pb3Br10–xClx. *J. Am. Chem. Soc.* **139**, 11956–11963 (2017).
106. Mao, L., Guo, P., Kepenekian, M., Hadar, I., Katan, C., Even, J., Schaller, R. D., Stoumpos, C. C., Kanatzidis, M. G. Structural diversity in white-light-emitting hybrid lead bromide perovskites. *J. Am. Chem. Soc.* **140**, 13078–13088 (2018).
107. Zhuang, Z., Peng, C., Zhang, G., Yang, H., Yin, J., Fei, H. Intrinsic broadband white-light emission from Ultrastable, cationic lead halide layered materials. *Angew. Chem. Int. Ed.* **56**, 14411–14416 (2017).
Non-perovskite lead halide hybrid materials with white-light emission.
108. Zhou, C., Lin, H., Worku, M., Neu, J., Zhou, Y., Tian, Y., Lee, S., Djurovich, P., Siegrist, T., Ma, B. Blue emitting single crystalline assembly of metal halide clusters. *J. Am. Chem. Soc.* **140**, 13181–13184 (2018).
Lead halide hybrid cluster with strong blue emission with a high IQY of 83%.
109. Zhou, C., Tian, Y., Yuan, Z., Lin, H., Chen, B., Clark, R., Dilbeck, T., Zhou, Y., Hurley, J., Neu, J, et al. Highly efficient broadband yellow phosphor based on zero-dimensional tin mixed-halide perovskite. *ACS Appl. Mat. Inter.* **9**, 44579–44583 (2017).
110. Fu, P., Huang, M., Shang, Y., Yu, N., Zhou, H.-L., Zhang, Y.-B., Chen, S., Gong, J., Ning, Z. Organic—Inorganic layered and hollow tin bromide perovskite with tunable broadband emission. *ACS Appl. Mat. Inter.* **10**, 34363–34369 (2018).
111. Zhou, C., Lin, H., Shi, H., Tian, Y., Pak, C., Shatruk, M., Zhou, Y., Djurovich, P., Du, M.-H., Ma, B. A zero-dimensional organic seesaw-shaped tin bromide with highly efficient strongly stokes-shifted deep-red emission. *Angew. Chem.* **130**, 1033–1036 (2018).
112. Khan, A., Zeb, A., Li, L., Zhang, W., Sun, Z., Wang, Y., Luo, J. A lead-free semiconducting hybrid with ultra-high color rendering index white-light emission. *J. Mater. Chem. C* **6**, 2801–2805 (2018).
113. Zhou, C., Worku, M., Neu, J., Lin, H., Tian, Y., Lee, S., Zhou, Y., Han, D., Chen, S., Hao, A, et al. Facile preparation of light emitting organic metal halide crystals with near-unity quantum efficiency. *Chem. Mater.* **30**, 2374–2378 (2018).
114. Toma, O., Allain, M., Meinardi, F., Forni, A., Botta, C., Mercier, N. Bismuth-Based coordination polymers with efficient aggregation-induced phosphorescence and reversible mechanochromic luminescence. *Angew. Chem. Int. Ed.* **55**, 7998–8002 (2016).
115. Shen, N., Li, J., Wu, Z., Hu, B., Cheng, C., Wang, Z., Gong, L., Huang, X. α- and β-[Bmim][BiCl4(2,2′-bpy)]: two polymorphic bismuth-containing ionic liquids with crystallization-induced phosphorescence. *Chem-Eur. J* **23**, 15795–15804 (2017).
116. Wang, S., Li, L., Sun, Z., Ji, C., Liu, S., Wu, Z., Zhao, S., Zeb, A., Hong, M., Luo, J. A semi-conductive organic–inorganic hybrid emits pure white light with an ultrahigh color rendering index. *J. Mater. Chem. C* **5**, 4731–4735 (2017).
117. Yangui, A., Pillet, S., Bendeif, E.-E., Lusson, A., Triki, S., Abid, Y., Boukheddaden, K. Broadband emission in a new two-dimensional cd-based hybrid perovskite. ACS Photonics **5**, 1599–1611 (2018).
118. Cheng, C.-C., Shen, N.-N., Du, C.-F., Wang, Z., Li, J.-R., Huang, X.-Y. Cadmium(II) chloride complexes of imidazole-based ligands: solvothermal syntheses, crystal structures and luminescent properties. *Inorg. Chem. Commun.* **85**, 21–25 (2017).
119. Shen, N.-N., Cai, M.-L., Song, Y., Wang, Z.-P., Huang, F.-Q., Li, J.-R., Huang, X.-Y. Supramolecular organization of [TeCl6]2– with ionic liquid cations: studies on the electrical conductivity and luminescent properties. *Inorg. Chem.* **57**, 5282–5291 (2018).
120. Xie, Y.-P., Jin, J.-L., Duan, G.-X., Lu, X., Mak, T. C. W. High-nuclearity silver(I) chalcogenide clusters: a novel class of supramolecular assembly. *Coord. Chem. Rev.* **331**, 54–72 (2017).
121. Connell, T. U., Sandanayake, S., Khairallah, G. N., White, J. M., O'Hair, R. A. J., Donnelly, P. S., Williams, S. J. Halide-ion-templated Ag8Cu6 rhombic dodecahedrons: synthesis, structure and reactivity of [Ag8Cu6(C≡CtBu)12X]BF4 (X=Cl, Br). *Dalton Trans* **42**, 4903–4907 (2013).
122. Bian, S.-D., Wu, H.-B., Wang, Q.-M. A Facile template approach to high-nuclearity Silver(I) alkynyl clusters. *Angew. Chem. Int. Ed.* **48**, 5363–5365 (2009).
123. Rais, D., Yau, J., Mingos, D. M. P., Vilar, R., White, A. J. P., Williams, D. J. Anion-Templated syntheses of rhombohedral silver–alkynyl cage compounds. *Angew. Chem. Int. Ed.* **40**, 3464–3467 (2001).
124. Kappes, M. M. Experimental studies of gas-phase main-group metal clusters. *Chem. Rev.* **88**, 369–389 (1988).
125. McCandlish, L. E., Bissell, E. C., Coucouvanis, D., Fackler, J. P., Knox, K. A new metal cluster system containing a cube of metal atoms. *J. Am. Chem. Soc.* **90**, 7357–7359 (1968).
126. Yam, V. W.-W., Lo, K. K.-W. Luminescent tetranuclear Copper(I) and Silver(I) chalcogenides. *Comments Inorg. Chem.* **19**, 209–229 (1997).
127. Yam, V. W.-W., Lo, K. K.-W., Cheung, K.-K. A Novel luminescent μ4-Selenido-Bridged Copper(I) tetramer. *Inorg. Chem.* **35**, 3459–3462 (1996).
128. Liu, C. W., Stubbs, T., Staples, R. J., Fackler, J. P. Syntheses and structural characterizations of two new Cu-S clusters of dialkyl Dithiophosphates: a sulfide-centered CuI8 Cube, {Cu8[S2P(O*i*Pr)2]6(.mu.8-S)}, and a distorted octahedral

DOI: 10.1016/j.enchem.2019.100008
EnergyChem 1, 100008 (2019)

{Cu6[S2P(OEt)2]6.cntdot·2H2O} cluster. *J. Am. Chem. Soc.* **117**, 9778–9779 (1995).
129. Wang, C.-R., Kam-Wing Lo, K., Wing-Wah Yam, V. Molecular orbital studies of luminescent silver(I) chalcogenido clusters [Ag4(μ-dppm)4(μ4-E)]2+ (dppm = Ph2PCH2PPh2). *J. Chem. Soc., Dalton Trans.*, 227–230 (1997).
130. Wang, C.-R., Lo, K. K.-W., Yam, V. W.-W. Ab initio study of luminescent chalcogenido silver(I) clusters [Ag4(μ-H2PCH2PH2)4(μ4-E)]2+. *Chem. Phys. Lett.* **262**, 91–96 (1996).
131. Zhou, K., Wang, X.-L., Qin, C., Wang, H.-N., Yang, G.-S., Jiao, Y.-Q., Huang, P., Shao, K.-Z., Su, Z.-M. Serendipitous anion-templated self-assembly of a sandwich-like Ag20S10 macrocycle-based high-nuclearity luminescent nanocluster. *Dalton Trans* **42**, 1352–1355 (2013).
132. Huang, R.-W., Wei, Y.-S., Dong, X.-Y., Wu, X.-H., Du, C.-X., Zang, S.-Q., Mak, T. C. W. Hypersensitive dual-function luminescence switching of a silver-chalcogenolate cluster-based metal–organic framework. *Nat. Chem* **9**, 689 (2017).
133. Huang, X., Li, J From single to multiple atomic Layers: a unique approach to the systematic tuning of structures and properties of inorganic−organic hybrid nanostructured semiconductors. *J. Am. Chem. Soc.* **129**, 3157–3162 (2007).
134. Li, J., Huang, X. Y., Yuen, T.. in Doped Nanomaterials and Nanodevices (2008). American Scientific Publishers.
135. Li, J., Huang, X. Y.. in Oxford Handbook of Nanoscience and Technology, Vol. 2. USA: Oxford University Press.
136. Smith, A. M., Nie, S. Semiconductor nanocrystals: structure, properties, and band gap engineering. *Acc. Chem. Res.* **43**, 190–200 (2010).
137. Bhargava, R. N., Gallagher, D., Hong, X., Nurmikko, A. Optical properties of manganese-doped nanocrystals of znS. *Phys. Rev. Lett.* **72**, 416–419 (1994).
138. Chen, Y., Wang, J., Li, J., Li, X., Wei, S. The luminescence inner filter effect of Mn2+-doped (ZnS)2·octylamine inorganic/organic hybrid thin films and their sensor application for environmental contaminants. *RSC Adv* **5**, 70238–70243 (2015).
139. Wallesch, M., Volz, D., Zink, D. M., Schepers, U., Nieger, M., Baumann, T., Bräse, S. Bright coppertunities: multinuclear CuI complexes with N–P ligands and their applications. *Chem-Eur. J* **20**, 6578–6590 (2014).
140. Barbieri, A., Accorsi, G., Armaroli, N. Luminescent complexes beyond the platinum group: the d10 avenue. *Chem. Commun.*, 2185–2193 (2008).
141. Yam, V. W.-W., Cheng, E. C.-C. Highlights on the recent advances in gold chemistry—a photophysical perspective. *Chem. Soc. Rev.* **37**, 1806–1813 (2008).
142. Tsubomura, T., Tsukuda, T., Matsumoto, K. Luminescent d^{10} transition metal complexes. *B. Chem. Soc. Jpn.* **52**, 29–42 (2008).
143. Sabin, F., Ryu, C. K., Ford, P. C., Vogler, A. Photophysical properties of hexanuclear copper(I) and silver(I) clusters. *Inorg. Chem.* **31**, 1941–1945 (1992).
144. Chan, C.-K., Cheung, K.-K., Che, C.-M. Structure and spectroscopic properties of a luminescent inorganic cyclophane from self-assembly of copper(I) and two ligand components. *Chem. Commun.*, 227–228 (1996).
145. Pawlowski, V., Knör, G., Lennartz, C., Vogler, A. Luminescence and theoretical studies of Cu(tripod)X [tripod = 1,1,1-Tris(diphenylphosphanylmethyl)ethane; X– = Halide, Thiophenolate, phenylacetylide]. *Eur. J. Inorg. Chem.* **2005**, 3167–3171 (2005).
146. Zhan, S.-Z., Li, M., Ng, S. W., Li, D. Luminescent metal–organic frameworks (MOFs) as a Chemopalette: tuning the thermochromic behavior of dual-emissive phosphorescence by adjusting the supramolecular microenvironments. *Chem-Eur. J* **19**, 10217–10225 (2013).
147. Armaroli, N., Accorsi, G., Cardinali, F., Listorti, A.. In: Balzani Vincenzo, Campagna Sebastiano, editors. Photochemistry and Photophysics of Coordination Compounds I. Springer Berlin Heidelberg. p. 69–115.
148. Kyle, K. R., Ryu, C. K., Ford, P. C., DiBenedetto, J. A. Photophysical studies in solution of the tetranuclear copper(I) clusters Cu4I4L4 (L = pyridine or substituted pyridine). *J. Am. Chem. Soc.* **113**, 2954–2965 (1991).
149. Raston, C. L., White, A. H. Crystal structure of the copper(I) iodide-pyridine (1/1) tetramer. *J. Chem. Soc., Dalton Trans.*, 2153–2156 (1976).
150. Tsuge, K., Chishina, Y., Hashiguchi, H., Sasaki, Y., Kato, M., Ishizaka, S., Kitamura, N. Luminescent copper(I) complexes with halogenido-bridged dimeric core. *Coord. Chem. Rev.* **306**, 636–651 (2016) Part 2.
151. Araki, H., Tsuge, K., Sasaki, Y., Ishizaka, S., Kitamura, N. Luminescence ranging from red to blue: a series of copper(i)−halide complexes having rhombic {Cu2(μ-X)2} (X = Br and I) units with N-Heteroaromatic ligands. *Inorg. Chem.* **44**, 9667–9675 (2005).
152. Perruchas, S., Le Goff, X. F., Maron, S., Maurin, I., Guillen, F., Garcia, A., Gacoin, T., Boilot, J.-P. Mechanochromic and thermochromic luminescence of a copper iodide cluster. *J. Am. Chem. Soc.* **132**, 10967–10969 (2010).
153. Benito, Q., Le Goff, X. F., Maron, S., Fargues, A., Garcia, A., Martineau, C., Taulelle, F., Kahlal, S., Gacoin, T., Boilot, J.-P, et al. Polymorphic copper iodide Clusters: insights into the mechanochromic luminescence properties. *J. Am. Chem. Soc.* **136**, 11311–11320 (2014).
154. Ortiz, A. M., Gómez-Sal, P., Flores, J. C., de Jesús, E. Learning about steric effects in NHC complexes from a 1D silver coordination polymer with fréchet dendrons. Organometallics **33**, 600–603 (2014).
155. Trivedi, M., Singh, G., Kumar, A., Rath, N. P. Silver(I) complexes as efficient source for silver oxide nanoparticles with catalytic activity in A3 coupling reactions. *Inorg. Chim. Acta* **438**, 255–263 (2015).
156. Yuan, S., Liu, S.-S., Lu, H.-F., Xu, M.-Z., Sun, D. A two-dimensional silver-iodide organic network constructed from a unique [Ag6I6] hexagonal prism-based one-dimensional column motif. *Acta Crystallogr. Sect. C* **69**, 216–218 (2013).
157. Kojima, A., Teshima, K., Shirai, Y., Miyasaka, T. Organometal halide perovskites as visible-light sensitizers for photovoltaic cells. *J. Am. Chem. Soc.* **131**, 6050–6051 (2009).
158. Lin, Q., Armin, A., Nagiri, R. C. R., Burn, P. L., Meredith, P. Electro-optics of perovskite solar cells. *Nat. Photonics* **9**, 106 (2014).
159. Green, M. A., Ho-Baillie, A., Snaith, H. J. The emergence of perovskite solar cells. *Nat. Photonics* **8**, 506 (2014).
160. Guner, T., Demir, M. M. A review on halide perovskites as color conversion layers in white light emitting diode applications. *physica status solidi (a)* **215**, 1800120 (2018).
161. Huang, H., Polavarapu, L., Sichert, J. A., Susha, A. S., Urban, A. S., Rogach, A. L. Colloidal lead halide perovskite nanocrystals: synthesis, optical properties and applications. *Npg Asia Mater* **8**, e328 (2016).
162. Kovalenko, M. V., Protesescu, L., Bodnarchuk, M. I. Properties and potential optoelectronic applications of lead halide perovskite nanocrystals. Science **358**, 745–750 (2017).
163. Hintermayr, V. A., Richter, A. F., Ehrat, F., Döblinger, M., Vanderlinden, W., Sichert, J. A., Tong, Y., Polavarapu, L., Feldmann, J., Urban, A. S. Tuning the optical properties of perovskite nanoplatelets through composition and thickness by ligand-assisted exfoliation. *Adv. Mater.* **28**, 9478–9485 (2016).
164. Mao, L., Wu, Y., Stoumpos, C. C., Wasielewski, M. R., Kanatzidis, M. G. White-Light emission and structural distortion in new corrugated two-dimensional lead bromide perovskites. *J. Am. Chem. Soc.* **139**, 5210–5215 (2017).
165. Sun, J., Yang, J., Lee, J. I., Cho, J. H., Kang, M. S. Lead-Free perovskite nanocrystals for light-emitting devices. *J. Phys. Chem. Lett.* **9**, 1573–1583 (2018).
166. Wang, G.-E., Xu, G., Wang, M.-S., Cai, L.-Z., Li, W.-H., Guo, G.-C. Semiconductive 3-D haloplumbate framework hybrids with high color rendering index white-light emission. *Chem. Sci.* **6**, 7222–7226 (2015).

DOI: 10.1016/j.enchem.2019.100008
EnergyChem 1, 100008 (2019)

167. Yang, S., Lin, Z., Wang, J., Chen, Y., Liu, Z., Yang, E., Zhang, J., Ling, Q. High color rendering index white-light emission from UV-Driven LEDs based on single luminescent materials: two-Dimensional perovskites (C6H5C2H4NH3)2PbBrxCl4–x. *ACS Appl. Mat. Inter.* **10**, 15980–15987 (2018).
168. Barkaoui, H., Abid, H., Yangui, A., Triki, S., Boukheddaden, K., Abid, Y. Yellowish white-light emission involving resonant energy transfer in a new one-dimensional hybrid material: (C9H10N2)PbCl4. *J. Phys. Chem. C* **122**, 24253–24261 (2018).
169. Dou, L., Wong, A. B., Yu, Y., Lai, M., Kornienko, N., Eaton, S. W., Fu, A., Bischak, C. G., Ma, J., Ding, T, et al. Atomically thin two-dimensional organic-inorganic hybrid perovskites. Science **349**, 1518–1521 (2015).
Strong purple-blue light emission from atomically thin 2D hybrid perovskite.
170. Zhang, Q., Ting, H., Wei, S., Huang, D., Wu, C., Sun, W., Qu, B., Wang, S., Chen, Z., Xiao, L. Recent progress in lead-free perovskite (-like) solar cells. *Materials Today Energy* **8**, 157–165 (2018).
171. Kamat, P. V., Bisquert, J., Buriak, J. Lead-free perovskite solar cells. *ACS Energy Lett* **2**, 904–905 (2017).
172. Chu, K.-B., Xie, J.-L., Chen, W.-J., Lu, W.-X., Song, J.-L., Zhang, C. A novel bismuth-based hybrid material with highly activity for fast removal of rhodamine B under dark conditions. Polyhedron **151**, 146–151 (2018).
173. Kulicka, B., Lis, T., Kinzhybalo, V., Jakubas, R., Piecha, A. Novel anionic water-containing inorganic fragment in [4-NH2PyH]8[Bi2Cl11] [Bi2Cl9(H2O)2]: structural characterization, thermal, dielectric and vibrational properties. Polyhedron **29**, 2014–2022 (2010).
174. Lin, R.-G., Xu, G., Wang, M.-S., Lu, G., Li, P.-X., Guo, G.-C. Improved photochromic properties on viologen-based inorganic–organic hybrids by using π-conjugated substituents as electron donors and stabilizers. *Inorg. Chem.* **52**, 1199–1205 (2013).
175. Rao, A. S., Babu, E. S., Swamy, K. C. K., Das, S. K. Isolation and structural characterization of 1,5-benzodiazepinium cation in an inorganic–organic hybrid compound [C12H17N2]3[Bi2Cl9]·2EtOH. Polyhedron **29**, 1706–1714 (2010).
176. Adonin, S. A., Sokolov, M. N., Fedin, V. P. Polynuclear halide complexes of Bi(III): from structural diversity to the new properties. *Coord. Chem. Rev.* **312**, 1–21 (2016).
177. Cao, Y., Wang, N., Tian, H., Guo, J., Wei, Y., Chen, H., Miao, Y., Zou, W., Pan, K., He, Y, et al. Perovskite light-emitting diodes based on spontaneously formed submicrometre-scale structures. Nature **562**, 249–253 (2018).
178. Yang, K., Li, F., Liu, Y., Xu, Z., Li, Q., Sun, K., Qiu, L., Zeng, Q., Chen, Z., Chen, W, et al. All-Solution-Processed perovskite quantum dots light-emitting diodes based on the solvent engineering strategy. *ACS Appl. Mat. Inter.* **10**, 27374–27380 (2018).
179. Liu, X., Zhang, T., Ni, T., Jiang, N., Liu, Z., Bian, Z., Lu, Z., Huang, C. Co-deposited Cu(I) complex for tri-layered yellow and white organic light-emitting diodes. *Adv. Funct. Mater.* **24**, 5385–5392 (2014).
180. Chondroudis, K., Mitzi, D. B. Electroluminescence from an organic−inorganic perovskite incorporating a quaterthiophene dye within lead halide perovskite layers. *Chem. Mater.* **11**, 3028–3030 (1999).
181. Tan, Z.-K., Moghaddam, R. S., Lai, M. L., Docampo, P., Higler, R., Deschler, F., Price, M., Sadhanala, A., Pazos, L. M., Credgington, D, et al. Bright light-emitting diodes based on organometal halide perovskite. *Nat. Nanotech.* **9**, 687 (2014).
182. Wang, J., Wang, N., Jin, Y., Si, J., Tan, Z.-K., Du, H., Cheng, L., Dai, X., Bai, S., He, H, et al. Interfacial control toward efficient and low-voltage perovskite light-emitting diodes. *Adv. Mater.* **27**, 2311–2316 (2015).
183. Cho, H., Jeong, S.-H., Park, M.-H., Kim, Y.-H., Wolf, C., Lee, C.-L., Heo, J. H., Sadhanala, A., Myoung, N., Yoo, S, et al. Overcoming the electroluminescence efficiency limitations of perovskite light-emitting diodes. Science **350**, 1222–1225 (2015).
Significant performance improvement of hybrid perovskite-based LED devices.
184. Ni, T., Liu, X., Zhang, T., Bao, H., Zhan, G., Jiang, N., Wang, J., Liu, Z., Bian, Z., Lu, Z, et al. Red emissive organic light-emitting diodes based on codeposited inexpensive CuI complexes. *J. Mater. Chem. C* **3**, 5835–5843 (2015).
185. Hu, P., Zhu, R.-Q., Zhang, W. Distinct dielectric transitions in 1-ethylimidazole-based cadmium(II) complexes. Polyhedron **115**, 137–141 (2016).
186. Xu, W.-J., He, C.-T., Ji, C.-M., Chen, S.-L., Huang, R.-K., Lin, R.-B., Xue, W., Luo, J.-H., Zhang, W.-X., Chen, X.-M. Molecular dynamics of flexible polar cations in a variable confined Space: toward exceptional two-step nonlinear optical switches. *Adv. Mater.* **28**, 5886–5890 (2016).
187. Ye, H.-Y., Zhang, Y., Fu, D.-W., Xiong, R.-G. An above-room-temperature ferroelectric organo–metal halide Perovskite: (3-Pyrrolinium)(CdCl3). *Angew. Chem. Int. Ed.* **53**, 11242–11247 (2014).
188. Qin, L.-L., Ye, H.-Y., Wang, D.-Y. Structural phase transition in catena-(1,2,3,6-tetrahydropyridine tris(μ2-chloro)-cadmium(II)). *Inorg. Chem. Commun.* **46**, 47–50 (2014).
189. Kuhn, N., Abu-Rayyan, A., Eichele, K., Schwarz, S., Steimann, M. Weak interionic interactions in 2-bromoimidazolium derivatives. *Inorg. Chim. Acta* **357**, 1799–1804 (2004).
190. Pietikäinen, J., Maaninen, A., Laitinen, R. S., Oilunkaniemi, R., Valkonen, J. Halogenation of tellurium by SO2Cl2. Formation and crystal structures of (H3O)[Te3Cl13]·1/2SO2, [(C4H8O)2H][TeCl5]·(C4H8O), [(Me2SO)2H]2[TeCl6], and [Ni(NCCH3)6][Te2Cl10]. Polyhedron **21**, 1089–1095 (2002).
191. Reich, O., Hasche, S., Bonmann, S., Krebs, B. [H3O·(Dibenzo-18-crown-6)][Te2Br9] and [H5O2][Te2Cl9]·2 C4H8O2: two new oxonium Halotellurates(IV) containing a novel type of [Te2×9]– Anions. *Z. Anorg. Allg. Chem.* **624**, 411–418 (1998).
192. Ryan, J. M., Xu, Z. [C6H5NH(CH3)2]2Te2I10: secondary I···I bonds build up a 3D network. *Inorg. Chem.* **43**, 4106–4108 (2004).

AUTHOR BIOGRAPHIES

Wei Liu received his B.S. in Chemistry from Nanjing University in China in 2010 and his Ph.D. from Rutgers University in the United States in 2017 with Prof. Jing Li. He is currently an associate professor in Hoffmann Institute of Advanced Materials (HIAM) at Shenzhen Polytechnic. His research focuses on developing functional inorganic-organic hybrid materials for energy-related applications.

William P. Lustig obtained his BS in chemistry from American University in 2010, joined the Jing Li Research Group in 2013, and obtained Ph.D degree in 2019 under Professor Jing Li's guidance. His research is centered on the synthesis and development of new luminescent materials with applications as sensor and phosphors. He is especially interested in studying the luminescence mechanisms at play in these systems and using theoretical methods to aid in their rational design.

Jing Li is a Distinguished Professor in the Department of Chemistry and Chemical Biology at Rutgers University. She received her Ph.D. degree from Cornell University in 1990 under the guidance of Professor Roald Hoffmann. She joined the chemistry faculty at Rutgers University in 1991 as Assistant Professor. She was promoted to Associate Professor in 1996, to Full Professor in 1999, and to Distinguished Professor in 2006. She has published +330 research articles, invited book chapters and reviews, and holds 14 issued and pending patents. She currently serves as Associate Editor for *Crystal Growth & Design*.

DOI: 10.1016/j.enchem.2019.100008
EnergyChem **1**, 100008 (2019)